Modelling and Optimisation for a Coordinated Interconnected Multi-Terminal DC Transmission Infrastructure for Integration of Offshore Wind Energy

SITI KHADIJAH HAMZAH

Modelling and Optimisation for a Coordinated Interconnected Multi-Terminal DC Transmission Infrastructure for Integration of Offshore Wind Energy

Siti Khadijah Hamzah

A thesis presented for the degree of
Doctor of Philosophy

Department of Engineering
Durham University
England
September 2024

Dedicated to:

My husband, Tony Sattar,
whose unwavering support, encouragement and love
have been my greatest strength in making this journey possible.
Thank you for standing by me every step of the way.

My family,
especially my mother and brother,
for their endless love and encouragement.

Modelling and Optimisation for a Coordinated Interconnected Multi-Terminal DC Transmission Infrastructure for Integration of Offshore Wind Energy

Siti Khadijah Hamzah

Abstract

The modern power system is undergoing significant modifications as a result of the integration of variable renewable energy system, particularly offshore wind farms. These modifications have increased the complexity of power grid operations, especially in terms of maintaining a balance between variable generation and demand. Consequently, operational planning has become notably more challenging, requiring greater flexibility (i.e., the ability to provide control and load-following throughout a wider operating range) to meet demands, whilst maintaining the security and reliability of the power system. This thesis presents a reinforcement model for transmission systems, designed to enhance the operational planning of hybrid AC/DC networks integrated with offshore wind farms, with a particular emphasis on the MT-HVDC link, through the utilisation of Voltage Source Converter (VSC) technology. A mathematical model for hybrid AC/DC networks is developed based on the Flexible Universal Branch Model (FUBM) to provide functionalities, which offer flexibility in both short-term and long-term operational planning, specifically addressing the optimisation problems of Optimal Power Flow (OPF) and Security Constrained OPF (SCOPF). This mathematical model has been tested using control techniques (i.e., conventional control and droop control) in the VSC in-model (one model in the FUBM) incorporated with the Remedial Action Scheme (RAS), known as RAS-FUBM (i.e., RAS-FUBM conventional control and RAS-FUBM droop control), whilst considering a range of scenarios (e.g., worst-case scenarios, multi-period scenarios, and multi-objective scenarios). The results clearly show that the model demonstrates greater flexibility and reliability, as well as mitigates the contingencies (following the standard N-1 rule) and congestion within the MT-HVDC link. These results provide a benchmark for modern operational planning and assist Transmission System Operators (TSOs) in making optimal decisions, thereby ensuring both reliability and economic feasibility in power system operation.

Declaration

The work in this thesis is based on research carried out at the Power Systems Research Group, the Department of Engineering, Durham University, England. No part of this thesis has been submitted elsewhere for any other degree or qualification and it is all my own work unless referenced to the contrary in the text.

Acknowledgements

Embarking on this PhD journey has been a challenging and rewarding experience, marked by countless hours of research, writing, dedication, reflection and personal growth. This journey would not have been possible without the support and encouragement of many individuals and organizations.

I would like to thank my primary supervisor, Dr. Behzad Kazemtabrizi, for his dedicated support, guidance, and insightful feedback. Throughout these three years, he was always willing and enthusiastic to assist me in every way possible. I would also like to thank my second supervisor, Dr. Mahmoud Shahbazi, for his openness in sharing comments and ideas. Their expertise and encouragement have been fundamental in shaping my work and growth as a scholar.

I am deeply grateful to my family for their support and encouragement, which motivated me to complete this strenuous work, especially to my husband, Tony Sattar, for never giving up and always believing in me during the past three years.

I sincerely thank my colleagues and administrative staff in the Department of Engineering at Durham University and AURA-CDT for their companionship and knowledge sharing. Special thanks to Martha Correa Delval, Gregorio Higuera-Gutierrez, Louise Gascoigne for their assistance during various stages of this journey. To my best friend, Iza Sazanita, who has always guided me over the years.

Finally, I would like to express my gratitude for the funding and resources provided by AURA-CDT, UKRI, and Durham University, which were instrumental in making this research possible. Their support has been essential in achieving the objectives of my work.

This work was financially supported by the Engineering and Physical Sciences Research Council (EPSRC) Centre for Doctoral Training (CDT) in Offshore Wind Energy and the Environment (AURA-CDT), with project reference number EP/S023763/1/2651009.

Contents

List of Figures

List of Tables

List of Acronyms

AC	Alternate Current
CA	Contingency Analysis
CDF	Cumulative Distribution Function
CSC	Current Source Converter
C-SCOPF	Corrective Security Constrained Optimal Power Flow
CTT	Control Tap Changing Transformer
DC	Direct Current
DWI	Demand and Wind Increased
ED	Economic Dispatch
EPS	Electric Power System
FACTS	Flexible AC Transmission System
FUBM	Flexible Universal Branch Model
GP	Geographic Partitioning
GTO	Gate Turn Off Thyristor
HVAC	High Voltage Alternate Current
HVDC	High Voltage Direct Current
HW	High Wind
HD	High Demand
IGBT	Insulated Gate Bipolar Transistor
LD	Low Demand
LW	Low Wind

MCT	Measure of Central Tendency
MD	Measure of Dispersion
MMC	Modular Multilevel Converter
MO-OPF	Multi Objective Optimal Power Flow
MT-HVDC	Multi-Terminal High Voltage Direct Current
NCER	Network Code on Emergency and Restoration
OPF	Optimal Power Flow
OPF-FUBM	Optimal Power Flow Flexible Universal Branch Model
OWFs	Offshore Wind Farms
PDF	Probability Distribution Function
PF	Power Flow
PI	Performance Index
PST	Phase Shifter Transformer
P-SCOPF	Preventive Security Constrained Optimal Power Flow
RAS	Remedial Action Scheme
RAS-FUBM	Remedial Action Scheme Flexible Universal Branch Model
RAS-FUBM CC	Remedial Action Scheme Flexible Universal Branch Model Conventional Control
RAS-FUBM DC	Remedial Action Scheme Flexible Universal Branch Model Droop Control
RMS	Root-Means-Square
SA	Security Assessment
SCOPF	Security Constrained Optimal Power Flow
SI	Severity Index
STATCOM	Static Compensator
TSCs	Transmission System Operators
VM	Voltage Magnitude
VSC	Voltage Source Converter

Chapter 1

Introduction

1.1 Problem Statement

The Electric Power System (EPS) faces significant challenges due to the increasing demand for energy consumption driven by population growth, which is projected to rise by 29% to 9.8 billion by 2050, up from the current world population of 7.6 billion [1]. Furthermore, ongoing modifications in power system infrastructure, as illustrated in Figure 1.1, are necessary not only to address this challenge but also to achieve the net zero target by 2050 [2]. These modifications involve the transformation of energy generation from fossil fuels to renewable energy sources [3], changing demand patterns (e.g., electric vehicles, storage devices, smart grids, etc.), the deployment of new technology trends (e.g., power-electronic devices, sensors, control devices, and grid services automation), regulatory requirements [4] and innovations in the transmission system (e.g., HVDC networks and Flexible AC transmission systems (FACTS) devices) [5]. However, many existing components within the EPS are aging, necessitating modernisation to facilitate the integration of renewable resources (e.g., offshore wind farms, photovoltaic solar farms, wave energy, etc.) [6]. This modernisation also needs to enhance operational flexibility (i.e., the ability to accommodate large-scale variable renewable generation sources) of the power system, whilst maintaining operational security and reliability to meet all demand requirements (i.e., stability and cost effectiveness) [7]. Therefore, the development of a modern EPS is essential not only for transmitting power over long distances, i.e., from regions with abundant renewable resources to regions with significant demand, but also for improving efficiency within the power system through a combination of AC and DC systems, which is vital for effectively incorporating renewable energy sources.

The hybrid AC/DC network, i.e., a power system with embedded HVDC links that are mainly used to facilitate integration of variable renewable generation, is a critical next step for the future growth of the EPS. Such a system however requires the establishment of new methodologies for planning and operational strategies, particularly with regards to controlling and managing interaction [8] between generator, transmission and demand sides within the power system. There

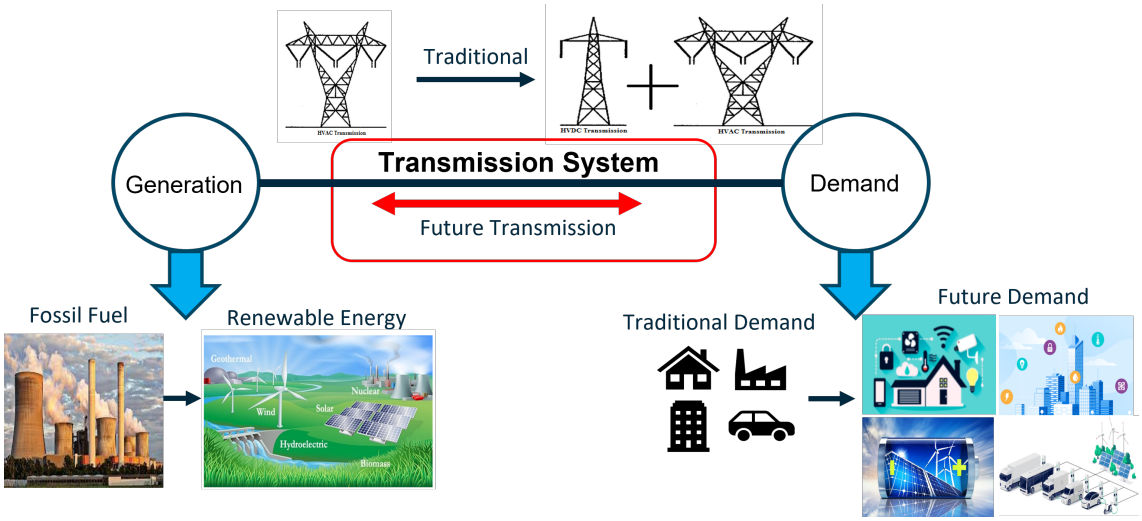

Figure 1.1: Power system structure

are inevitably new technical challenges in the route to adopting hybrid AC/DC networks as the next evolutionary step in the development of a modern and flexible power systems infrastructure. Challenges such as the requirement for coordinated control between both AC and DC components, achieving power quality, maintaining stability, ensuring a reliable communication infrastructure, addressing protection issues, and implementing energy management systems [9] create additional complexity when planning and operating hybrid AC/DC networks. On the other hand, in an effort to become a global leader in green energy, the United Kingdom (UK) has established a Ten Point Plan for a Green Industrial Revolution, one of which is to double the offshore wind energy capacity to 40GW by 2030 [10]. This transition implies that the power system is becoming increasingly dependent on weather conditions, which inevitably leads to uncertainty and variability in power production during operational planning. In the past, the operational planning process did not consider these uncertainties and variability on the generation side. Modern hybrid AC/DC networks require the inclusion of these factors (i.e., uncertainty and variability) along with numerous scenarios in the ensuing operational planning models, which are optimization problems related to solving optimal power flow, and security-constrained optimal power flow problems. Considering these factors and scenarios are essential for ensuring the safety and reliability of power system operations at all times, as well as for delivering electricity in the most economical manner whilst adhering to acceptable power quality standards [11]. Furthermore, it will assist and enable Transmission System Operators (TSOs) and policymakers to make informed decisions (i.e., decision considered all factors, scenarios, and insights before making a choice), which is critical for effective real-world applications [12]. Therefore, for modern hybrid AC/DC networks, it is imperative to develop comprehensive operational planning models that account for all factors and scenario events across various operating conditions.

A Multi-Terminal HVDC (MT-HVDC) link embedded within an AC network represents an ad-

vanced topology of the hybrid AC/DC network and has been proposed as a future energy solution, which can effectively harness electricity from large Offshore Wind Farms (OWFs) (i.e., DC system) and transmit it to onshore system (i.e., AC system). Furthermore, the MT-HVDC link can enhance the flexibility and reliability of the power system through the deployment of converters (i.e., Current Source Converter (CSC) or Voltage Source Converter (VSC)). Nevertheless, the offshore industry has not yet realised this link, especially the interconnection of OWFs clusters [13]. This is due to the technical constraints such as standards and interoperability in DC systems, strong AC system connection points, substation-to-substation communication, protection and grounding [14]. Therefore, this thesis presents analyses of transmission system reinforcement centred on the MT-HVDC link integrated with Offshore Wind Farms (OWFs), deploying the VSC under various operating conditions (i.e. normal and abnormal conditions) and through different scenarios (e.g., worst-case wind generation, multiple periods and multiple objectives). The proposed analyses can provide greater flexibility by leveraging the high controllability of VSC technology to independently regulate power system variables [15], including voltage and power, in both AC and DC systems.

1.2 Research aims and objectives

The main aim of this thesis is to model the reinforcement of transmission systems through the utilization of VSC technology, employing a Flexible Universal Branch Model (FUBM) within the context of a MT-HVDC link integrated with OWFs. This comprehensive modelling approach has the potential to expedite the development of a Supergrid infrastructure. The FUBM model has been chosen due to its ability to replicate the operation of standard AC branches and AC/DC interfaces within a single frame of reference. Additionally, it can represent real-world devices (e.g., voltage source converter, phase shifter transformer, and control tap changer transformer), whilst providing additional degrees of freedom in the form of additional state variables, a topic that will be discussed in more detail in Chapter 3. This thesis subsequently entails an extensive analysis of reliability in the power system, with the following objectives related to this critical analysis:

1. To develop a flexible transmission system operation strategy taking advantage of controllability and flexibility of VSC devices, with applicability spanning for both short-term operational planning and long-term planning horizons

2. To devise a novel, state of the art approach for solving the SCOPF problem for hybrid AC/DC networks, accounting for the worst-case scenarios of demand and Offshore Wind generation, as well as incorporating a multi-period OPF framework.

3. To rigorously investigate the techno-economic impacts of strategic VSC placement within the hybrid AC/DC networks architecture, through the formulation of a comprehensive multi-objective infrastructure planning problem.

1.3 Research questions and challenges

The EPS has experienced considerable transformation in recent years, in order to meet the rising demand and accommodate the integration of intermittent, variable renewable generation sources, particularly OWFs. This thesis seeks to investigate the modelling of power system infrastructure (i.e., VSC), emphasising on the reinforcement and strengthening of the transmission system. The study will explore the implementation of control strategies that could have potential to enhance the flexibility and reliability of the performance power system. Overall, the research questions are outlined as follows:

(a) What are the greatest challenges facing the electric power system today especially related to large-scale integration of variable renewable generation?

(b) How can the EPS system be strengthened in order to overcome these challenges, particularly at the transmission system?

(c) How can the current transmission system be reinforced in order to enhance the production from OWFs, considering the control actions?

(d) Why is it important to consider the control actions, particularly in context of short-term operational planning and long-term planning in the EPS?

(e) To what extent is the control actions' implementation within the EPS flexible and reliable?

From these research questions, this thesis delves into the more challenging aspects of:

1. **A Mathematical Model for MT-HVDC links:** To present a concept of MT-HVDC link as an optimal solution for integrating large scale VSC-interfaced variable renewable energy sources, particularly OWFs, providing an appealing approach for creating interconnected DC network hubs, enabling the maximisation of power sharing amongst renewable generation resources and facilitating long-distance power exchange between otherwise independently operated regions. In this thesis, this objective is addressed in Chapter 3.

2. **A holistic operational planning framework:** To establish an innovative modelling framework for operational planning of hybrid AC/DC networks taking advantage of the additional control actions promised by the VSCs that exist in such networks to enhance their operational flexibility. In this thesis, we call this framework, RAS-FUBM, which is introduced in Chapter 4.

3. **Application and impact assessment of additional control strategies in hybrid AC/DC networks with embedded MT-HVDC links:** To implement the VSC control strategies framework, considering a variety of scenarios (e.g., worst-case scenarios, multi-period scenarios and multi-objective scenarios). To this end, the implementation should be

able to demonstrates the flexibility and reliability of the power system, particularly related to contingency and congestion. In this thesis, this objective is addressed in Chapters 4 and 5.

1.4 Publications

Table 1.1 presents a list of the papers that have been presented and published, along with prospective future publications, which have been produced during the PhD research. The content and results from these papers have been incorporated into Chapters 3, 4, and 5 of this thesis.

Table 1.1: List of Publications and Presentations.

Type of Paper	Details of the Paper	Chapter
Conference publication	Optimum operational planning of wind-integrated power systems with embedded Multi-terminal High Voltage Direct Current Links using the Flexible Universal Branch Model. IEEE International Conference on Environment and Electrical Engineering and 2023 IEEE Industrial and Commercial Power Systems Europe (EEEIC/I&CPS Europe), pp. 1-6. IEEE, 2023.	3
Conference presentation	Operational Network Planning for Different Multi-Terminal High Voltage Direct Current Offshore System Interfaced Wind Integration. 19th EAWE PhD Seminar on Wind Energy, 6 - 8 September 2023, Hanover, Germany	4
Conference publication	Minimizing the Impact of Contingency in Multiple-Period Short-Term Operational Planning with RAS-FUBM for Wind Integration. IET Conference Proceedings, 2024, p. 180-187, DOI: 10.1049/icp.2024.2155. (13th International Conference on Power Electronics, Machines and Drives(PEMD 2024))	4
Journal Under Review	The Effect of Voltage Variations at the Reference VSC within the Multi-Terminal HVDC System Integrated with Offshore Wind Farms. IEEE IAS Publication	5

1.5 Chapter summary

This chapter provides a general introduction to the thesis, beginning with a problem statement that describes the challenges and ongoing modifications within the power system structure, the necessity of developing a modern EPS (i.e., hybrid AC/DC network) planning framework that accounts for uncertainty and variability, particularly when arising from weather-dependent power generation, whilst incorporating multiple scenarios into the operational planning models, and proposing advanced topology in hybrid AC/DC network with MT-HVDC link, as future energy solutions.

Chapter 2

Literature Review

This chapter provides an overview of two key components, the transmission system and converters (sections 2.1 and 2.2), which supports the thesis's aim of investigating the reinforcement of the transmission system through the utilization of VSC technology for purposes of large-scale offshore wind generation capacity integration. The remainder of this chapter contains the following: Section 2.3 provides a brief overview of the elements of operational planning and security assessment within the power system. In section 2.4, a detailed explanation of power flow is presented as a fundamental mathematical framework for purposes of power system's operational planning and security assessment. Section 2.5 introduces a general concept and standard formulation of optimisation problems applied to the power systems operational planning, encompassing several specific models, including economic dispatch, optimal power flow and security constrained optimal power flow. This section also discusses two types of control actions (i.e., preventive and corrective) to emphasise their significance, particularly in relation to assessing the performance of power system's operational security and its reliability. Finally, section 2.6 provides a summary of this chapter.

2.1 Transmission System

The transmission network, which is responsible for transmitting electricity from power plants (generation) to load centers (demand), is one of the primary components in the Electrical Power System (EPS) [16]. Furthermore, it has an enormous influence on the production side, influencing aspects such as the location of the power plants (i.e., where to build), operation of the power plants (i.e., which generators need to be operated) and the production of the power plants (i.e., how much power needs to be generated from each generator) [17]. However, the integration of variable renewable energy systems, particularly Offshore Wind Farms (OWFs), in the modern power system increases the complexity of the power grid's operation especially with regards to maintaining balance between variable generation and demand, making the operation of such transmission systems significantly more challenging [18]. In order to maximise the energy output from OWFs, trans-

mission system reinforcement is essential, resulting in reduced consumer cost by necessitating an economically prudent investments for both the OWFs and transmission systems [19]. It can be concluded that the planning of the transmission systems and the planning of OWFs are closely interrelated. Consequently, when undertaking analysis of OWFs, it is essential to also consider the planning of the associated transmission systems. Considering of these aspects, it is important to comprehend the system and structure of the transmission system, in order to optimise the integration of OWFs and ensure the sustainability and affordability of the power system.

An optimal operational planning in the transmission system typically seeks to establish the most economical operating point in the system given a specific generation and demand profile through minimising generating costs, generation re-dispatching expenses, or investment costs, in cases of long term planning problems. These problems can also be formulated such that they aim to find the best operating points to alleviate network congestion and maximising social welfare [20]. The Transmission System Operators (TSOs) have to consider uncertainties and variability in various scenarios, in order to propose an economically viable transmission investment plan that addresses all possible outcomes, including the intermittency nature of renewable energy and demand uncertainties in the future [21]. The only way the wind generators are compensated for their power is to offer at zero price through the Locational Marginal Price (i.e., the marginal cost of supplying the increment of electric energy at a certain bus, taking into account the cost of generation and the physical characteristics of the transmission system [22]) of the bus where these generators are located. Therefore, the current and future growth transmission network strategies determine the revenue and profitability of wind generating installations [23]. The current operational planning strategies for the transmission system need to be updated to account for transmission reinforcement measures [24]. These updated plans should be able to capture the various scenarios of uncertainty and variability inherent in wind power generation, thereby ensuring the overall reliability of the power system. The transmission system can be classified in general into types: High Voltage AC (HVAC) system and High Voltage DC (HVDC) system. A Multi-Terminal HVDC (MT-HVDC) system represents an advancement of the traditional HVDC system, and the details of these transmission systems will be elaborated upon in the following section. MT-HVDC systems will be key to integrating large-scale OWF generation capacity into the conventional AC systems.

2.1.1 High Voltage AC System

The HVAC transmission system is a well-established technology, which is primarily used for bulk electric power transmission using transformers for stepping up and down the transmission voltages [25]. Most existing OWFs connectivity utilises this type of transmission [26], due to the installation of OWFs close to the shore, where the transmission distance is minimal (i.e., typically around 50km) and has a low voltage (i.e., less than 175kV) resulting in lower transmission losses [27].

Despite the maturity and considered desirable choice for short distances, HVAC transmission has some limitations, particularly for longer distances (i.e., more than 700km). The capacitance of the HVAC cables, which maintain the voltage across the cable and allows charging current to flow along it, limits the amount of active power (P) that can be transferred, affecting cable length in offshore applications [28]. The charging current, I_c is defined as:

$$I_c = 2\pi f C V \tag{2.1}$$

Where f is frequency, C and V are the capacitance and voltage. It is clear from (2.1) that the frequency (f = 50Hz or 60Hz) determines the amount of I_c. If the amount of I_c lower, the available cable capacity to carry a useful load current, I_n, will also be decreased, as shown by the following equation:

$$I_n^2 = I_r^2 - I_c^2 \tag{2.2}$$

Where I_r is the ampacity rating of the cable. This equation shows that the flows of the I_c in the HVAC cable is not uniform [29].

a. Reactive Power Consumption of AC Transmission Lines

Reactive power is an essential component of some electric power system, arising from the characteristics of both capacitance and inductance (also called reactance) within the load and the transmission line, which lead to the production and absorption of this power in AC systems [30]. In fact, the performance of the AC transmission line, particularly medium-length lines (ranging from 80 km to 160 km) and long-length lines (more than 160 km) [31], is significantly affected by this power, and without it, active power could not be transmitted at all. Furthermore, the stability of these length lines and voltage magnitude are depends on the reactive power transfer, which will be further explained further.

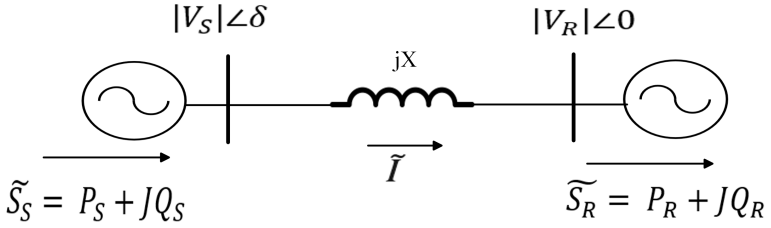

Figure 2.1: General power system diagram

Based on Figure 2.1, the complex power at the receiving end (S_r) can be expressed as:

$$\tilde{S}_R = P_R + jQ_R = \tilde{V}_R \tilde{I}^* \tag{2.3}$$

where P_R, Q_R and $\tilde{V}_R$ are the active power, reactive power and voltage at the receiving end.

$\tilde{I}^*$ is the conjugate current, which can be expressed as:

$$\tilde{I}^* = \left[\frac{\tilde{V_S} - \tilde{V_R}}{jX}\right]^* \tag{2.4}$$

where X is the reactance. Then, substituting (2.4) into (2.3), the new complex power equation is:

$$\tilde{S_R} = \tilde{V_R}\left[\frac{\tilde{V_S} - \tilde{V_R}}{jX}\right]^* \tag{2.5}$$

$$\tilde{S_R} = V_R\left[\frac{V_R\cos\delta + jV_S\sin\delta - V_R}{jX}\right]^* \tag{2.6}$$

Equation 2.6 can be divided into active power (P) and reactive power (Q) as shown below: At the receiving end:

$$P_R = \frac{V_S V_R}{X}\sin\delta \tag{2.7}$$

$$Q_R = \frac{V_S V_R\cos\delta - V_R^2}{X} \tag{2.8}$$

At the sending end:

$$P_S = \frac{V_S V_R}{X}\sin\delta \tag{2.9}$$

$$Q_S = \frac{V_S^2 - V_S V_R\cos\delta}{X} \tag{2.10}$$

Equations (2.7) to (2.10) describe how active and reactive powers are transmitted in a transmission line. Let's interpret this in more detail by considering the differences in voltage magnitudes and angles.

i Condition 1: $\delta = 0$

The receiving and sending active powers (P) becomes 0.

$$P_R = P_S = 0 \tag{2.11}$$

The reactive power (Q) at both ends will be:

$$Q_R = \frac{V_R(V_S - V_R)}{X} \tag{2.12}$$

$$Q_S = \frac{V_S(V_S - V_R)}{X} \tag{2.13}$$

If $V_S > V_R$, the reactive power at both ends (Q_R and Q_S) will become positive, indicating that reactive power is being transmitted from the sending end to the receiving end. If $V_S < V_R$, the reactive power at both ends (Q_R and Q_S) will become negative, indicating that reactive

power is flowing from the receiving end to the sending end. The phasor diagram for this statement is shown in Figure 2.2.

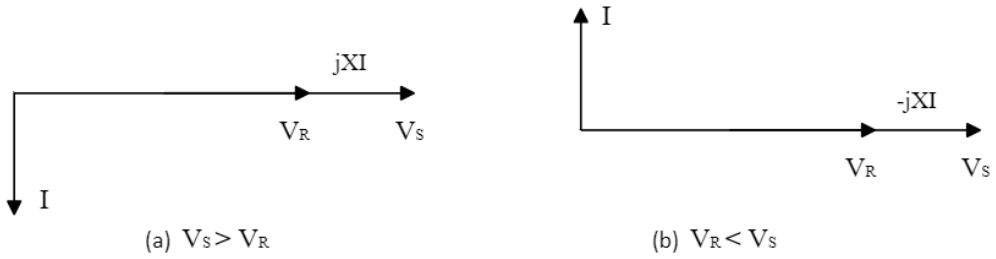

Figure 2.2: Phasor diagram with $\delta = 0$

From Figure 2.2, it can be interpreted that:

- Lagging current (I) in transmission lowers the voltage at the receiving end (V_r).
- Leading current (I) in transmission increases the voltage at the receiving end (V_r).

Therefore, the following formulation describes the amount of reactive power consumed in the transmission line:

$$Q_S - Q_R = \frac{(V_S - V_R)^2}{X} = XI^2 \tag{2.14}$$

ii Condition 2: $\delta \neq 0$, $V_S = V_R$

The receiving and sending active powers (P) now can be expressed as:

$$P_R = P_S = \frac{V^2}{X} \sin \delta \tag{2.15}$$

The reactive power (Q) at both end will be:

$$Q_S = -Q_R = \frac{V^2}{X}(1 - \cos \delta) = \frac{1}{2} XI^2 \tag{2.16}$$

If δ is positive, the active powers (P_R and P_S) at both ends will be positive, indicating that active power flow from sending to receiving ends. If the δ is negative, the active powers at both ends will be negative, indicating the active power flow in reverse direction.

Figure 2.3 shows the phasor diagram for second condition, which stated that there is no reactive power transfer from one end to other, instead each end (receiving and sending) supply half of the reactive power as shown in (2.16).

iii Condition 3: $\delta = 1$, (Unity)

If power factor (δ) is unity, means the current and voltage in an AC electrical system are perfectly in phase, the magnitude of sending voltage (V_S) is slightly larger than receiving

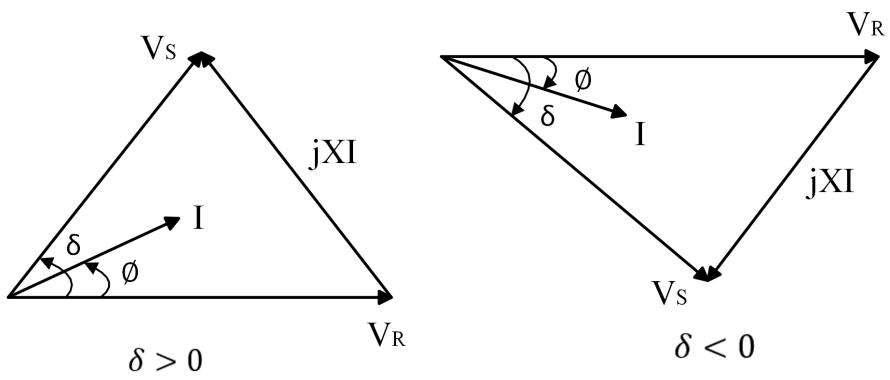

Figure 2.3: Phasor diagram with $\delta \neq 0$, $V_S = V_R$

voltage (V_R). The reactive powers are supplied by the sending end. The phasor diagram for this condition is shown in Figure 2.4.

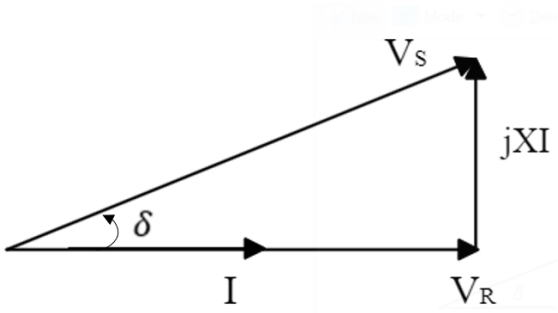

Figure 2.4: Phasor diagram with $\delta = 1$

iv Condition 4: Any values of δ, (V_S) and (V_R)

The current (I) at this condition can be calculated as below:

$$I = \frac{V_S \cos\delta + jV_S \sin\delta - V_R}{jX} \tag{2.17}$$

From (2.8) (2.10) and (2.17), the total reactive power between the sending and receiving ends is given by:

$$Q_S - Q_R = \frac{V_S^2 + V_R^2 - 2V_S V_R \cos\delta}{X} = \frac{(XI)^2}{X} = XI^2 \tag{2.18}$$

If the series resistance (R) is considered, the power losses (both active and reactive) at the transmission lines can be calculated as follows:

$$Q_{\text{loss}} = XI^2 = X\frac{P_R^2 + Q_R^2}{E_R^2} \tag{2.19}$$

$$P_{\text{loss}} = RI^2 = R\frac{P_R^2 + Q_R^2}{E_R^2} \tag{2.20}$$

It can be seen from (2.18) that the reactive power absorbed by the reactance (X) under all

conditions can be defined by XI^2. This leads to a concept of reactive power loss, similar to active power loss, defined by RI^2, which is associated with the resistive elements. Equations (2.19) and (2.20) demonstrate that an increase in reactive power within the transmission line corresponds to a rise in losses for both active and reactive power, thereby impacting the efficiency of power transmission and voltage regulation. The reactive power flow in the transmission lines can be summarised as follows, based on the aforementioned conditions [32]:

(a) Reactive power flow depends on voltage magnitude, which is transmitted from the higher voltage side to the lower voltage side.

(b) Reactive power cannot be transmitted over long distances, as this would require a large voltage gradient (i.e., the potential difference between receiving and sending ends voltages divided by the distance between them).

(c) An increase in reactive power flow results in higher loses for both active and reactive power.

The concept of line loadability, which refers to the permissible degree of line loading expressed as a percentage of Surge Impedance Load (SIL) for given thermal or voltage drop steady-state stability limits, plays an important role in the power transfer capability of the lines, affecting voltage levels as well as the length of overhead AC transmission lines [33].

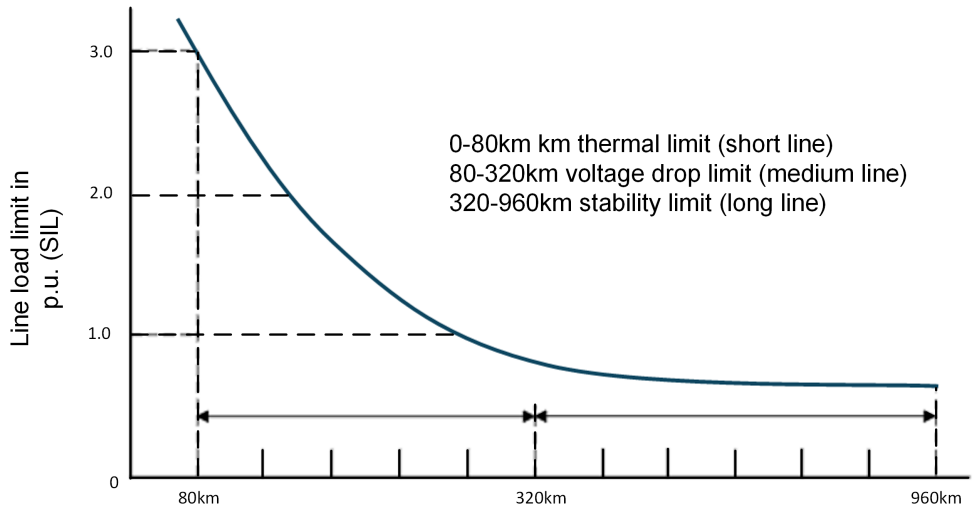

Figure 2.5: Transmission line loadability curve

Figure 2.5 illustrates the general loadability curve for uncompensated lines, which is applicable across all voltage levels, and indicates the limiting power transmission values in relation to line length. The figure clearly shows that for short-length lines, the steady state limit loading exceeds the thermal loading; therefore, loadability is primarily determined by the thermal loading rather than steady state loading. In the case of medium-length lines, voltage levels become a critical

consideration for line loadings. Conversely, for long-length lines, the steady-state stability limit loading is the predominat factor as the loading is typically less than the surge impedance loading [3].

Given that reactive power affects the voltage profile and stability of transmission lines, as previously discussed, compensation within a transmission system is essential for enhancing the quality of supply, particularly over long distances. Transmission compensation involves the management of reactive power through reactive compensation, which refers to the installation of reactive devices on AC transmission lines. The aims of this installation are to:

1. Generate a constant voltage profile across all levels of power transmission

2. Enhance the stability of the AC transmission line by increasing the maximum transmitted active power; and

3. Supply reactive power requirements in a cost-effective manner

The primary objective of compensation is to modify the SIL by adjusting the capacitive and inductive reactance of the AC transmission lines. There are two types of compensators:

1. passive compensators that include shunt reactors, capacitors and series capacitors; and

2. active compensator, which typically consist of shunt-connected devices that aim to maintain a constant voltage at their terminals

These compensators can be located anywhere along the line, including the midpoint, line terminals or at the 1/3 or 1/4 points of the terminals. However, the midpoint location offers several advantages, as the relaying requirements are less complicated when compensation is less than 50% [31]. Furthermore, at this midpoint, the compensators can supply or absorb the reactive power remaining in the central half of the line after the synchronous machines at both end sides (receiving and sending ends) have supplied and absorbed the reactive power for the leftmost and rightmost halves of the line [33].

Overall, although reactive powers do not perform any useful work in AC transmission lines or loads, its necessity is crucial for maintaining voltage levels and ensuring the efficient operation of power system equipment. Excessive reactive power can cause voltage levels to rise, leading to inefficiencies in power system equipment, higher operational cost and increased stress on the equipment that can shorten its lifespan. Conversely, insufficient reactive power can result in voltage drops, particularly under heavy load conditions, as well as voltage instability, poor power factor, and increased losses for both active and reactive powers. Therefore, effective management of reactive power is critical not only for ensuring power system stability but also for enhancing the constraints on the amount of active power that can be transmitted along AC transmission lines.

2.1.2 High Voltage DC System

The HVDC transmission system emerged as a viable solution to address the challenges encountered by the HVAC transmission system (i.e., higher transmission loss over long distances, reactive power consumption of the line, and limited active power transmission capability). Furthermore, the development of the HVDC system has been driven by: a) the escalating need for transmitting electrical power on a global scale; b) the optimal utilisation of transmission lines; and c) the operational flexibility [34]. On the other hand, the development of OWFs would evolve toward larger capacity that will lead to farther away from the shore, with OWFs located more than 80km offshore. Over these distances, long cable transmissions will be used to connect the OWFs to the onshore stations to generate a substantial amount of power [35]. With the advantages of no charging current (I_c=0) in the HVDC transmission due to the zero frequency (f=0), which lead to no reduction of cable's rating (I_r) as $I_n^2 = I_r^2$ (refer to (2)), the HVDC system is able to transmit more power over long distances. Additionally, the HVDC system offers more flexible control techniques [36] with the integrated Flexible AC Transmission Systems (FACTS) devices (e.g. Voltage Source Converters (VSC) and Current Source Converters(CSC)) [37] that enable the AC and DC systems to be adjusted to adapt to the intermittent nature of output from OWFs. Despite the numerous benefits offered by the HVDC system, the investment cost associated with this technology exceeds those of the HVAC system. The converters are the main component of the HVDC system and more than 50% of the cost of the HVDC transmission system is related to this equipment. Due to this, the cost comparison related to the converter station is the key component between HVAC and HVDC systems, as illustrated in Figure 2.6. From this Figure, it can be seen that the initial cost (i.e >$150million) for the HVDC station is significantly higher compared to the initial cost (i.e., <$50million) of the HVAC station. However, the HVDC transmission system becomes more cost-effective when the transmission distance exceeds 450 miles, as compared to the HVAC transmission system. Therefore, the HVDC system is a more cost-effective option for long -distance transmission than the HVAC system [38].

The prevalent connection configuration in existing HVDC systems is the point-to point transmission architecture, which is similar to the topology commonly found in the HVAC systems. As shown in Figure 2.7, this configuration consists of two converters connected between the onshore and offshore system, where the converters depicted in this figure are based on multi-modular converter technology [39].

2.1.3 Multi-Terminal High Voltage DC Systems

A Multi Terminal HVDC (MT-HVDC) link is an extension of a point-to-point HVDC system (i.e., two converters) that represents an interconnection of nodes and branches, which has more than two converters connected in radial or meshed topologies. This link interconnects various AC systems to the power grid through converters (i.e., hybrid AC/DC networks), enabling them to

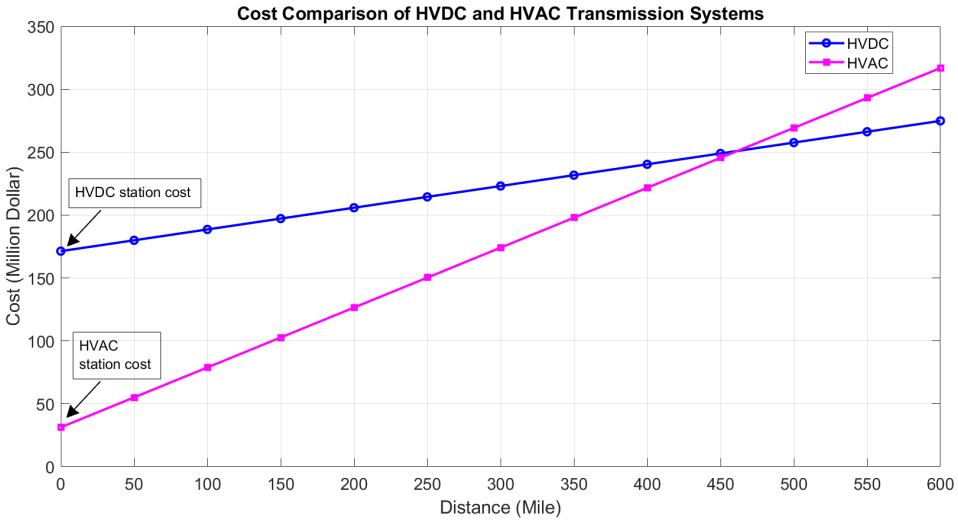

Figure 2.6: A comparison of costs between HVAC and HVDC systems.

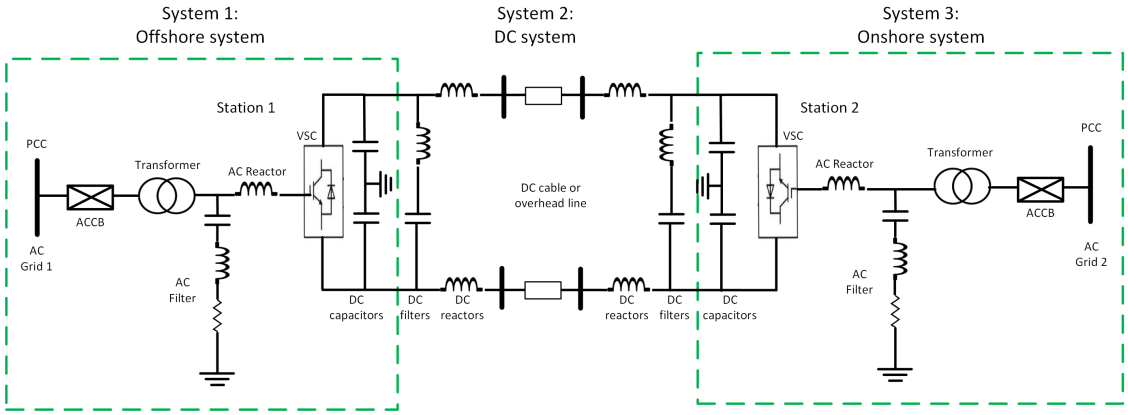

Figure 2.7: Point-to-point topology

function as either input or output power nodes, depending on whether power is being fed into or drawn from the EPS. Figure 1 illustrates an example of a simplified layout of an offshore HVDC grid in an MT-HVDC link, which consists of m AC systems that inject power into the EPS, n AC system that extract power from the EPS, p intermediate connection nodes and r branches. It can be seen from this figure that the number of p and r depend on the particular interconnection pattern [40] (i.e., layout topology). The MT-HVDC link is an appealing option, especially for integrating multiple offshore wind farms into onshore AC systems, as it facilitates the transmission of renewable energy sources [41], which are typically located in remote areas, over long distances and across international borders [42]. Furthermore, this system can resolve issues such as remote offshore generating connection, undersea or long-distance interconnection, power injection into a weak node, power grid reinforcement, isolated load connection, and asynchronous grid coupling that currently exist in AC technology [43].

The MT-HVDC can be configured in a number of topologies depending on the design specifica-

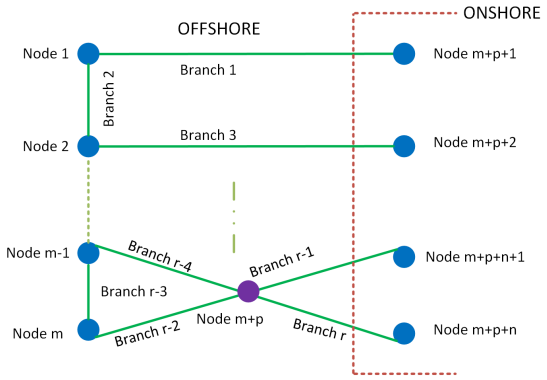

Figure 2.8: Offshore HVDC Grid Configuration in an MT-HVDC Link

tions and operating conditions. The selection of network topologies is a critical consideration, as it significantly impacts the investment requirements, operational modes, complexity of the network architecture, and power generation factors such as the choice of wind turbine type. Critical elements include the total complexity of the wind farm interconnections as well as the arrangements of the connections, which are designed to maximise power output. These layouts need to be made to provide a robust and appropriate solution in the case of an outage or equipment malfunction. Furthermore, the selected network topology has to facilitate future expansion, particularly with respect to converters or power generation assets [44]. The MT-HVDC topology can be broadly categorized into two main types of layout configurations: radial connections and meshed connections, or combinations of both [40].

The parallel MT-HVDC configuration, as shown in Figure 2.9, also known as the radial topology, represents an extension of the point-to-point topology HVDC transmission architecture. This topology is characterised by a string connection composed of several VSCs connected side by side. Figure 2.9a shows the illustration of general radial topology, which has the benefit of being simple to construct and requiring low investment. However, the drawback is that it has very low reliability compared to other topologies [45]. The star topology represents another type of parallel MT-HVDC layout configuration, where VSCs are connected to a central DC switching station (i.e., central star node), as displayed in Figure 2.9b. This configuration is formed from the point-to-point link and then tapping to other terminals for the integration of AC networks or power sources such as renewable energy. The star topology is a more economic investment as compares to the ring or mesh design due to the fewer number of cable connection [46]. The main drawback of this layout type is that if there is a fault at the central node, it can affect the entire system, potentially leading to a complete shutdown of the system.

Figure 2.10 depicts a configuration of a meshed MT-HVDC system, which represents a combination of radial and star topologies. This layout architecture has been developed to enhance the reliability and economic operation of HVDC systems. Additional advantage of this topology includes increased flexibility for power exchanges between areas, reduced shortest connection dis-

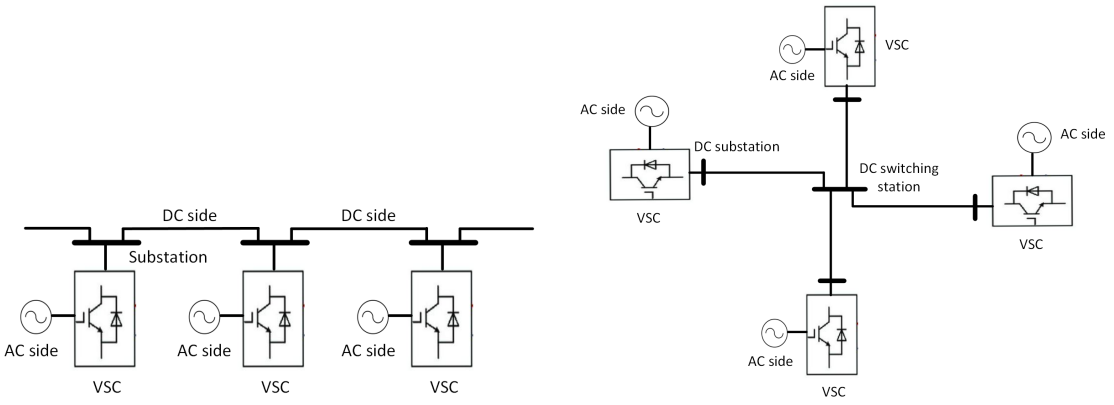

(a) Radial MT-HVDC (b) Star MT-HVDC

Figure 2.9: Parallel MT-HVDC configurations: a) Radial topology b) Star topology

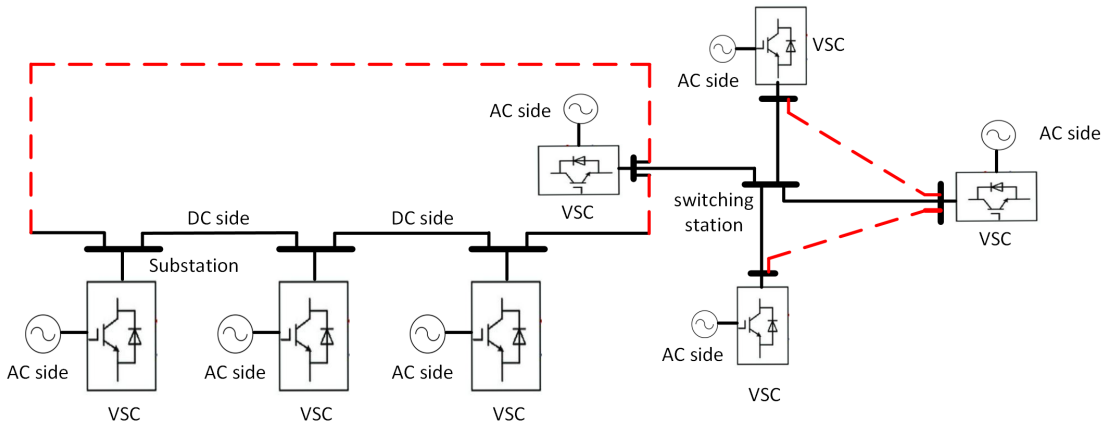

Figure 2.10: Meshed topology

tances between two points and improved security compared to radial network designs. However, the primary drawback of this configuration is the higher cost incurred by the need for longer cable lengths [45]. Furthermore, meshed topology can contribute to the formation of a Supergrid system, as illustrated in Figure 2.11, which consists of a special node (i.e., SuperNod) that interconnects multiple DC links with wind farms through an islanded AC network. This special node is a VSC-based AC hub within HVDC transmission that connects HVDC systems via AC systems to form a hybrid system, which offers effective solutions for integrating either OWFs or oil and gas platforms. More importantly, the VSC-HVDC device can be regulated to maintain stable voltages in the AC hub. This hub will constitute a comprehensive power electronics-linked network, effectively eliminating natural system inertia in offshore AC systems that lack synchronous generators. The coordination of the VSC-HVDC is crucial for ensuring stability, control and regulation of voltage and frequency within Supergird system [40]

The ring topology is a configuration where all the nodes are arranged in a circular pattern, as display in Figure 2.12. This topology provides flexibility in controlling the power flow between the

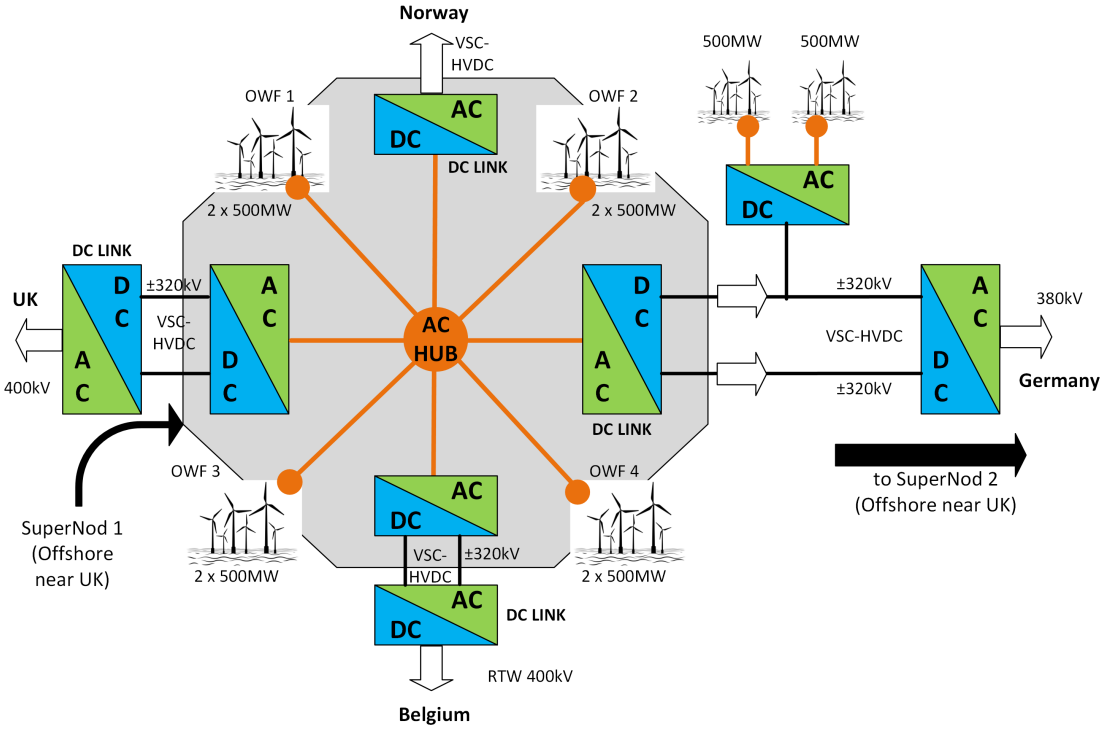

Figure 2.11: Supergrid system

wind farms and the onshore substations. Furthermore, the ring topology can be operated in two different modes: a) closed loop (i.e., all circuit breakers and isolators remain closed during normal operation, which allows power to flow through the entire path); and b) open loop (i.e., all circuit breaker or isolator are kept open during regular operation, which effectively breaking the loop if there is failure or malfunction equipment) [47]. This type of topology has generated significant interest from the research community [48], due to the benefit of being simple to construct and operate. However, it also has low reliability and significant losses due to the lengthy transmission lines [45].

2.2 Converter

2.2.1 Current Source Converter

A classical converter system, known as a Current Source Converter (CSC) or Line Commutated Converter (LCC), uses valves based on thyristor as switching devices. These devices are only able to be turned on; however, external circuits are required to turn them off and perform valve commutation. Furthermore, the CSC requires a strong AC voltage system between its two terminals to maintain stable operation and operates efficiently. Connection to a weak AC voltage may result in issues with the converter itself, such as commutation failure especially at the inverters [49], which can lead to significant power loss. In spite of this CSC is typically employed in higher-

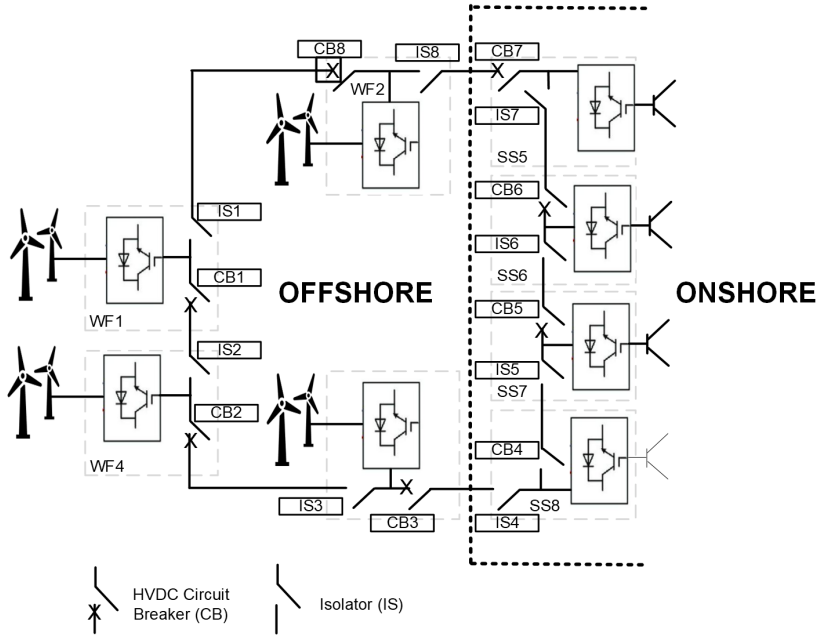

Figure 2.12: Ring topologies

power levels (i.e., normally above 1000MW), it is unable to independently control the active and reactive powers [50]. The power flow direction is determined by reversing DC voltage polarity; nevertheless, this converter only permits current to flow in one way within the DC system [51]. However, reversing the voltage polarity leads to increased complexity in the required switching arrangements [52]. Due to the necessity of commutation voltage during operation, the CSC is unable to perform black start and supply power to a passive network. This poses challenges, particularly in the case of wind farms where there is no commutation voltage available before the startup, to solve this problem, external devices such as a Static Synchronous Compensator (STATCOM) are required to supply a stable AC voltage in the CSC [53].

Figure 2.13 illustrates the steady state model of CSC components, which include reactive power compensation, AC and DC filters, transformers, thyristor valves and a smoothing reactor. The AC filters are responsible for reducing the current harmonics generated on the AC side of the converter. On the other hand, the DC filter in the CSC serves two functions; a) to reduce or avoid the DC voltage ripple (i.e., fluctuating AC component of the DC output); and b) to reduce or eliminate unwanted interference present on the DC line. Noteworthy, this filter is only necessary for overhead line and is not required in the case of underground cable or back-to-back transmission [54]. As the CSC generates significant harmonics on both the AC and DC sides, filters are required on both sides to reduce or filter out the harmonics in the power system [55]. Reactive power compensation is responsible for increasing the stability of the power system and optimising power availability. In the CSC operation, the AC current lags voltage and this process demands reactive power. This power is provided by the AC filters that exhibit capacitive behaviour at the fundamental frequency

(i.e., 50Hz or 60Hz) and can also be supplied by shunt banks or series capacitors, which are essential components for this converter. If there is an insufficient or excess reactive power supplied from these sources, the AC system will need to adjust to accommodate the reactive power differences. In order to maintain the desired voltage tolerance, tight control over reactive power exchange becomes more important especially when the CSC is further from the generator [56]. This is one of the biggest drawbacks of the CSC, as its reactive power requirement can exceed 50% of the active power rating [57].

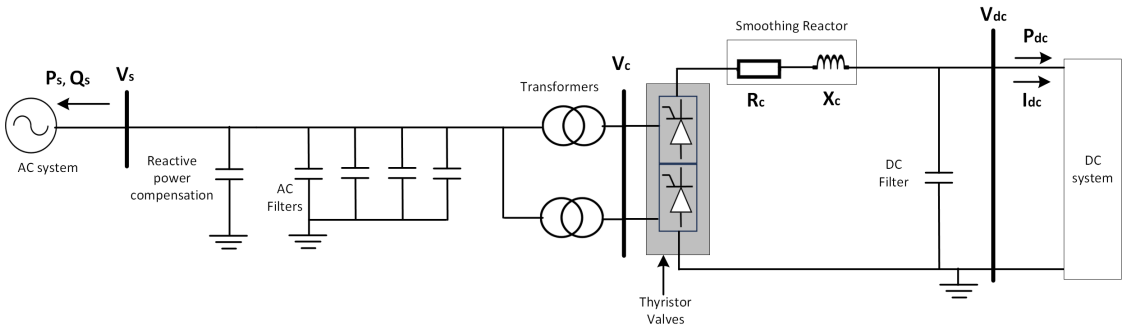

Figure 2.13: The steady state CSC model

The constraints of CSC as discussed earlier, reversing voltage polarity and high reactive power requirements, restrict the feasible connection options of this component to radial or two-terminal configurations within the MTDC link [58]. Another challenge is the size and weight of this component, which is larger and heavier compared to the VSC, making it more difficult to implement offshore. To date, the CSC system has not been implemented in Offshore Wind Farms (OWFs), gas or oil extracting platforms connection, with installations only existing on onshore power grids [59]. Despite these drawbacks, this system has been credited for its high reliability and better performance in high-power applications, due to the low voltage drop of the semiconductor used [60]. However, due to its disadvantages, this classical technology is considered unsuitable candidate for the MT-HVDC link, particularly in integration with offshore wind farms. Therefore, this study sets out to explore the VSC rather than the CSC due to its flexibility and efficiency in connection with the MT-HVDC link.

2.2.2 Voltage Source Converter

A Voltage Source Converter (VSC) is a self-commutated converter based on Gate Turn Off Thyristor (GTO) or Insulated Gate Bipolar Transistor (IGBT) valves to enable current to flow through, which can be either positive or negative [33]. This feature allows a VSC to individually control the magnitude (i.e., amplitude) and phase angle of an AC voltage, which in turn permits the independent control of both active and reactive power outputs [61]. Despite having a lower power rating, the power flow reversal capabilities of the VSC make it a superior option for connecting

to the MT-HVDC link, because of its constant voltage polarity and its ability to alter power direction through current reversal [62]. The latest offshore wind project, the Dogger Bank HVDC connections (i.e., Dogger Banks A, B, and C), has a power rating of 1200 MW and symmetrical poles with ±320 kV DC. Each project is scheduled for commissioning in 2023 (Dogger Bank A), 2024 (Dogger Bank B), and 2026 (Dogger Bank C) [63]). Furthermore, this device has the ability to control both AC and DC systems by regulating two control variables: power and voltage, as depicted in Figure 2.14.

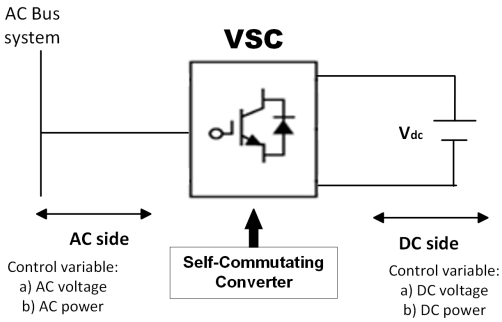

Figure 2.14: VSC converter schematic diagram.

The structure of the VSC in the steady-state model of the hybrid AC/DC system, as shown in Figure 2.15, consists of a transformer, an AC filter (i.e., low pass filter) and a phase reactor. The variables of this model are as follows [64]:

(a) P_s and Q_s represent both active and reactive powers injected by the VSC into an AC system.

(b) V_s is the voltage of an AC bus.

(c) R_c and X_c are the resistance and reactance of the phase reactor.

(d) V_c is the voltage of the converter at the AC side.

(e) V_d is the voltage of the converter at the DC side.

(f) P_{dc} is the power of VSC injected to the DC bus.

The equivalent circuit of the VSC model (i.e., steady state) is illustrated in Figure 2.16, which has a controllable voltage source (V_c) on the AC side and active power control using a current source (I_{dc}) on the DC side [65]. The parameters of this model are described below:

(a) Impedance of the transformer: $Z_t = R_t + jX_t$.

(b) The susceptance of the low-pass filter: j_{Bf}.

(c) Impedance of the phase reactor: $Z_c = R_c + _{Xc}$.

(d) The active (P_f) and reactive (Q_f) powers of the low pass filter.

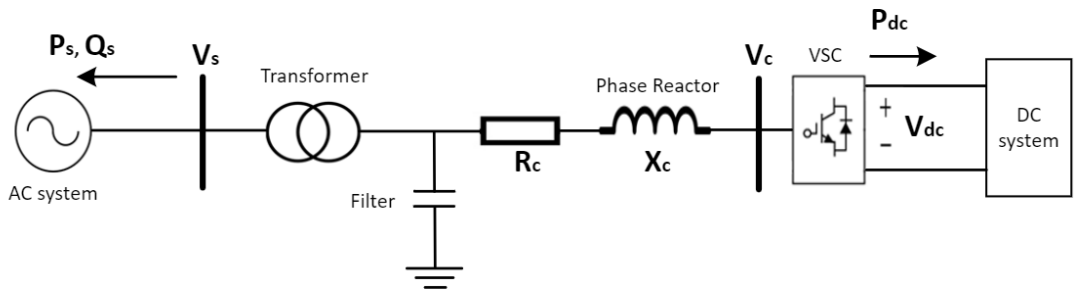

Figure 2.15: The steady state VSC model.

(e) The VSC active (P_c) and reactive (Q_f) powers on the AC side.

(f) The VSC active power on the DC side: (P_{dc}) .

(g) Power losses: P_{loss}.

In the equivalent circuit of VSC converter, the division between AC and DC systems are noticeable. In order to find a solution for this circuit, three sets of equations need to be solved: one for the AC system, one for the DC system and the last one is a coupling equation representing active power exchange between the AC and DC systems for the VSC. In the steady state analysis, this coupling is modelled using two dummy generators (refer to Figure 2.16). The power balance equation for this circuit can be mathematically expressed as follows:

$$P_{ac} + P_{dc} + P_{loss} = 0 \tag{2.21}$$

where P_{ac}, P_{dc} and P_{loss} refer to active power injection on AC system, active power injection on DC system and active power losses in the VSC.

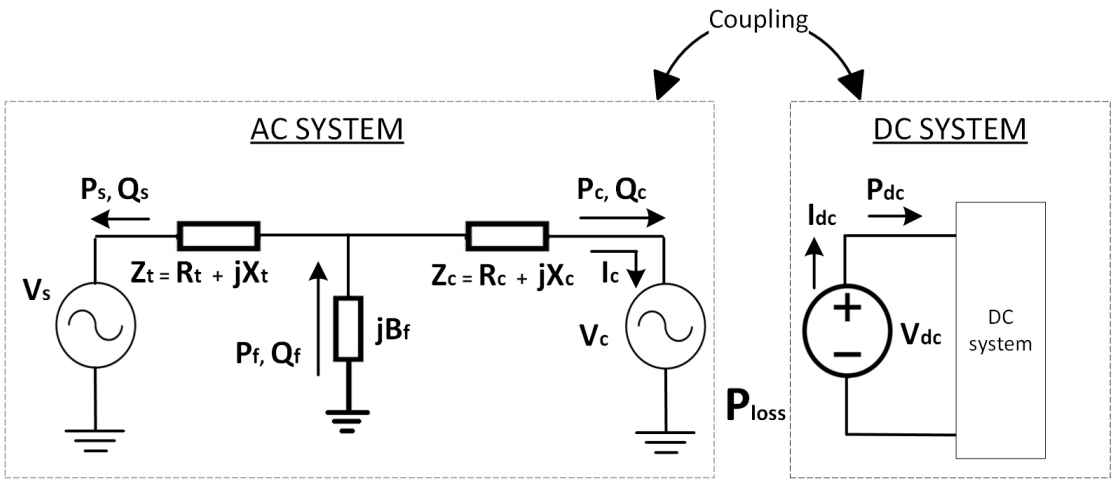

Figure 2.16: The equivalent circuit of VSC converter.

Given that the VSC is a self-commutated converter that commonly employ high-power semiconductor components such as Insulated Gate Bipolar Transistor (IGBT), developing an accurate model for power loss is essential, as these losses significantly affect the efficiency of the VSC's performance. Normally, the power losses in a VSC can be categorised into two types: conduction loss and switching loss [66]. The conduction loss typically occurs in the freewheel diodes and switches in the semiconductor (e.g., IGBT and MOSFET) during the on state, where the voltage varies non-linearly with current [67], as illustrated by the $I-V$ characteristics in Figure 2.17 [68]. The calculation of conduction power losses is different for each semiconductor. For example, the conduction losses that occur in IGBTs, both for the IGBT switches (P_{csIGBT}) and the IGBT diode (P_{cdIGBT}) can be calculated using the formula below:

$$P_{csIGBT} = U_{ceo} \cdot I_{sav} + r_c \cdot I^2_{srms} \tag{2.22}$$

$$P_{cdIGBT} = U_{do} \cdot I_{dav} + R_d \cdot I^2_{drms} \tag{2.23}$$

Where U_{ceo}, I_{sav}, r_c and I^2_{srms} represent on-state zero current collector-emitter voltage, average switch current, collector-emitter on-state resistance and RMS switch current for the IGBT, respectively. Whilts U_{do}, I_{dav}, R_d and I^2_{drms} indicate diode on-state voltage, average diode current, diode on-state resistance and RMS diode current [69], respectively.

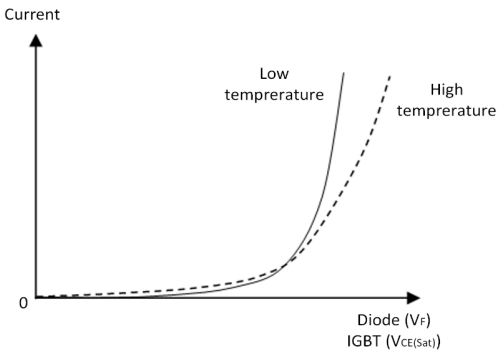

Figure 2.17: Characteristics of the $I-V$ Relationship of IGBTs

A commonly used approach for modelling power losses in the VSC is through a generalised loss formula, which expresses converter losses as quadratically dependent on the magnitude of the converter current (I_c) [70], as shown below:

$$P_{loss} = \alpha_1 I_c^2 + \alpha_2 I_c + \alpha_3 \tag{2.24}$$

where α_1, α_2, and α_3 are parameter values referring to the quadratic, linear and constant of the losses on the converter current (I_c).

2.3 Operational Planning in the Power System

Operational planning in the power system refers to the utilisation of the existing components (e.g., generators, transmission systems, distribution systems, FACTs devices, etc) in the most efficient manner [71], by developing a decision-making framework to generate, transmit and deliver the electricity [72], whilst maintaining the reliability [73] and economic feasibility [74] of the associated interconnected system. The associated decision framework can be categorised into long-term, medium-term and short-term [75], with studies influenced by the respective time horizon spanning from milliseconds to seconds (i.e., real time operation) [76] up to 30 years. Each categorised planning has different timeline and different purposes: a) long-term reaching timeline for more than three years that includes the generation and transmission expansion planning, as well as policy development [77]; b) medium term planning related to the asset management that involves maintenance scheduling and allocation components, with time horizon from a month up to three years [78]; and c) short-term planning deals with minimizing operational costs and ensuring network reliability, as well as stability [79] with time spanning from milliseconds to a day. Figure 2.18 shows the visual representation pertaining to operational planning terms at each stage. However, increased climate change escalates the penetration of variables renewable energy sources, which makes power grid operation more challenging [80]. As a result, a comprehensive approach to operational planning is required to deal with the current changes occurring in the power system.

The decisions made in every phase and stage of operational planning are considered as strategies to solve the problem facing by current power system, as a result of the transition from fossil fuel to renewable energy generation and growing demands. There are certain considerations that need to be accounted for each planning. Some of the important questions that need to be kept in mind when conducting a short-term planning are [81]:

1. What are the voltages throughout the system?
2. What are the loads of components such as transmission lines, transformers and generators?
3. What are the options to mitigate the congestion on the transmission lines?
4. What are the options to provide continued service as equipment fails unexpectedly?

The proposed long-term planning requires an assessment of the power system modification that will be implemented. The assessment queries are [81]:

1. Where is the new transmission line/generation site located?
2. Which new FACTS devices will provide the necessary control to maintain system reliability and a secure operating state?
3. Where is the new demand able to be added given the present system design?

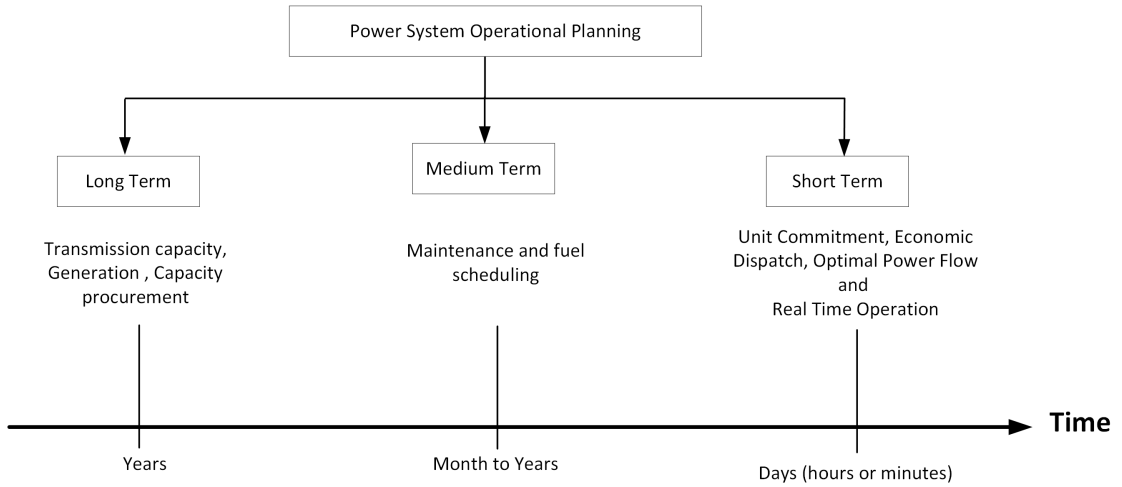

Figure 2.18: Operational Planning in the Power System

2.3.1 Security Assessment

The performance of the power system is assessed through the reliability (i.e., probability of the power system operating satisfactorily in the prolonged duration and the capacity to provide adequately uninterrupted energy supply for a lengthy period of time [82]), which relies on the security and adequacy of the power system [83]. The adequacy is defined [84] as the ability of power system to supply aggregate power requirements to meet the demand and energy needs of all times, considering all scenarios (i.e., scheduled and unscheduled outages of the power system elements), whilst security refers to the ability of the power system to withstand the sudden disturbances such as an outage of components or natural disaster. In order to assess this security, a comprehensive Security Assessment (SA) needs to be performed that involves a thorough evaluation, including assessment system performance related to the security criteria or operational limits. The objective of the SA is to evaluate whether the power grid is operating under secure or insecure conditions [85]. Traditional SA is based on deterministic criteria. These criteria (N-1 or N-k) refer to whether or not the system can withstand contingencies, when one or more elements are out of service [86]. The static security analysis method typically involves the execution of a significant number of computer simulations, in order to determine a set of network topologies, a range of system operating conditions, a list of contingency scenarios and the associated performance evaluation criteria [87]. However, the deterministic method is inappropriate for modern power systems, particularly when dealing with uncertainties in renewable energy. The method does not consider a lot of factors including uncertain nature of customer demands, stochastic nature of system behavior and probabilities of contingencies and components failure [88]. Therefore, the probabilistic method has been introduced in SA methodology. This technique combines both effects and probabilities that are much more attractive for representing system risk [89].

Figure 2.19 displays the structure of the SA framework for both the deterministic and prob-

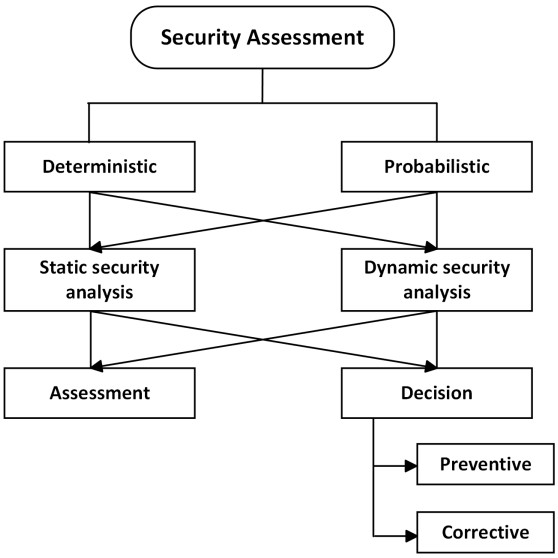

Figure 2.19: Security Assessment

abilistic criteria. Each of these criteria can be further categorised under either static security or dynamic security, with the ability to be utilised interchangeably between the respective methodologies. These criteria, both deterministic and probabilistic, will then be evaluated through an assessment and decision-making process. However, the decision-making component, which consists of preventative and corrective actions, will only be conducted through the dynamic SA methodology, as this strategy mimics the operation of the power system in the real world. The preventive actions are implemented during the pre-contingencies period, with the objective of protecting the network system from breaching operational limit violations, which may occur during contingency events. On the other hand, the corrective actions are utilised to ensure that any violations of the predetermined limits are resolved within specified time frames in the event of a contingency scenario [90]. Further details on these actions are provided in Section 2.5.

Static security analysis, a technique commonly employed in both planning and dispatching operation [91], refers to the ability of the power grid to restore to a steady state within a predetermined secure region (defined by bounding limits) following a contingency event [92]. The primary concerns in this analysis are the violations of thermal limits on transmission lines and bus voltage limits, as such violations can potentially trigger a cascading outage scenario leading to a large-scale blackout. Normally, the evaluation of static security is conducted through analytical network modelling and iterative solving of algebraic load flow equations, with each prescribed outage scenario assessed individually [93]. Furthermore, this security approach neglects the transient behaviour and other time-dependent variations that arise due to changes in load generation conditions, instead solely focusing on the post contingency steady-state evaluation. Due to the significant computational burden associated with the assessment in static security analysis, most TSOs utilise SA predictors such as sensitivity matrix, distribution factors or performance indicators to reduce the number of

critical contingencies that need to be specifically calculated in real-time [94].

Dynamic security analysis refers to the evaluation of the dynamic behaviour of the power system [95], by analysing the time-dependent transition from the pre-contingent to post-contingent steady state [96]. A conventional off-line study method called transient stability program is applied in dynamic security analysis, to simulate the dynamic behaviour of the machines along with their electrical network connection [97]. The main purpose of dynamic security analysis is to identify and evaluate the impact of contingencies arising from outages or severe system faults under various system operating states [98], by assessing the security criteria such as dynamic under/over frequency, dynamic under/over voltages, overload transmission lines, stability limits and low frequency oscillations [99]. Furthermore, online dynamic security analysis plays an important role in modern power systems to predict the future operating conditions, particularly those related to the uncertainty and variability from the generation side (i.e., renewable energy sources). However, the effectiveness of this analysis is reliant upon the quality of the underlying system model, particularly if the assessment performed relies on fully defined system models computations [100]. Additional challenges arise from the constraint on the time available for computation and interpretation as well as the qualification of the results. These drawbacks present significant challenges for dynamic security analysis, especially with regards to online analysis, where the required time performance is typically set to 10 minutes, with each simulation run lasting 10 seconds, in order to process 30 contingencies for a 2,000 bus, 250 generators [101].Figure 2.20 provide a summary of the assessment analyses conducted for both static and dynamic security considerations.

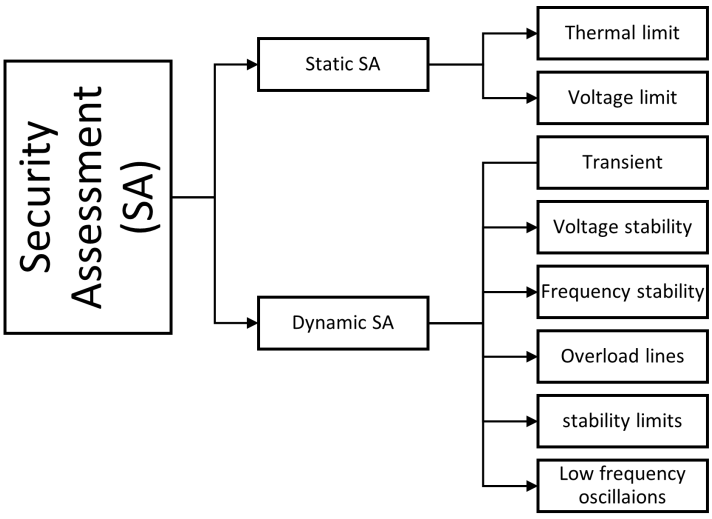

Figure 2.20: Static and Dynamic Security Assessments.

2.4 Power Flow

The Power Flow (PF) problem consists of solving complex voltages (i.e., angle and magnitude) at each bus in the network, which deliver the active and reactive powers (i.e., power flows) to each transmission line and transformer [102] in a steady state analysis [103]. It is represented by a set of equations for active and reactive power flows. Considering the system is typically balanced, a single-phase representation of the power network is used for power flow studies [104]. The power flow is a fundamental tool for power system planning and operation, which is represented through a set of equations and nonlinear algebraic inequalities that correspond to the Kirchhoff law and the system's operational constraints, respectively, in network modelling [105]. The fundamental principles and basic power flow concepts will be thoroughly discussed in the next part.

2.4.1 Fundamental principles

1. **Phasor and complex number**

   The Voltage (V) and current (I) at the node power system is assumed to be purely sinusoidal and constant frequency. A complex number, denoted by the quantities of 'V' and 'I', is a phasor representation of sinusoidal voltages and currents. The phasor is a fundamental concept that has been extensively used for efficient calculations in AC circuit analysis. It represents the sine waveform in time domain by specifying the magnitude (i.e., Root -Means- Square (RMS) values) and phase angle (i.e., in relation to a reference). This phasor representation allows for the simplification of the mathematical analysis (i.e., techniques and principles) of AC circuits, as the time-varying sinusoidal signals can be reduced to constant-magnitude and constant-phase angle quantities. The sinusoidal or sine wave function is defined by three variables: amplitude, angular frequency and phase angle, and Figure 2.21 illustrates the relationship between these three variables.

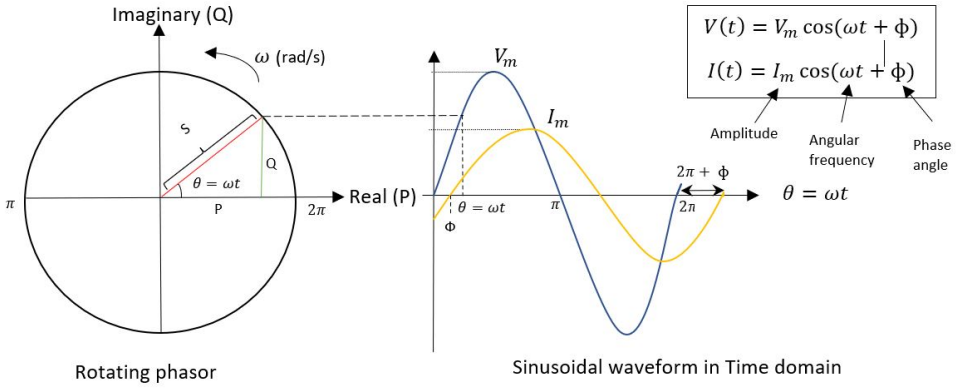

Figure 2.21: Phasor representation

Regarding the voltage and current, the magnitude of phasors is designated by $|V|$ and $|I|$

and their angles is denoted by θ_V and θ_I [106]. The phasor concept can be developed using Euler's identity, which relates the exponential function to trigonometric functions:

$$e^{\pm j\theta} = \cos\theta \pm j\sin\theta \tag{2.25}$$

The cosine (con) and sine (sin) function provide alternative to (2.25), which also can be represented as the real part and imaginary part of the exponential functions, respectively. These exponential functions can be expressed as [107]:

$$\cos\theta = \Re\{e^{j\theta}\} \tag{2.26}$$

$$\sin\theta = \Im\{e^{j\theta}\} \tag{2.27}$$

Where $\Re$ refers to the real part and $\Im$ refers to the imaginary part. Figure 2.22 illustrates the exponential function in a complex number, which will be explained further in a simple manner. Let say Z is a complex number that can be written in the form of rectangular coordinates as:

$$Z = a + \mathbf{j}b \tag{2.28}$$

where a is a real part and b is the imaginary part. The complex conjugate of a complex number Z is denoted by Z^*, then this complex conjugate can be written in the form of:

$$Z = a - \mathbf{j}b \tag{2.29}$$

'Z' in a Euler's identity (i.e., polar coordinates) is denoted as:

$$Z = |Z|e^{i\theta} \tag{2.30}$$

$$Z = |Z|\cos\theta + i|Z|\sin\theta \tag{2.31}$$

From (2.28) and (2.31), the a (i.e., real part) and b (i.e., imaginary part) can be expressed as:

$$a = |Z|\cos\theta \tag{2.32}$$

$$b = |Z|\sin\theta \tag{2.33}$$

The complex number is important as it provides a powerful and flexible tool for representing the flow of energy and power in electrical power systems [108], which have sinusoidal quantities that can be divide into real and imaginary parts to represent the magnitude and phase angle, respectively. In network modelling, most of power system parameters and components used complex number modelling such as voltages, currents, impedances, generators

or transmission lines.

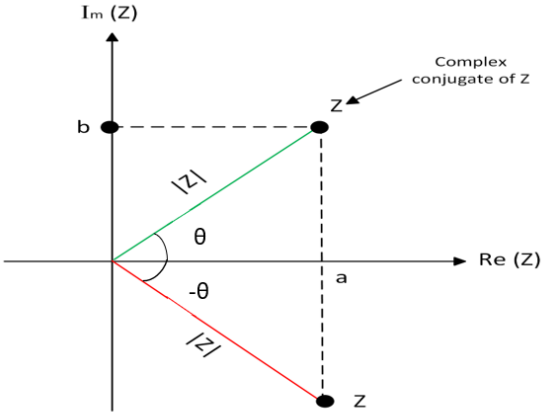

Figure 2.22: Complex number

2. **Per Unit System**

Transmission line power transfer often involves high voltage levels (i.e., kilovolt amperes or megavolt amperes) and large power amounts (i.e., kilowatts or megawatts), which complicate calculations. The per unit (p.u) method was developed by properly defining base quantities, in order to simplify equivalent circuits and convert them into the same unit values. These values are expressed as a percentage or per unit of a specified base value. Furthermore, the advantages of p.u could avoid making serious calculation errors when referring quantities from one side of a transformer to the other. The p.u value of any quantity is the ratio of the actual value of that quantity to the base value for that quantity [109] [110] , which can be mathematically express as:

$$\text{Quantity in per unit} = \frac{\text{actual quantity}}{\text{Base value of quantity}} \tag{2.34}$$

In the p.u system, there are four p.u values that are important in the power system: Power (S), Voltage (V), Current (I) and Impedance (Z), and the expression for each value is shown below:

$$S_{\text{p.u}} = \frac{S}{S_B} \tag{2.35}$$

$$V_{\text{p.u}} = \frac{V}{V_B} \tag{2.36}$$

$$I_{\text{p.u}} = \frac{I}{I_B} \tag{2.37}$$

$$Z_{\text{p.u}} = \frac{Z}{Z_B} \tag{2.38}$$

In the three-phase system, S and V will always be the base value and I and Z will be

dependent on these two values. These are displayed as follows:

$$\text{Current:} \quad I_B = \frac{S}{\sqrt{3}V_B} \tag{2.39}$$

$$\text{Impedance:} \quad Z_B = \frac{(V_B)^2}{S_B} = \frac{(kV_B)^2}{MV_AB} \tag{2.40}$$

The impedances of the machines and transformer are normally specified by the manufacturer and are expressed as a percentage or in the nameplate rating, whilst the impedance of the transmission lines is generally given in ohmic values. During power system analysis, all impedance values have to be in p.u. on a common system basis, which requires the specification of a random apparent power base that is typically set to 100MVA. Subsequently, the voltage base is selected, and this reference value is then designated as a point of reference. The remaining voltage bases can no longer be regarded as independent after the reference value is established as the point of reference. For this particular case, the p.u. impedance is expressed as follows:

$$Z_{\text{p.u}}^{\text{old}} = \frac{Z_\Omega(\text{actual})}{Z_B^{\text{old}}} = Z_\Omega \left(\frac{S_B^{\text{old}}}{V_B^{\text{old}}}\right)^2 \tag{2.41}$$

In the case of $Z_{p.u}$ being based on a new power, the new p.u value is calculated as follows:

$$Z_{\text{p.u}}^{\text{new}} = \frac{Z_\Omega(\text{actual})}{Z_B^{\text{new}}} = Z_\Omega \left(\frac{S_B^{\text{new}}}{V_B^{\text{new}}}\right)^2 \tag{2.42}$$

Then, the old and new p.u values have the following relationship:

$$Z_{\text{p.u}}^{\text{new}} = Z_{\text{p.u}}^{\text{old}} \left(\frac{S_B^{\text{new}}}{S_B^{\text{old}}}\right) \left(\frac{V_B^{\text{old}}}{V_B^{\text{new}}}\right)^2 = \frac{MV_{\text{AB}}^{\text{new}}}{MV_{\text{AB}}^{\text{old}}} \left(\frac{kV_B^{\text{old}}}{kV_B^{\text{new}}}\right)^2 \tag{2.43}$$

If the voltage reference values are the same, (2.43) become:

$$Z_{\text{p.u}}^{\text{new}} = Z_{\text{p.u}}^{\text{old}} \left(\frac{S_B^{\text{new}}}{S_B^{\text{gold}}}\right) \tag{2.44}$$

2.4.2 Power Flow Problem Formulation

The most important law in the power system is an ohm' law, which stated the relationship between three parameters: current, voltage and resistance [111]. Given the current, voltage and resistance, the ohm' law can be defined as:

$$V = IZ \tag{2.45}$$

$$I = \frac{V}{Z} \tag{2.46}$$

i **Power flow equation between two buses**

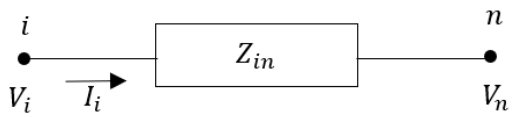

Figure 2.23: Nodes between two buses

Based on Figure 2.23 and (2.46), the current at bus 'i' can be calculated as follows:

$$I_i = \frac{V_i - V_n}{Z_{\text{in}}} \tag{2.47}$$

The bus admittance between two buses is:

$$\tilde{Y}_{\text{in}} = \frac{1}{Z_{\text{in}}} \tag{2.48}$$

Substituting (2.48) into (2.47), the $I_i$can be expressed as:

$$\tilde{I}_i = \tilde{Y}_{\text{in}}(\tilde{V}_i - \tilde{V}_n) \tag{2.49}$$

Complex power at node i:

$$S_i = \tilde{V}_i \tilde{I}_i \tag{2.50}$$

Then, substitute (2.49) into (2.50), and the complex power at node 'i' can be expressed as:

$$S_i = \tilde{V}_i(\tilde{Y}_{\text{in}}(\tilde{V}_i - \tilde{V}_i)) \tag{2.51}$$

$$= \tilde{V}_i(\tilde{V}_i\tilde{Y}_{\text{in}} - \tilde{V}_n\tilde{Y}_{\text{in}}) \tag{2.52}$$

$$= |\tilde{V}_i|^2\tilde{Y}_{\text{in}} - \tilde{V}_i\tilde{V}_n\tilde{Y}_{\text{in}} \tag{2.53}$$

ii **Power flow equation at node i:**

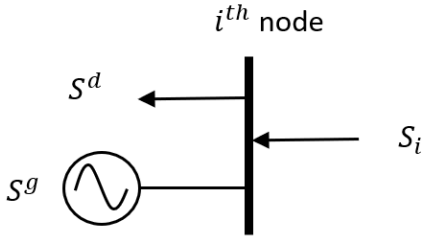

Figure 2.24: Powers at node i

The complex power injected into the system at node i:

$$S_i = P_i + jQ_i = \tilde{V}_i \tilde{I}_i \tag{2.54}$$

The total current injected at node i:

$$I_i = Y_{i1}V_1 + Y_{i2}V_2 + \cdots + Y_{in}V_n \tag{2.55}$$

$$I_i = \sum_{k=1}^{n} Y_{ik}V_k \tag{2.56}$$

Where n is the number of buses. Substituting (2.56) into (2.54), the complex power can then be expressed as:

$$S_i = V_i \sum_{k=1}^{n} Y_{ik}V_k \tag{2.57}$$

$$= \sum_{k=1}^{n} |V_i V_k Y_{ik}| e^{j(\delta_i - \delta_k - \theta_{ik})} \tag{2.58}$$

$$= \sum_{k=1}^{n} |V_i V_k Y_{ik}| \cos(\delta_i - \delta_k - \theta_{ik}) + j \sum_{k=1}^{n} |V_i V_k Y_{ik}| \sin(\delta_i - \delta_k - \theta_{ik}) \tag{2.59}$$

By separating the complex power into active power (P_i) and reactive power (Q_i), the expression becomes:

$$P_i = \sum_{k=1}^{n} |V_i V_k Y_{ik}| \cos(\delta_i - \delta_k - \theta_{ik}) \tag{2.60}$$

$$Q_i = \sum_{k=1}^{n} |V_i V_k Y_{ik}| \sin(\delta_i - \delta_k - \theta_{ik}) \tag{2.61}$$

iii **The nodal power balance equation at node i:**

For the complex nodal power balance (g_S) at bus i (refer to Figure 2.24), it can be represented as:

$$g_s(x) = S_i^g - S_i^d + S_i = 0 \tag{2.62}$$

This complex nodal power balance can be divided into active (g_P) and reactive (g_Q) powers:

$$g_P(x) = P_i^g - P_i^d + P_i = 0 \tag{2.63}$$

$$g_Q(x) = Q_i^g - Q_i^d + Q_i = 0 \tag{2.64}$$

The aim of power analysis in the nodal power balance equation is to find a feasible operating point of state variable x, which is a set of voltages (i.e., magnitude and angle) in the matrix

form of:

$$x = (\theta, V) = [\theta_1, \theta_2, \theta_3, \ldots, \theta_n, V_1, V_2, V_3, \ldots, V_n]^\top$$

There are three types of nodes in the power systems, and each node has two assumed known variables and the other two variables are state variables that need to be calculated [112]. These nodes and variables are explained below:

(a) **Slack node:** There should be one node assigned for a slack node (i.e., reference node) in the power system, which specified the constant voltage (i.e., magnitude and phase angle). Therefore, in this node, the Voltage Magnitude (VM) and voltage angle (θ) are the known variables, whilst active power '(P)' and reactive power '(Q)' are the unknown variables that need to be solved.

(b) **PQ nodes:** These nodes also known as load nodes, where the 'P' and 'Q' are the known variables due to the fixed values, whilst the unknown variables are 'VM' and 'θ' that need to be calculated. These sorts of nodes represent the majority of the nodes in the power system.

(c) **PV nodes:** These nodes are referred to generator nodes, where the 'P' and 'VM' are known variables, whilst the unknown variables that need to be calculated are 'Q' and 'θ'. These nodes are also known as voltage-controlled nodes, because they have ability to regulate voltage using the reactive power capacity of their generators.

2.5 Optimisation in the power system

There are a wide range of optimisation problem in the power system that related to the planning, design, operation, and maintenance of the electrical infrastructure (e.g., generator, transformer, transmission lines, FACTS devices) [113]. In order to solve this problem, a set of mathematical formulations (i.e., known as mathematical model) is utilised to identify the best optimisation model [114]. According to [115] the optimisation model consists of three steps, which are :

1. **The selection set of variables:** These variables specify different states of a power system, such as voltage magnitude, voltage angle, active power and reactive power.

2. **The selection of objective function:** The objective is the function (criterion) that needs to be optimised, either by minimising or maximising its value.

3. **The determination of constraints:** The solution must meet all the constraints imposed on the model, which are equalities, inequalities, etc.

The objective function (i.e., a quantitative measure of the performance of the system under study) is represented by a scalar (i.e., a single number) that could be either profit, time, potential

energy or any other quantities or combination of those quantities [116]. Generally, the power system optimisation problems can be mathematically formulated as follows:

$$\min_{x} f(x) \tag{2.65}$$

subject to:

$$g(x) = 0 \tag{2.66}$$

$$h(x) \leq 0 \tag{2.67}$$

where $f(x)$ is the objective function, x is the variables, $g(x)$ and $h(x)$ represent the equality constraints and inequality constraints respectively. The point x satisfies all the constraints that called the feasible solution [117]. There are several traditional optimisation models for power system analysis, including unit commitment, economic dispatch, optimal power flow, security constrained optimal power flow, etc. Whilst the physics of the power has not been changed, the inputs have changed drastically over the years such as renewable energies, storage, HVDC links and demand responds [118]. A detailed discussion of several of these optimisation problems will be provided in the upcoming section.

2.5.1 Economic Dispatch

The Economic Dispatch (ED) problem is an important tool in the operation and planning of the power system [119]. It is a process that determines how much power each individual generating unit, within a varied generation mix should produce in order to most effectively meet the overall demand for electricity at the cost-effective way, whilst accounting for network losses without considering security constraints [120] (i.e., transmission line limits). The objective function (f) is to minimise the total generation cost by satisfying a set of equality constraint (g) (i.e., balancing supply and demand without accounting for network losses, and at the same time ensuring the power system and generating units operate at their respective bounds) [121]. This statement can be mathematically formulated as:

$$\min_{x,u} f(x,u) \tag{2.68}$$

subject to:

$$g(x,u) = 0 \tag{2.69}$$

Where x refers to the state variables that is a set of voltage (i.e., magnitude (VM) and angle (θ)), whilst u refers to the control variables such as active power and reactive power controls. The power balance equation in (2.69) at node k can be divided into active power ($g_{(P,k)}$) and reactive

power ($g_{(Q,k)}$), as per below:

$$g_{P,k}(x) = P_k^g - P_k^d = 0, \quad \forall k \in N \tag{2.70}$$

$$g_{Q,k}(x) = Q_k^g - Q_k^d = 0, \quad \forall k \in N \tag{2.71}$$

where P_k^g is the active power generation and P_k^d is the active power demand at node k. The Q_k^g and Q_k^d represent the reactive power generation and reactive power demand at node k, respectively. N refers to the set of all nodes. Traditionally, the objective function is the summation of individual cost functions (f_g) of active power injections (P_g) for each unit of generator (g).

$$\min \quad F = \sum_{g=1}^{n_g} f_g(P_g) \tag{2.72}$$

where F is a quadratic function that represents the total individual cost functions and n_g is the number of generators in the power system. The individual generator cost functions at unit k, ($f_{(g,k)}$), can be defined as:

$$f_{(g,k)} = a_k + b_k P_{(g,k)} + c_k P_{(g,k)}^2 \tag{2.73}$$

Where a_k, b_k and c_k are the cost coefficients of that measured in units \$, $\$/MW$ and $(\$/MW)^2$ respectively.

2.5.2 Optimal Power Flow

Optimal Power Flow (OPF) is another important optimisation problem, which is normally used to find the immediate optimal operation of power system whilst complying with system constraints, feasible operation and security [122]. In other words, the aim is to identify an economic resource dispatch schedule ahead of real-time operation based on the network's realistic operational constraints (i.e., nodal voltage magnitudes and active power limits in transmission lines.) [123] [124]. Typical problems solved using OPF include improving energy efficiency through new technology and policies [125], optimising electrical systems in the presence of offshore wind farms [126], and searching for the optimal point of maximum loadability at a load bus [127], etc. Based on these types of problems, the optimisation of the objective function can vary such as total generation cost, transmission line losses, FACTS cost, voltage stability, voltage deviation, etc [128]. Furthermore, the OPF problem that is normally solved in this context is useful for identifying any control actions, by generators, transformers, and any other available control devices in the system under both normal and abnormal operating conditions [129]. The TSOs therefore solves instances of OPF problems to account for any changes in the system's steady-state operating points (i.e., generators' resource dispatch, transformers' tap changer positions, and other controller actions) to plan the system operation in a reliable and economic manner ahead of real-time operation. Generally, OPF is formulated as a nonlinear, nonconvex optimisation problem, which is expressed in the following

form:

$$\min_{x,u} f(x,u) \tag{2.74}$$

subject to:

$$g_k(x,u) = 0, \quad \forall k \in N \tag{2.75}$$

$$h_l(x,u) \leq 0 \quad \forall l \in L \tag{2.76}$$

In (2.74), f represents the objective function, x and u are the state variables and control variables, respectively. The equality constraint (g) in (2.75) refers to the nodal network power balance (i.e.,balanced supply and demand) during steady state operation. N is the set of all nodes with k being indexed over this set, and L is the set of all transmission lines with l being indexed over this set. The equality constraint can be expressed in terms of active power ($g_{(P,k)}$) and reactive power ($g_{(Q,k)}$) as follows:

$$g_{P,k}(x) = P_k^g - P_k^d + P_k^{bus} = 0, \quad \forall k \in N \tag{2.77}$$

$$g_{Q,k}(x) = Q_k^g - Q_k^d + Q_k^{bus} = 0, \quad \forall k \in N \tag{2.78}$$

where N refers to the set of all nodes with k being indexed over this set. At this node, the active power generation is denoted by P_k^g, the active power demand by P_k^d, and the active power injections at node k are denoted by P_k^{bus}. The Q_k^g is the reactive power generation, Q_k^d is the reactive power demand, and Q_k^{bus} is the reactive power injections, respectively, at node k. Equation (2.76) represents the inequality constraints (h) pertaining to the limits on the transmission lines and physical constraints on the components (e.g., generators' power limits, transformers' tap ratios and VSC power rating). The constraint related to the transmission line limit at line'l is defined as follows:

$$h_l^R(x) = R_l - L^R(max) \leq 0, \quad \forall l \in L \tag{2.79}$$

where L is the set of all transmission lines with l bein indexed over this set. The variable R_l can be either an apparent power (S) in unit MVA, an active power (P) in unit MW or a current (I) in Ampere. The $L_l^R(max)$ refers to the upper limit of the variable R_l. The expression for the general physical constraint related to the components at node k, can be expressed as follows:

$$x_k^{min} \leq x_k \leq x_k^{max}, \quad \forall k \in N \tag{2.80}$$

where x_k^{min} and x_k^{max} refer to the lower and upper limits of variables below:

(a) Active power generation constraints:

$$P_g^{min} \leq P_g \leq P_g^{max}, \quad \forall g \in G \tag{2.81}$$

(b) Reactive power generation constrains:

$$Q_g^{min} \leq Q_g \leq Q_g^{max}, \quad \forall g \in G \tag{2.82}$$

(c) Voltage magnitude constraints at node k:

$$V_k^{min} \leq V_k \leq V_k^{max}, \quad \forall k \in N \tag{2.83}$$

where G is the set of all generators with g being indexed over this set, whilst N is the set of all nodes with k being indexed over this set. Presently, the standard PF and the OPF formulations are only suited for AC systems [90].Furthermore, most software implementation of PF/OPF solvers lack the model libraries [130] and realistic network element representations required for implementing and solving a system with embedded VSC-HVDC links and their associated controls (voltage and power control), to provide a quick and an accurate solution for hybrid AC/DC networks. Besides that, existing OPF formulations mostly employ a sequential methodology to independently solve the AC and DC elements of the hybrid networks. As a result, the governing equations for the AC and DC system models are different. Yet, developing accurate models that are capable of representing the control actions of Flexible AC transmission systems (FACTS), particularly converters in the context of operating in a meshed MT-HVDC network is still an area of active research [131] [132].

2.5.3 Security Constrained Optimal Power Flow

The Security Constraint OPF is an extension of an OPF problem that mathematically models for contingency scenarios. This model was developed to eliminate the constraint violations [133] and ensure that even if the contingency occurs, the post-contingency state is always feasible [134], which can increase the security level of the network system operation. The security in this context refers to the ability of power system to tolerate sudden disturbances (e.g., unexpected loss of system elements or faults, often called $N-1$ condition [135]) and transition to an acceptable operating state [136]. The SCOPF objective function (f) is to minimise the overall cost of electricity generation, by: a) satisfying a set of equality constraints (g) (i.e., balancing supply and demand); b) inequality constraints (h) related to the operational security limits (e.g., power flows in the transmission lines); c) physical equipment limits (x) (e.g., generators powers, transformers ratios, etc.); and d) coupling constraints (Δu_c). The mathematical presentation of this statement can be presented as below:

$$\min_{x_0, u_0 \ldots\ldots x_c, u_c} f(x_0, u_0) \tag{2.84}$$

subject to:

$$g_{k,c}(x_c, u_c) = S^g_{(k,c)} - S^d_{(k,c)} + S^{bus}_{(k,c)} = 0, \quad \forall k \in N, \quad \forall c \in C \tag{2.85}$$

$$h_{l,c}(x_c, u_c) \leq S_{l,c}^{max}, \quad \forall l \in L, \quad \forall c \in C \tag{2.86}$$

$$|u_c - u_0| \leq \Delta u_c, \quad \forall c \in C \tag{2.87}$$

Where N, C and L are the set of all nodes, the set of all contingencies and the set of all transmission lines, respectively, with k, c and l being indexed over these sets. The state and control variables represented by x_o (basecase scenarios), x_c (contingency scenarios), u_o (basecase scenarios), and u_c (contingency scenarios) consist of the following: a) N_b x1 vectors of voltage angles (θ) and magnitudes (VM); and b) N_g x1 vectors of generator active (P^g) and reactive (Q^g) power injections, which can be specified in the following form:

$$(x, u) = (\theta, \text{VM}, P^g, Q^g)^\top$$

The $g_{(k,c)}$ is the equality constraint pertaining to the network's nodal power balance during steady-state operation. These constraints must be equal to the difference between the complex power injections ($S^g_{(k,c)}$) and the sum of complex power demands ($S^d_{(k,c)}$) and net complex power injections ($S^{bus}_{(k,c)}$) at node k for each contingency case (c). These complex powers (S) can be represented by a set of nonlinear active (P) and reactive (Q) power balance equations as per follows:

$$S_P = P^g - P^d + P^{bus} = 0 \tag{2.88}$$

$$S_Q = Q^g - Q^d + Q^{bus} = 0 \tag{2.89}$$

The coupling constraints in (2.87) represents the maximum allowed variations in control between pre- and post-contingency [90]. Generally, the control actions have been formulated into two type of modes: preventive and corrective, which will be further explained in the next section. The SCOPF emphasise three criteria that are removal cost congestion, maximum power transfer computation, and minimisation of generation cost [137]. The solution of the SCOPF problem allows for the evaluation of the optimal trade-off between the objective function and the number of control actions employed in the optimisation process, maximum number of controls and the amount of flexibility available in the event that any control actions fail [138].

2.5.4 Security Constrained Optimal Power Flow: Preventive Action

The problem formulation of Preventive SCOPF (P-SCOPF) is the same as the standard SCOPF. In (2.87), Δu_c is defined as a vector of maximum allowed adjustments after contingency c has occured. Within the P-SCOPF framework, the control variables (u_0) are constrained such that they are not permitted to undergo any changes once the contingency has occurred, consequently, the Δu_c is set to zero. It can be mathematically express as:

$$\Delta u_c = 0 \rightarrow u_c = u_0, \quad \forall c \in C \tag{2.90}$$

Where C is the set of all contingencies with c being indexed over this set. The actions in the P-SCOPF include generator re-dispatch, topology configuration and load shedding, which aims to eliminate the constraint violations during post-contingency. P-SCOPF is a traditional approach and is regarded as an expensive method, as no actions are permitted ($\Delta u_c = 0$) during post-contingency scenarios to eliminate violations, and additional costs must be incurred during normal operations to prevent contingencies, which may result in infeasibility during severe events. Nevertheless, industry practice often favours this type of action, despite the higher operational costs (i.e., additional costs included in normal operations) associated with the relative simplicity of solving the optimisation problem. In conclusion, P-SCOPF actions are generally perceived as a safer alternative compared to other methods, thereby enhancing confidence and perceptions of safety among industry practitioners [139] [140].

2.5.5 Security Constrained Optimal Power Flow: Corrective Action

The second mode of SCOPF actions is the Corrective SCOPF (C-SCOPF), which is based on the assumption that violations of operational limits (e.g., voltage, power flows, etc) can be tolerated for a minimum of several minutes without causing damage to the corresponding equipment. This corrective action can continue until the post contingency control actions (e.g., automatic or human interactions) are implemented [141]. The vector Δu_c in (2.87) for the C-SCOPF framework exhibits a distinct definition compared to the P-SCOPF. In C-SCOPF the vector Δu_c contains the vector of maximal allowed for control adjustment of variables in u_c between the pre-contingency and $c-th$ post-contingency state. The Δu_c can be further explained as:

$$\Delta u_c = T_c \frac{du_c}{dt}, \quad \forall c \in C \tag{2.91}$$

Where C is the set of all contingencies with c being indexed over this set, T_c is the assumption of time horizon allowed for corrective actions to ensure the feasibility of the post-contingency state, and $\frac{du_c}{dt}$ is the rate of change of the control variables in response to contingency [142]. The actions in the C-SCOPF include post-contingency generation rescheduling, load shedding or generation shedding. The key difference between the P-SCOPF and C-SCOPF actions lies in their objective formulations. The P-SCOPF aims to identify an optimal solution that ensure security in both normal and post-contingency conditions, whilst the C-SCOPF focuses on mitigating security violations specifically during post-contingency conditions [143]. In order to meet both the normal and post-contingency modes, the P-SCOPF only considers a single set of control variables that will be the same for both states. Regarding the C-SCOPF, it needs 'n' sets of adjustment variables for the 'c' contingency scenarios in addition to one set of control variables under normal states. As a result, the C-SCOPF has more constraints and variables, which lead to higher computational time [144].

Due to the same control variables being used for both pre- and post-contingency periods, the P-SCOPF may incur high operational costs, as adjustments to control variables are not permitted during contingency scenarios. This situation is exacerbated when a feasible operating point does not exist for both normal and contingency constraints. Conversely, the C-SCOPF approach may achieve lower operating costs and a more flexible strategy due to the permitted adjustment in control variables. However, there are several disadvantages associated with the C-SCOPF approach, such as the requirement to adjust the output levels of a large number of generators for optimal solutions to be feasible, and there may be substantial rescheduling of active power (P) between normal and contingencies states [145]. Generally, the C-SCOPF is considered a cost-effective control because post-contingency adjustments to control variables are allowed. However, in the context of instantaneous cost comparisons, the C-SCOPF may incur a relatively higher cost than the P-SCOPF. Nevertheless, this significant initial cost is expected to be minimised in the long term due to the low probability of contingency scenario [146]. Furthermore, the utilisation of VSC controls in an MT-HVDC network provides an advantage for C-SCOPF. Hence, the TSO can viably apply C-SCOPF in critical situations to alleviate the impacts of post-contingency disturbances. In conclusion, C-SCOPF represents a more economically viable long-term solution, whereas P-SCOPF provides a simple solution to the optimisation problem.

2.6 Chapter summary

This chapter presents a comprehensive overview of the concepts and theories related to power systems in steady-state analysis, beginning with the structure and topology of transmission systems in section 2.1 and discussing two types of converters in section 2.2. These two sections form the main focus of this thesis and are of great importance for the operational planning discussion that will follow in the next section. In section 2.3, operational planning is discussed in detail, as it is an essential element that establishes a framework for decision-making, ensuring both reliability and economic feasibility in power system operations. One crucial aspect of the operational planning that has been covered in the same section is the security assessment, which is used to examine the performance of the power system in order to ensure operational adequacy and security in the event of a contingency. Before fully understanding the optimisation problem, it is necessary to be familiar with the fundamental principles underlying the power system and the concept of basic power flow, which are covered in section 2.4. Finally, section 2.5 provides a comprehensive overview of optimisation problems in the power system, describing the general formulation of optimisation problems and presenting further details on specific models, including ED, OPF and SCOPF. These specific models are the central focus of this thesis, forming the foundation for the development of multiple scenario cases in Chapters 3, 4, and 5. In the SCOPF problem, corrective control actions have received attention due to their core importance in this thesis and their pivotal role in developing greater flexibility in the power system, which is incorporated into the development

of multiple scenarios and periods in Chapter 4. The VSC control strategies are developed to demonstrate and evaluate their effectiveness within the hybrid AC/DC system in relation to OPF problems, which will be discussed in detail in the next chapter.

Chapter 3

Mathematical Modelling of Multi Terminal HVDC Links for Hybrid AC/DC Networks

The Multi-Terminal HVDC (MT-HVDC) link is envisioned as a viable solution for the integration of large-scale offshore wind resource capacity and enabling long-distance power exchange between different independent operating regions (e.g., countries). MT-HVDC links normally consist of several converters forming a meshed DC link. In practical applications, power converters can be categorised into two types: Current Source Converter (CSC) and Voltage Source Converter (VSC). The CSC is a mature technology and classified as a conventional converter, whilst VSC is considered a modern converter that has gained significant attention in current research, specifically since it can be used to easily form multi-terminal meshed DC networks, which would be suitable for offshore wind transmission. VSC has more advantages compared to CSC, which are: a) offering more operational flexibility in terms of independent active and reactive power control in their AC side; b) having a smaller footprint due to smaller sized filters; c) capability of performing black start (i.e., the process of restoring power system operation, after a complete shutdown or blackout situation using its internal resources and capabilities, without requiring external power sources [147]); and d) capability of connecting and energising weak AC systems, due to the characteristics of the VSC, as discussed in section 2.2.2 of Chapter 2. The current topology of the VSC, the Modular Multilevel Converter (MMC), has gained interest among researchers and industry worldwide, particularly in HVDC transmission due to its high quality of voltages and currents, high modularity and high voltage ratings [148]. The higher conversion efficiency within the submodule of the MMC contributes to lower total power losses [149], and it also exhibits reduced switching losses when compared to two-level and three-level VSCs. Furthermore, the MMC, characterised by its reduced stress on switches that facilitates high-voltage applications such as HVDC systems and its ability

to generate high-quality waveforms, has emerged as an integral component in the development of MTDC and DC grids [150]. Although the benefits of the VSC, particularly the MMC topology, are appealing, it nonetheless has drawbacks from an economic perspective, specifically the high cost compared to the CSC [151]. The main focus of this research is VSC technology, as it is key to the hybrid AC/DC networks.

The hybrid AC/DC network is currently in the early stage of research development, in contrast to the well established AC system. One of the limitations of this hybrid system lies in its modelling for power flow and optimal power flow analyses, which requires further development and improvement from the current state of the art. This modelling is related to the structure (i.e., arrangement, configuration or framework) that regulates how AC and DC system integrate and interact with one another. The Flexible Universal Branch Model (FUBM) first introduced in [152] is presented in this study in order to address the limitations of the steady state analysis, providing a simpler and condensed form to solve the optimisation problems in the hybrid AC/DC network. Therefore, this research establishes an innovative modeling framework for developing and incorporating additional control actions, utilizing one of the FUBM models (i.e., VSC in-model) for short-term operational planning of hybrid AC/DC networks, specifically an MT-HVDC link, whilst taking into consideration the additonal control capabilities and flexibilities that are available to the network operator from the VSCs. The MT-HVDC link integrated with several wind farms is a complex network, which requires appropriate planning of its operation particularly with regards to scheduling VSC control actions to achieve optimal economic and operational performance (e.g., power transfer capability, voltage stability, response to contingencies, etc). This reinforced system performance is greatly influence by the control strategies, which depend on the converter, the HVAC connection and the HVDC network topology. Several types of control strategies have been implemented in the MT-HVDC link, including DC voltage controls, active and reactive power controls, droop control, main-follower control, margin voltage control, priority control and ration control [153]. Two types of control strategies have been developed in this research for the MT-HVDC link, comprising DC voltage control, active power and droop control. Section 3.3 will provide further discussion about these control strategies.

In the context of the MT-HVDC link, there are several elements and components involved that need more investigation and development. This development and research are indispensable, as they enhance understanding and improve the functionality and performance of each element and component, thereby contributing to the comprehensive advancement of the MT-HVDC link. The mathematical modelling of hybrid AC/DC networks constitutes a fundamental aspect of the topics covered in this chapter. The remainder of this chapter contains the following: Section (3.1) explains the FUBM components and the OPF-FUBM formulation structure. Section (3.3) provides a detailed explanation of the control strategies related to the VSC model in the FUBM, considering three control types (i.e., DC voltage control, active power control, and droop control) that have

been implemented in the case study. Section 3.4 presents the case study and the discussion of results, and finally, section 3.5provides a summary of this chapter.

3.1 Flexible Universal Branch Model (FUBM)

The Flexible Universal Branch Model (FUBM) first introduced by Alvarez-Bustos in Durham [152] is a general-purpose mathematical model that can represent the real-world devices in power systems (e.g., Voltage Source Converter (VSC), Static Compensator (STATCOM), Phase Shifter Transformer (PST), and Control Tap Changing Transformer (CTT)) for purposes of solving steady-state computational problems used in short-term operational planning (e.g., Optimal Power Flow (OPF) and economic dispatch). This model is powerful because it offers greater freedom and flexibility, by introducing additional state variables to solve the ensuing optimisation problems (e.g., power flow, OPF, Security Constraned OPF (SCOPF) and contingency analysis) used for operational planning of hybrid AC/DC networks. Furthermore, the model is scalable and efficient since the equations for all system (i.e., AC system, DC system and coupling) elements are similar, as the entire system is conceptually modelled as an AC system. FUBM can be utilised to accurately simulate the operation of typical AC branches or AC/DC converters on a single frame of reference (i.e., no need for solving coupling equations for such devices). To this end, it allows Transmission System Operators (TSOs) to plan different control actions (voltage control, independent active/reactive power control) available in VSC stations for example in a MT-HVDC link in hybrid AC/DC networks. It therefore provides researchers with a powerful tool to gauge the effectiveness of additional operational flexibility (promised by VSC control actions) and their impact on the power system behaviour under different operating conditions [152]. To this end, this thesis makes use of the FUBM mathematical model, more importantly its VSC in-model to present a unique planning framework for both short-term and long-term planning of hybrid AC/DC networks.

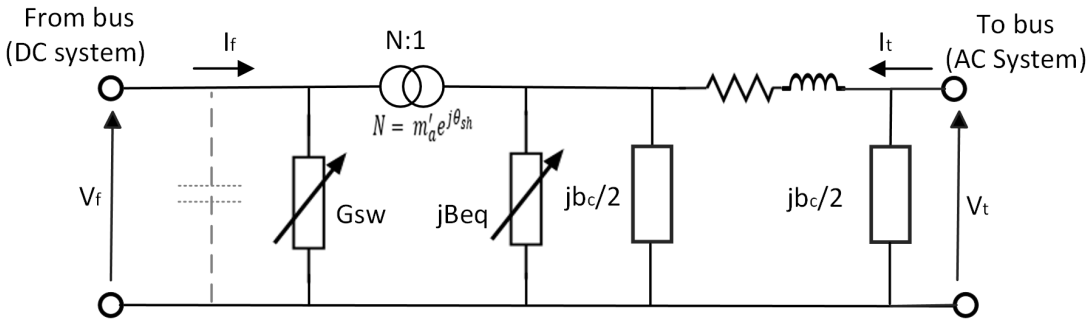

Figure 3.1: General Equivalent Circuit of the FUBM Model in Steady State

There are five internal models (also known as *in-models*) in the FUBM: a) AC branch; b) DC branch; c) Transformer (i.e., Controlled Tap Transformer (CTT) and Phase Shifter Transformer

(PST)); d) Voltage Source Converter (VSC); and e) Static Synchronous Compensator (STATCOM). One of the FUBM requirements states that there should be only one in-model for each transmission line in the power system model. Figure 3.1 illustrates a general equivalent circuit for the FUBM in steady-state,which can be used to model a variety of in-models depending on the available degrees of freedom in the model. For example, to model a simple AC branch it is sufficient to have the complex tap ratio in the transformer behave as simply a fixed parameter or to simply turn it off by setting the complex valued N to zero, which will reduce the FUBM to a simple π AC transmission model. The core components of the FUBM which allows this level of modelling flexibility are listed below:

(a) Complex Tap Transformer (CTT)

The core component of the FUBM which allows precise mapping of VSC controls such as voltage and power flow control is the transformer with the complex tap ratio shown in (3.1). This component allows for modelling of VSC's voltage control (AC and DC sides) and active power flow control by simply mapping the amplitude modulation control in a VSC to the variable m'_a and phase angle control to the variable θ_{sh}. To this end, variable θ_{sh} controls the amount of transmitted active power through the VSC, and variable m_a corresponds to the VSC's amplitude modulation co-efficient, when controlled using an appropriate pulse-width modulation scheme.

$$N = m'_a e^{j\theta_{sh}} \tag{3.1}$$

(b) Variable susceptance (jB_{eq})

Responsible for absorbing or supplying reactive power at the AC side of the FUBM when it is used to model AC/DC interfacing converters such as the VSC. It specifically represents the reactive power control capabilities and is activated exclusively during the modelling of the VSC and STATCOM components.

(c) Shunt conductance (G_{sw})

This variable relates to the switching losses in the VSC and is exclusive to the VSC in-model. Further explanation about these losses will be discussed in the next section.

3.1.1 VSC in-model

The VSC in-model within the FUBM is an enhancement of the conventional VSC model presented in Figure (2.16) which makes it feasible to solve the entire hybrid AC/DC networks within a single frame of reference without needing to solve an additional coupling equation. There are two main differences between the VSC in-model and the traditional VSC, as clearly shown in Figure 3.2. The first difference is that the coupling equation for the traditional VSC is represented by two dummy generators, whilst for the VSC in-model there is no coupling equation. Instead, it has a physical interaction consisting of two components: CTT and variable susceptance (jB_{eq}). The AC

and DC sides are seamlessly connected in this model. From this Figure, the VSC only needs to satisfy reactive power compensation on the AC side using the jB_{eq}. To this end, a zero reactive power constraint is defined for the DC side of the converter, which is mapped to jB_{eq} variable allowing for either injection or absorption of reactive power at the AC side (exactly like an actual VSC station), whilst preventing any flow of reactive power to the DC side of the converter [152]. Active power flow is regulated using the variable phase shifter angle, θsh, and therefore power balance can be maintained at the DC side without the need for a coupling equation. The other differences include the calculation of losses, where the switching losses in the VSC in-model are considered by including a shunt conductance (G_{sw}) on the converter's side, which accounts for both the converter current (i_G^{sw}) and voltage on the DC side (v_{dc}). The calculation of active power losses in the FUBM (P_{loss}^{FUBM}) is shown below:

$$P_{loss}^{FUBM} = v_{dc} i_G^{sw} = v_{dc} \left(G_{sw} v_{dc} \right) = v_{dc}^2 G_{sw} \tag{3.2}$$

$$P_{loss}^{FUBM} = \alpha + \beta i_c + \gamma i_c^2 \tag{3.3}$$

$$0 = -P_{\text{loss}}^{FUBM} + \alpha + \beta i_c + \gamma i_c^2 \tag{3.4}$$

Where α, β and γ represent the co-efficient losses of constant, linear, and quadratic terms. The G_{sw} can be calculated as follows:

$$G_{sw} = \frac{P_{\text{Traditional loss}}}{|V_{dc}|^2} \tag{3.5}$$

Where $P_{Traditionalloss}$ represents the active power losses in the traditional VSC and $|V_{dc}|^2$ is the magnitude of the DC voltage. Although there is a difference in the calculation of losses between the traditional VSC and the VSC in-model, the loss calculations for both models adhere to the same standard recommendations outlined in IEC 62751-2, which is based on a quadratic function. As a result, the power losses for both models are expected to be the same, as expressed mathematically by the following equation:

$$P_{\text{Traditional loss}} = P_{\text{FUBM loss}} \tag{3.6}$$

The VSC in-model is also capable of simulating the separation (i.e., isolation) of AC and DC systems, enabling the modelling of scenarios in which these two systems operate independently. Despite this isolation, the VSC in-model still allows for the transfer of active power between AC and DC systems. This demonstrates the advanced capabilities of the VSC in the FUBM by ensuring that active power can be exchanged efficiently, in addition to simulating real-world device operations.

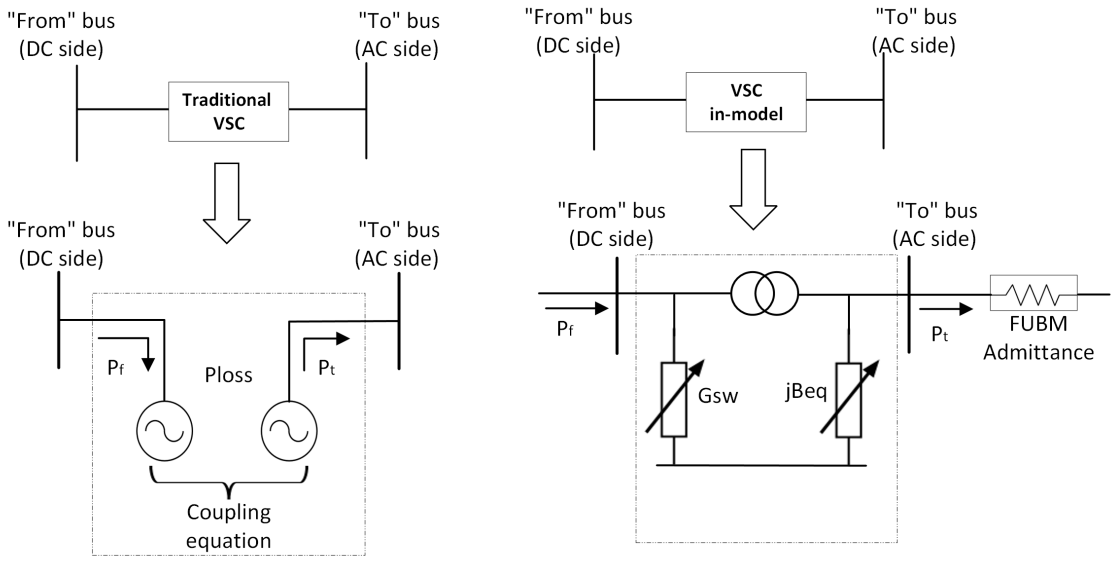

Figure 3.2: VSC in model compared to traditional VSC.

3.2 OPF Formulation using FUBM for Hybrid AC/DC Networks

The structure of the OPF formulation when the power system is modelled using the FUBM is the same as the general OPF (see Chapter 2, section 2.5.2), with the exception of an additional set of equality constraints that represents all VSC in-model controls, as specified in Table 3.1. In this table, it shows that the VSC in-model has three types of control and seven modes. In each mode, there are two active control constraints that govern the behaviour of the VSC. Control type I has three modes and the constraints for mode 1 are the phase shift angle (θ_{sh}) and AC voltage (v_{ac}), whilst modes 2 and 3 have constraints that combine DC active power (P_f) with reactive power (Q_{ac}) and voltage (v_{ac}) on the AC side, respectively. Type II control has two modes (i.e., modes 4 and 5) with constraint 1 being the DC voltage (v_{dc}) and constraint 2 being the reactive power (Q_{ac}) and voltage (v_{ac}) on the AC side for each mode. The last control, type III, which is related to droop control has two modes (i.e, modes 6 and 7). The constraint combination for this type includes voltage droop control ($v_{dc}droop$), whilst the second constraints are reactive power (Q_{ac}) and voltage (v_{ac}) on the AC side for modes 6 and 7, respectively. These constraints ensure the stability, reliability and desired performance of the power system by imposing specific limits on the operation of the VSC.

The injected nodal powers that are active and reactive for any devices in the power system can be calculated by evaluating the branch admittance matrix pertaining to the FUBM general model, which is given below [152] defined for the equivalent circuit given in Figure 3.1:

Table 3.1: Type of control mode in VSC in-model

Mode	Constraint 1	Constraint 2	Control Type
1	θ_{sh}	v_{ac}	
2	P_f	Q_{ac}	I
3	P_f	v_{ac}	
4	v_{dc}	Q_{ac}	
5	v_{dc}	v_{ac}	II
6	$v_{dc}droop$	Q_{ac}	
7	$v_{dc}droop$	v_{ac}	III

$$Y_{fubm} = \begin{bmatrix} G_{sw} + \left(y_s + j\frac{b_c}{2} + jB_{eq}\right) & \dfrac{-y_s}{m'_a e^{-j\theta_{sh}}} \\ \dfrac{-y_s}{m'_a e^{j\theta_{sh}}} & y_s + j\frac{b_c}{2} \end{bmatrix} \tag{3.7}$$

where variable G_{sw} represents the actual losses in the VSC, y_s is series admittance, b_c and B_{eq} are shunt and variable susceptances, m_a is the magnitude of the complex tap ratio (N) representing the amplitude modulation index and θ_{sh} is the phase angle of the complex tap ratio (N) representing phase shift between voltage in either side of the in-model. This admittance matrix is used to represent the VSC in-model together with its associated controls, enabling the calculation of associated nodal powers (i.e., following the general form $S = diag\{V\}(YV)^*$ to compute the nodal active and reactive power pertaining to the VSC. All the controls in the VSC given in Table 3.1 are therefore mathematically represented in the OPF problem, as explicitly defined by the equality constraint equations below. These equations, which represent nodal power balance equations, are an additional set of equality constraints added to the original OPF formulation as presented in (2.75).

1. Active power control:

$$g^n_{P_f}(x) = \text{Real}\left\{S^n_f(x)\right\} - P^{\text{set}(n)}_f = 0, \quad \forall n \in J_{sh} \cup J_{vsc} \tag{3.8}$$

In this type of control, only two internal models can utilise it: transformer (i.e., PST) and the VSC. The control variable, shift angle (θ_{sh}), can be adjusted to regulate the active power at the 'From' DC side (P_f). Here, n refers to the number of nodes, J_{sh} represents a set of PSTs and J_{vsc} represents a set of all VSCs. It can be stated that n is a member of either the set of shift angles or the set of VSCs, or it belongs to both sets.

2. Reactive power control (AC Side):

$$g^n_{Q_t}(x) = \text{Imag}\left\{S^n_t(x)\right\} - Q^{\text{set}(n)}_t = 0, \quad \forall n \in J_{vsc} \cup J_{cct} \tag{3.9}$$

For this type of control, only transformer (i.e., CTT) and VSC are able to utilise this control.

The control variable, referred to as modulation amplitude (m_a) for the VSC and normal tap for the transformer, can be adjusted to regulate the reactive power at the 'To' AC side (Q_t). Here, n refers to the number of nodes, J_{vsc} represents a set of all VSCs and J_{cct} represents a set of CTTs. It can be stated that n is a member of either the set of VSCs or the set of CTTs, or it belongs to both sets.

3. Reactive power compensation (DC Side):

$$g^n_{Q_z}(x) = \text{Imag}\left\{S^n_f(x)\right\} - \text{ zero } = 0, \quad \forall n \in J_{vscI} \tag{3.10}$$

This type of control is exclusive to the VSC and is also known as zero constraint, as it ensures that there is no reactive power flow in the DC system. The control variable, variable susceptance (B_{eq}), can be adjusted to regulate the reactive power at the 'From' DC side (Q_f) to achieve zero constraint, ensuring zero reactive power in the DC system. Here, n refers to the number of nodes, J_{vcs1} represents a set of VSC type I, indicating that this type of control is only applicable for converter type I.

4. AC voltage control:

$$g^n_{V_t} = \left\{V^n_t - V^{set}_t\right\}, \quad \forall n \in J_{vsc} \cup J_{cct} \tag{3.11}$$

In this type of control, only two internal models can utilise it: transformer (i.e., CTT) and the VSC. The control variable can be adjusted to regulate the AC voltage at the 'To' AC side (V_t), whilst simultaneously adjusting the reactive power. The Voltage Magnitude (VM) can then be configured to the set point (VM^{set}_t) at the AC terminal. For the VSC, this control variable is known as modulation amplitude (m_a) and for the CTT it is known as controllable tap ratio. Notably, the bus type at the node switches from PQ to PV when this control is implemented. Here, n refers to the number of nodes, J_{vsc} represents a set all VSC and J_{cct} represents a set of CTTs. It can be stated that n is a member of either the set of VSCs or the set of CTTs, or it belongs to both sets.

5. DC voltage control

$$g^n_{V_f} = \left\{V^n_f - V^n_{set}\right\}, \quad \forall n \in J_{vsc_{II}} \subset J_{vsc} \tag{3.12}$$

This type of control is exclusive to the VSC, specifically control type II (refer to Table 3.1). The control variable, variable susceptance (B_{eq}), can be adjusted to regulate the DC voltage at the 'From' DC side (V_f), and then the VM can be configured to the set point (VM^{set}_f) at the DC terminal. Similar to AC voltage control, this control also switches the bus type when implemented, changing it from PQ to PV nodes. Here, n refers to the number of nodes, $J_{vsc_{II}}$ represents a set of VSC type II and J_{vsc} represents a set of all VSCs. It can be stated that n is a member of either the set of control type II VSC or the set of all VSCs, or it belongs to both sets.

6. Voltage droop control:

$$g^n_{PV_{dp}}(x) = -\operatorname{Real}\left\{S^n_f(x)\right\} + P_f^{\text{set}(n)} - k_{dp}\left(VM^n_f - VM_f^{\text{set}(n)}\right) = 0$$
$$\forall n \in J_{vsc_{III}} \subset J_{vsc} \quad (3.13)$$

This type of control is exclusive to the VSC, specifically control type III (refer to Table 3.1). The control variable, shift angle (θ_{sh}), can be adjusted to regulate the DC voltage at the 'From' DC side (V_f), whilst simultaneously adjusting the active power flow (P_f). The VM and active power can then be configured to the set points (VM_f^{set} and P_f^{set}) at the DC terminal, as well as the droop gain (k_{dp}). The parameter k_{dp} represents the characteristic of the linear slope for ($v_{dc} - P_f$), as shown in Figure 3.7. Notably, when this control is implemented, the bus type at the 'From' DC side is set to PQ node. Here, n refers to the number of nodes, $J_{vsc_{III}}$ represents a set of VSC type III and J_{vsc} represents a set of all VSCs. It can be stated that n is a member of either the set of control type III VSC or the set of all VSCs, or it belongs to both sets.

7. Converter Losses:

$$g^n_{G_{sw}}(x) = -V_f^{2(n)}G^n_{sw} + \gamma i_t^{2(n)} + \beta i_t^{(n)} + \alpha = 0$$
$$\forall n \in J_{vsc} \quad (3.14)$$

This loss formulation is only related to the VSC station as it exchanges power (i.e., active and reactive) between the converter and the AC system. The calculation of active power losses in the FUBM uses a constant value G_{sw}, as explained in detail in (3.2) to (3.5) in section 3.1.1. The parameter of interest is the current at the 'To' AC side (i_t), which depends on the no-load losses, constant losses (α), linear losses (β) and quadratic losses (γ), as shown in the equation above. Here, n refers to the number of nodes, J_{vsc} represents a set of all VSCs. It can be stated that J_{vsc} is the set of all VSCs with n being indexed over this set. It should be noted that in the above equations, the subsets, J_{vsc_I} , $J_{vsc_{II}}$, and $J_{vsc_{III}}$ refer to the subsets of VSCs in the system that are of type I, II, or III depending on their control configurations as per Table 3.1.

Meanwhile, these equations are complemented by the following inequality constraints:

8. Line limits (including limits for the MT-HVDC DC lines):

$$h^k_{s_f}(x) = \{P^k_f(x)\}^2 + \{Q^k_f(x)\}^2 \leq \{L^k_S\}^2, \quad \forall k \in K \quad (3.15)$$
$$h^k_{s_t}(x) = \{P^k_t(x)\}^2 + \{Q^k_t(x)\}^2 \leq \{L^k_S\}^2, \quad \forall k \in K \quad (3.16)$$

Where $h^k_{S_f}$ and $h^k_{S_t}$ refer to the thermal limits at the 'From' and 'To' of line k pertaining to

the complex power, L_S^k refers to the thermal upper limit at line k pertaining to the complex power. The variables P_f^k and Q_f^k represent the active and reactive powers 'From' line k, whilst P_t^k, and Q_t^k represent the active and reactive powers 'To' line k, respectively. K is the set of all transmission lines with k being indexed over this set.

9. Upper and lower bounds on all state variables (for all VSCs and other internal models in the FUBM):

$$x_n^{\min} \leq x_n \leq x_n^{\max} \quad \forall n \in N \tag{3.17}$$

Where N is the set of all nodes with n being indexed over this set. The variables x_n^{min} and x_n^{max} refer to the lower and upper limits of the FUBM models.

3.3 Control Strategies in hybrid AC/DC system using VSC

The control strategy that applies to MT-HVDC links using the VSC in-model, represents an advanced version of the conventional VSC control strategy. As stated earlier in this chapter, the two variables, modulation amplitude ($m_a^{'}$) and shift angle (θ_{sh}), represent the Pulse Width Modulation (PWM) control of an actual VSC device. These variables can model the control capabilities for individual active and reactive powers. The VSC in-model is able to compensates for the reactive power flow at the DC side (i.e., From bus) using variable susceptance (jB_{eq}). This variable will be automatically adjusted in the OPF solution process to maintain zero reactive power injection in the DC link. This means that the reactive power at the "From bus" side is being monitored by this variable. This solution process is mathematically represented by the "zero constraint" in the FUBM OPF formulation which is illustrated in Figure 3.3.

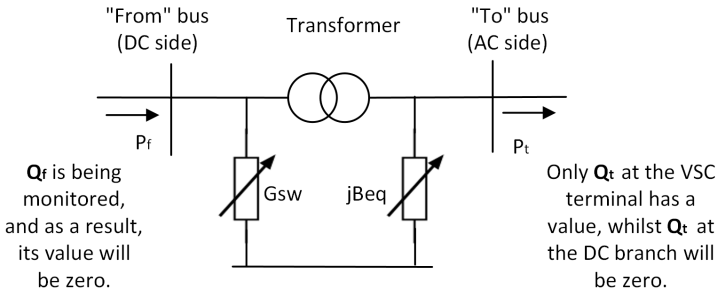

Figure 3.3: Control in the VSC in-model

The VSC can be configured to operate in different control modes such as voltage control, active power control, reactive power control or a combination of both powers and voltage. This specific selection of control types depends on the operational and control requirements of the power system. The OPF problem in the hybrid AC/DC networks can be effectively and mathematically solved using the FUBM model. However, there are certain rules that must be adhered to in order to be able to model and solve AC/DC networks with embedded MT-HVDC links using the FUBM VSC

in-model. The first rule is that there needs to be one VSC acting as a reference converter (i.e., slack VSC), which can be either types II or III - this is functionally equivalent to the VSC station setting a DC link voltage within an MT-HVDC link. Meanwhile, the slack VSC functions to ensure that the DC voltages and power flows do not exceed the limits, thereby, the power systems can remain stable and secure. The second rule states that if converter type II is chosen as the slack VSC, the other VSCs must be of type I, and there should be only one VSC of type II within each DC system. Morevoer, the third rule states that if converter type III is selected as a slack VSC, there must be j converters type III and m converters set to type I, with only one converter allowed to be designated as the slack VSC under this rule. The final rule sets out that type I converters must be used if there is a connection to renewable energy sources (i.e., wind farms and photovoltaic power plants).

Table 3.2: Rules for VSC in the FUBM model

Rule	Explanation of the rules
1	One VSC needs to be a reference VSC, which can be either type II or III.
2	**Slack VSC type II:** One VSC is of type II, whilst the remaining VSCs are of type I. There can only be one VSC of type II in each DC system.
3	**Slack VSC type III:** "j" VSCs of type III and "m" VSCs of type I There can only be one slack VSC in each DC system.
4	**Converter type I** must be used if connected to the renewable energy sources (i.e., wind farms and photovoltaic power plants)

The control in the VSC in-model can be divided into five types of control that are:

(a) DC Voltage Control.

This type of control related to assign one converter as a slack VSC.

(b) AC voltage control.

The variables that need to be set are AC voltage (V_{ac}) and limits for the modulation amplitude (m_a).

(c) Active power control (DC Side).

The variables setting are active power control on AC side (P_{ac}) and boundaries for the shift angles (θ_{sh}).

(d) Reactive power control (AC side).

The configuration variables are reactive power control on AC side (Q_{ac}) and the modulation amplitude limits(m_a)

Table 3.3: Types of control and setting variables in the VSC in-model.

No	Type of control	Setting Variables
1	DC Voltage control	V_{dc}
2	AC Voltage control	V_{ac} and $\overline{m_a}, \underline{m_a}$
3	Active power control	P_{dc} and $\overline{\theta_{sh}}, \underline{\theta_{sh}}$
4	Reactive power control	V_{ac} and $\overline{m_a}, \underline{m_a}$
5	Droop control	P_{dc}, V_{dc}, k_{dp}, $\overline{B_{eq}}, \underline{B_{eq}}$ and $\overline{\theta_{sh}}, \underline{\theta_{sh}}$

(e) Droop control.

The configuration variables are active power control on AC side (P_{ac}), DC voltage (V_{dc}), converter constant (k_dp), boundaries both for the variable susceptance (B_{eq}) and shift angles (θ_{sh}).

This thesis employs three types of control strategies in the VSC model, which have been proposed in many literature to investigate the operation of the hybrid AC/DC networks, specifically the model with the MT-HVDC link, namely: a) DC voltage control; b) active power control; and c) droop control. These controls are subsequently classified into two primary types:

(a) **Conventional control:** A combination of a DC voltage control and an active power control

(b) **Droop control:** A generalisation of traditional control.

The aforementioned controls are discussed in detail in the OPF-FUBM formulation in section 3.2. The next section will discuss these types of controls in further detail.

3.3.1 Conventional control

A conventional control in the VSC has two types of controls: a) DC voltage; and b) active power. DC voltage control is considered as the most straightforward approach that assigns one VSC, also known as a reference VSC or a slack bus at the DC node, to regulate the voltage within a predetermined range (i.e., upper and lower bounds of voltage). Controlling voltage with the reference VSC is essential, as it ensures that the total amount of active power entering the power system (P^{vsc}_{enter}) equals the sum of the power exiting the power system (P^{vsc}_{exit}) , accounting for losses (P_{loss}). This statement can be mathematically expressed as:

$$P^{vsc}_{enter} = P^{vsc}_{exit} - P_{loss} \tag{3.18}$$

Equation (3.18) known as the VSC power balance equation, provides further insight into necessity of maintaining the required active power in the DC system. Specifically, it states that the active power required in the DC system must not exceed the active power rating of the reference converter

in order to maintain stable operating conditions and promptly mitigate abnormal voltage conditions (i.e., undervoltage or overvoltage) or alleviate congestion. [154][18]. Furthermore, the MT-HVDC link is primarily dependent on the DC voltage regulation, which supplies and absorbs any power imbalance in the power systems to ensure stable operation and power balance among all the system's buses (i.e., AC and DC nodes). Thus, the availability and capabilities of this type of control is fundamental to the power balance in the MT-HVDC links [155][19].

The second traditional control is an active power control, which is the simplest technique similar to the DC voltage control. This control also known as a power angle control, due to the fact that angle is the main variable in controlling and maintaining the stability of the power system.

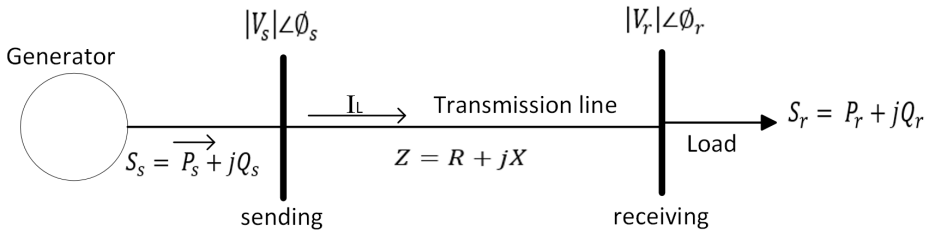

Figure 3.4: Two bus system

The transmission model (refer to Figure 3.4) can be mathematically expressed as below, in terms of sending (s) and receiving (r) voltages, currents and phase angle.

$$V_s = V_s e^{-j\emptyset_s} \tag{3.19}$$

$$V_r = V_r e^{-j\emptyset_r} \tag{3.20}$$

where V_s, $\emptyset_s$, V_r, $\emptyset_r$ are the voltage sending end, phase angle sending end, voltage receiving end and phase angle receiving end, respectively. The complex impedance (Z) and current (I_L) are expressed in the form of:

$$Z = R + jX \tag{3.21}$$

$$I_L = \frac{V_s - V_r}{Z} \tag{3.22}$$

where R and X are the resistance and reactance (i.e., a capacitor or inductor), respectively. The complex AC power at both sending and receiving ends can be calculated as follows:

$$S_s = P_s + jQ_r = V_s I_s^* \tag{3.23}$$

$$S_r = P_r + jQ_r = V_r I_r^* \tag{3.24}$$

The power transfer across the transmission line can be calculated using the formula provided

below.

$$S = V_r I^* = V_r \left[\frac{V_s - V_r}{jX}\right]^* \tag{3.25}$$

$$S = \frac{V_s V_r}{X}\sin\delta + j\frac{V_r}{X}\left(\frac{V_s V_r}{X}\cos\delta - V_r\right) \tag{3.26}$$

The active and reactive power transfers in (3.26) for the transmission line can be formulated as:

$$P = \frac{|V_s|\,|V_r|}{X}\sin\delta \tag{3.27}$$

$$Q = j\frac{V_r}{X}\left(V_s\cos\delta - V_r\right) \tag{3.28}$$

From (3.27), it can be inferred that the transmission angle (δ) is an important variable, as it defines the amount of power transmitted between two buses and also affect the stability of the overall power system. This expression also states that power will only flow when there is a phase difference between the voltages at the sending and receiving ends. Figure 3.5 illustrates the relationship between power and transmission angle. In this curve, power transmission needs to be controlled to keep the transmission angle (δ) within safe limits, which are below P^{max}. In theoretical limit, the maximum power (P^{max}) occurs when the transmission angle (δ) is 90°, representing the steady state stability limit. If the transmission angle (δ) exceeds 90°, the whole power system becomes unstable and can lead to sudden power loss. In the worst-case scenario, the power system can collapse, resulting in a blackout. However, the power transfer capability of the transmission line is always constrained by various other factors, such as thermal loading limits and temperatures not solely relying on differences in the transmission angle [156]

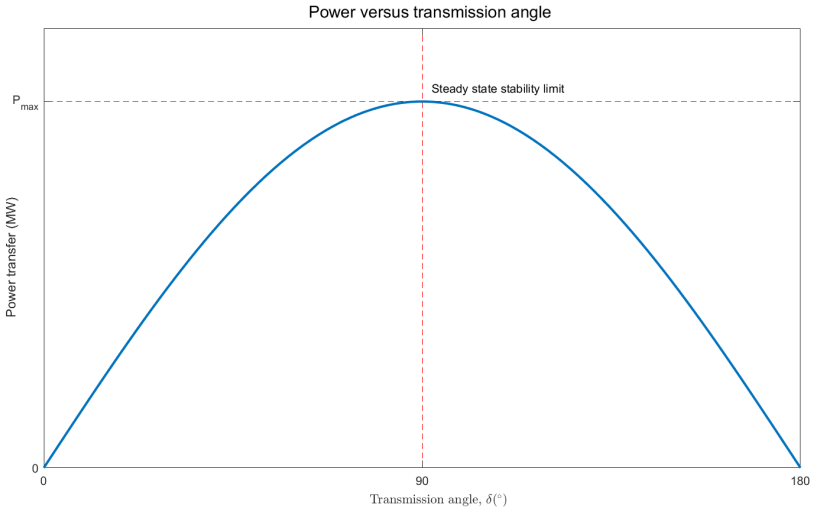

Figure 3.5: Power versus transmission angle

3.3.2 Droop control

Droop control is a proportional type of control for power sharing mode among the converters. The principle of this control is similar as frequency droop control, which is to achieve a distributed frequency control in the synchronous generator in conventional AC system. Droop control normally refers to Voltage Droop Control (VDC), which has been receiving attention, especially in research related to the MT-HVDC link, due to its advantages over other controls, such as: a) higher reliability and robustness resulting from less requirements for a communication infrastructure [157]; and b) the minimal impact on the transmission system due to a continuous and smooth relationship between voltage and power. However, the drawback of this control is the stable voltage rises as the proportional constant (i.e., converter constant) increases. There are various types of droop characteristics under this control, namely voltage-power ($V-P$), voltage -current ($V-I$), adaptive control and voltage droop with different dead-bands and limits [158] [159]. Figure 3.6 shows several characteristic curves associated with these droop control types. The development of VDC aimed to overcome the difficulty of achieving efficient power sharing among converters operating within a shared DC system.. The structure of this control is similar to the master-slave configuration, except the converter constant (k_{dp}) is added in the voltage deviation input for the power flow equation. This constant is the key to determine the proportion sharing of power among the converters. The higher the power sharing, the higher the converter constant and vice versa [160]. Therefore, it can be stated that the converter constant is vital to optimising the operation of the power system. Normally, this constant is preferred to be higher in order to avoid large voltage deviation, but if it too high it can lead to non-linearity in the power control circle, potentially causing instability or inefficiency in the power control mechanism.

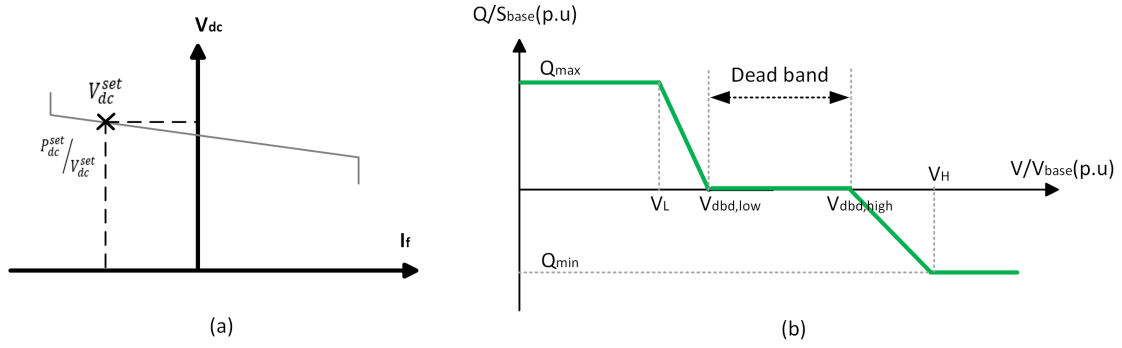

Figure 3.6: Characteristic curve of droop control: a) $v_{dc} - I_f$. b) voltage droop with dead-band and limit.

The FUBM model utilises a voltage-power ($v_{dc} - P_f$) droop characteristic, whilst the VSC in-model classifies this control as type III (refer Table 3.1). In this type of control, the active power (P_f) and voltage magnitude (V_m) are obtained from the "From bus" at DC side of the VSC in-model (refer to Figure 3.3). The power controlled in the converter at bus 'n', as determined by

this control, can be expressed using the following equation:

$$-P^{cal}_{f(n)} + P^{set}_{f(n)} - k_{dp}\left(V^{cal}_{mf(n)} - V^{set}_{mf(n)}\right) = 0, \quad \forall n \in N \tag{3.29}$$

Where N is the set of all nodes, with n being indexed over this set, and the voltage and power references of the droop line are denoted by $V^{cal}_{mf(n)}$ and $P^{cal}_{(f(n))}$. This equation indicates that the voltage magnitude at the "From bus"at DC side ($V_{mf(n)}$) is varied in proportion to the active power ($P_{f(n)}$) being exchange between the generators. As active power increases, the magnitude of the voltage decrease and vice versa, maintaining a proportional balance between power generation and demand. The converter constant (k_{dp}) quantifies the sensitivity of the converter's output power to the local DC voltage source. This constant defines the linear slope that characterises the relationship between the converter power and the DC voltage, as illustrated in Figure 3.7 and described by (3.29).

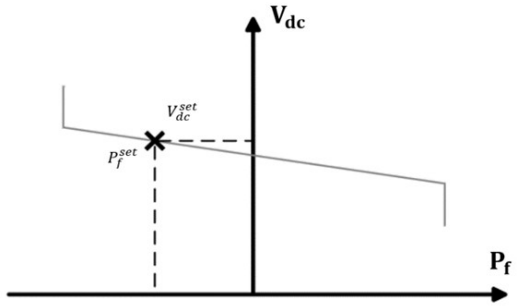

Figure 3.7: Characteristic curve of linear slope: $v_{dc} - P_f$

3.4 Case Study: Flexibility in the MT-HVDC Link through Control Strategies

This section presents the simulations of the VSC model in the MT-HVDC link that attempt to solve the OPF problem in a three-terminal MT-HVDC link. The system is connected to three OWFs (i.e., Wind Farms A, B and C) as illustrated in Figure 3.8. The AC system is an IEEE30 bus system consisting of six generators, 41 transmission lines and 24 loads. The data for this system is available in an open-source programming package called MATPOWER [130] [12], which is also provided in Appendix B. The DC system highlighted by red line consists of six DC lines (i.e., B001, B002, B003, B004, B005 and B006), three transformers (i.e., Tx1, Tx2 and Tx3) and three converters (i.e., VSC1, VSC2 and VSC3). For this case study, the transformers and converters located after all the wind farms are not considered in the simulation. Therefore, the wind farms (i.e., Wind Farm A (WFA), Wind Farm B (B) and Wind Farm (C) are directly connected to the lines (i.e., WFA to line B004, WFB to line B005 and WFC to line B006). This modified system (i.e.,

the MT-HVDC link) has been used as a model to address hybrid AC/DC network optimization problems. There are nine parameters in the MT-HVDC, which are listed below. Table 3.4 provides the setup values for each parameter.

(a) Voltage rating for the VSCs and DC lines.

(b) Maximum and minimum DC Voltage.

(c) Maximum and minimum variable susceptance (jB_{eq}).

(d) Resistance (r_s) and reactance (x_s) for each VSC.

(e) DC line Resistance (r_s).

(f) Loss coefficient for the VSCs (quadratic loss (α), linear loss (β) and constant loss (γ))

(g) The upper power limit of the VSC

(h) Thermal limit (i.e., transmission limit) for the DC line

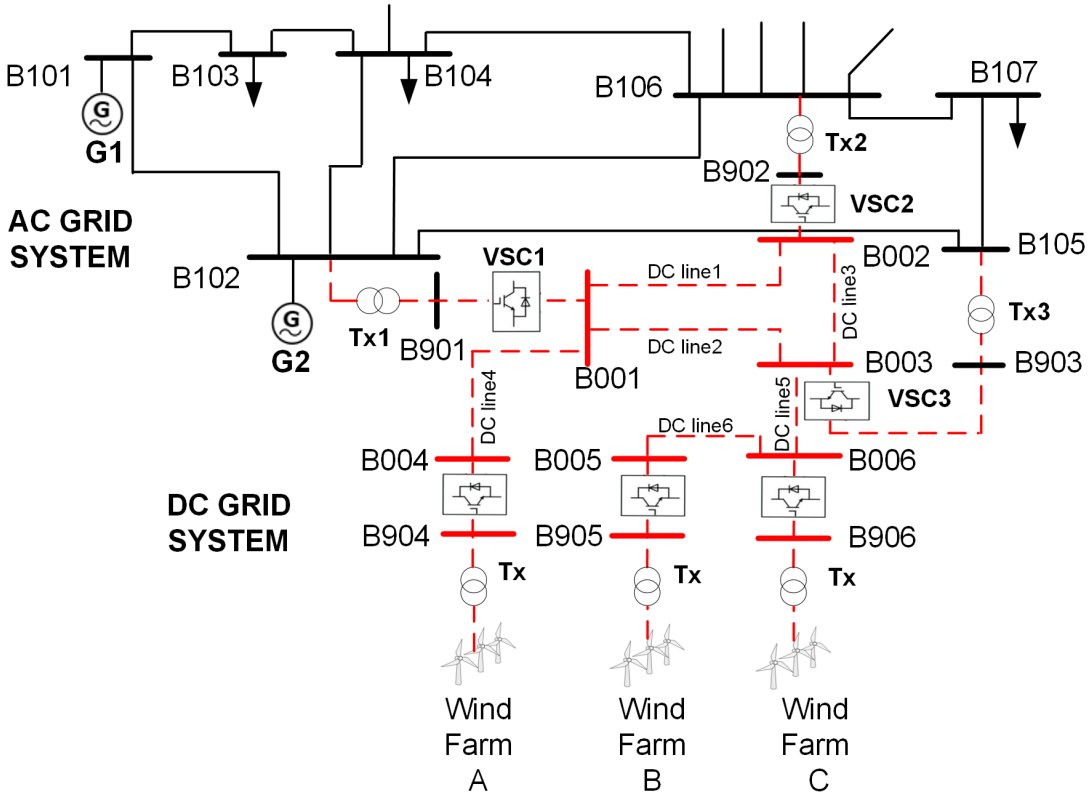

Figure 3.8: MT-HVDC system

There are four cases considered in this study: a) Basecase; b) DC voltage control; c) 20% increase active power control; and d) droop control. Table 3.5 provides the control settings for VSC variables, with VSC 1 (i.e., the reference VSC) designated as type II with mode 4 in the base

Table 3.4: Parameters of the converter and DC grid.

Parameter	Values	
Rating VSC/DC Voltage	100MVA	200kV
Max/Min DC Voltage	1.15p.u	0.9p. u
Ma (Max/Min)	1.2	0.8
Beq (Max/Min)	0.5p. u	-0.5p. u
VSCs (rs/xs)	0.0001p.u	0.1643p.u
DC lines (rs)	0.05p.u	
VSCs loss coefficient	$\alpha = 0.0001$, $\beta = 0.015$, $\gamma = 0.2$	
VSC's upper power limit	100MVA	
DCs transmission limit	200MVA	

case scenario. Whilst, both VSC2 and VSC3 are classified as type I with mode 3. DC voltage and DC active power are the control constraint variables for these VSCs (i.e., VSC2 and VSC3), and their respective setup are as follows: VSC1: V_f = 1.0p.u; VSC2: P_f = 25MW; and VSC3: P_f = 15MW. For both the DC voltage control and the 20% increase in active power control cases, the designated VSC types, modes and control constraints follow the basecase scenario. The setup parameter values for DC voltage are as follows: VSC1: V_f = 0.98p.u; VSC2: P_f = 25MW; and VSC3: P_f = 15MW. For active power control, the parameter values are as follows: VSC1: $_f$ = 1.0p.u; VSC2: P_f = 30MW; and VSC3: P_f = 18MW. In the case of droop control, VSC1 is chosen as a slack VSC with type III, whilst the other VSCs are type I. As for the chosen mode, VSC1 is set to mode 7, while VSC2 and VSC3 are set to modes 3 and 2, respectively. The parameter settings for all VSCs are shown in Table 3.5.

3.4.1 Result and Discussion

Each simulation case has successfully converged. Tables 3.6, 3.7, and 3.8, as well as Figure 3.9 and 3.10 show the results pertaining to convergence times, generation costs, voltage and power profiles, respectively. Table 3.6 shows the results of the convergence time, indicating that the fastest convergence (131.6 seconds) occurs during DC voltage control, whilst the slowest convergence time is 196.7 seconds, which occurs when droop control is adopted. Meanwhile, the basecase converged at 177.76 seconds, whilst the active power control converged at 151.29 seconds. Convergence time (i.e., computational time) is an important factor in solving PF and OPF problems, especially given that power system topology changes frequently during the short-term or long-term operational planning [161]. Faster convergence is crucial because it reduces the computational time needed to obtain solutions for optimization problems in power systems. Using an unsuitable method can

Table 3.5: Settings for the VSC.

No	Type of control	Converter	Type	Mode	Control constraint
1	Basecase	VSC1	II	4	Vf=1.0p. u
		VSC2	I	3	Pf = 25MW
		VSC3	I	3	Pf= 15MW
2	DC voltage control	VSC1	II	4	Vf=0. 98p.u
		VSC2	I	3	Pf = 25MW
		VSC3	I	3	Pf= 15MW
3	Active power control (+20%)	VSC1	II	4	Vf=1.0p. u
		VSC2	I	3	Pf = 30MW
		VSC3	I	3	Pf= 1MW
4	Droop control	VSC1	III	7	Vf=1.0p. u, Pf = 25MW, Kdp = -0.1
		VSC2	I	3	Pf = 25MW
		VSC3	I	2	Qt = 25MW

prolong the processing time for solving optimisation problems, which poses a significant challenge in the real time operations involving large power systems. Based on these findings, DC voltage control demonstrated fast convergence followed by active power control. This implies that the conventional method performs better in terms of computational efficiency compared to the basecase and droop control. It is important to highlight that, when formulating any OPF problems, it is fundamental to carefully consider which optimal controls are appropriate for the objectives and application problems. Whilst accuracy, feasibility and robustness are key factors to consider, the rapid convergence (i.e., related to hardware and algorithm) [162] of the OPF modelling solution provides a significant advantage in the MT-HVDC link.

Table 3.6: Time converged and generation cost.

Case	Basecase	DC Voltage Control	Active power control (+20%)	Droop control
Converged (Second)	177.86	131.6	151.29	196.47
Generation cost ($/hr)	472.54	469.46	476.89	475.07

The objective function, as outlined in the standard OPF formulation in (2.74) in Section 2.5.2, is to minimize the overall generation cost of power in this case study, which includes the costs of fuel consumption as well as the operation and maintenance of conventional generators. For a thermal unit, the generation cost is represented by a quadratic function of fuel consumption, measured

in British thermal unit per hour (Btu/h or $MBtu/h$). This cost is expresses in terms of dollars per hour ($\$/h$) and includes operating cost such as labour, maintenance and fuel transportation. However, due to the complexity of directly modelling these costs as a function of the thermal unit's output, these costs are included as a fixed portion of the overall operating cost [163]. Minimizing the power generation cost is a prominent goal in the power system, as it offers significant advantages, including economic efficiency for businesses, affordable electricity prices for consumers, and investment in infrastructure. Furthermore, it helps energy companies operate their resources and equipment at appropriate levels, avoiding both overutilisation and underutilisation. This can also optimise energy usage and prevent energy spillage (i.e., the wastage of energy in the power system). Table 3.6 provides the results of this objective for four different scenarios. From this table, it can be observed that the active power control has the highest generation cost, $476.89\$/hour$, followed by the droop control and basecase, with production costs $475.07\$/hour$ and $472.54\$/hour$, respectively. The lowest overall cost for electricity occurs when the DC voltage control is activated, with a price of $469.46\$/hour$. The overall generation cost is higher in active power control because all generators in this case injected more active power (i.e., a 20% increase) into the power system to satisfy the demands. Conversely, the DC voltage has the lowest generation cost due to the fact that this type of control focuses only on voltage stability.

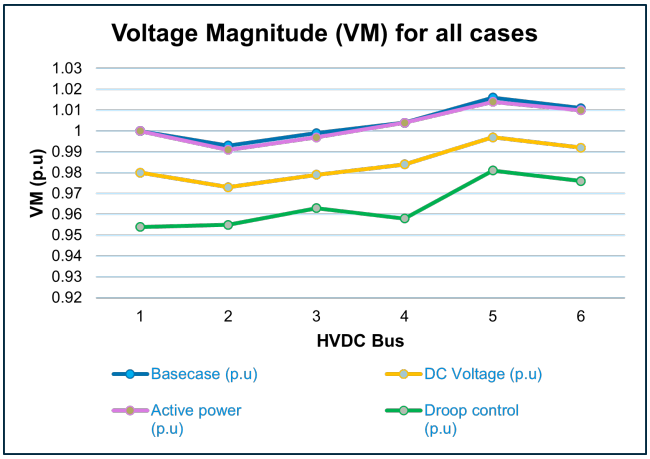

Figure 3.9: Voltage Magnitude result

Figure 3.9 presents the results of the voltage profile (i.e., VM), which shows that all voltages are within their boundaries, with the upper and lower values being 1.02 p.u. and 0.95 p.u., respectively. It also can be observed that the highest voltages occur by far at buses 5 and 6 in all cases. The most surprising aspect of this result is that the voltage values are lowest in the droop control case compared to other cases. The concept of Voltage Droop Control (VDC) is not the same as the voltage drop, even though this control allows for a controlled reduction in voltage, by creating proportional relationship between voltage and the control base (e.g., power or current) [164]. This is because this control primarily focuses on adjusting the output power of converters in response to changes in demand, as discussed in section 3.3.2. It involves dividing

demands in proportion to their output power based on the converter constant (k_{dp}) value. This constant value indicates how much the voltage levels differ from their nominal values in response to changes in power demands, ensuring that the power system can effectively respond to varying levels of demand while maintaining stability. Consequently, when demand increases, the converters with this control slightly reduce their voltage output, allowing power to be distributed among the various demands, which results in a lower overall system voltage. The DC voltage control has the second lowest voltages compared to other cases, as its function is to regulate the voltage within a predetermined range at the reference converter, ensuring the balance of active power (i.e., power in equals power out plus losses) in the DC system. DC voltage is also a vital control to keep the power system operating under stable conditions, ensuring that the power flow does not exceed the ratings of the reference converter and avoiding abnormal voltage conditions (i.e., undervoltage and overvoltage). The last control is active power control, which has a voltage profile slightly similar to the base case. This type of control involves managing the active power output of the converters to maintain stability and meet the demands.Stability is an important criterion in the power system operation, defined in [82] as, *the ability of an electric power system, for a given initial operating condition, to regain a state of operating equilibrium after being subjected to a physical disturbance, with most system variables bounded so that practically the entire system remains intact.* In hybrid AC/DC networks, stability operation is classified based on rotor angle, frequency and voltage as well as two new stability introduced in [165]: converter-driven stability and resonance stability. However, this thesis focuses on the standard classification of voltage stability, defined as the ability of a power system to maintain steady voltages near nominal values for all buses, particularly during outages ($N-1$ or $N-k$), and the capacity of generation and transmission systems to supply power to meet electricity demand [166].

Table 3.7: Voltage Angle result.

Branch	Basecase	Control		
		DC Voltage	Active power (+20%)	Droop control
	PF (MW)	PF (MW)	PF (MW)	PF (MW)
1	-1.357	-1.551	-2.376	-4.524
2	-1.357	-1.551	-2.376	-4.524
3	-1.357	-1.551	-2.376	-4.524
4	-1.357	-1.551	-2.376	-4.524
5	-1.357	-1.551	-2.376	-4.524
6	-1.357	-1.551	-2.376	-4.524

Table 3.7 shows the Voltage Angle (VA) results, which have the same values at all buses for each case. These values are expected to be the same because the FUBM model only allows active power flows in the DC links. This means that there is no injection or absorption of reactive powers in the links due to the activation of zero-constraint, as stated in the OPF-FUBM formulation. Additionally, these angles are constant because the FUBM model is notionally derived from the AC

system, rather than being a separate component within the power system. This notion eliminates the need for separate network elements as typically applied in a conventional method.

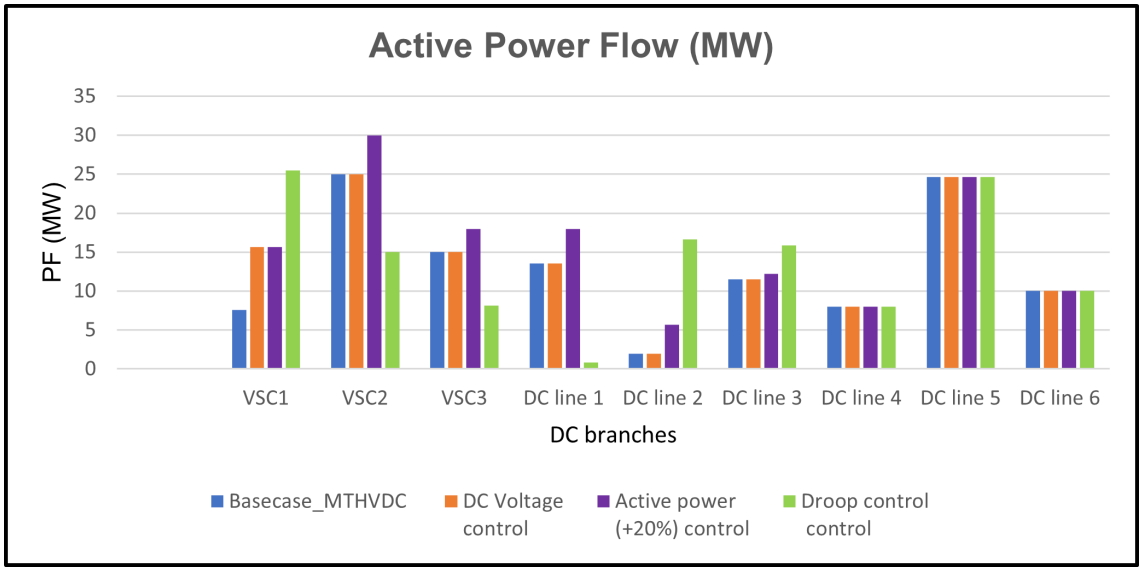

Figure 3.10: Active power flow result

The result of the active Power Flow (P_{PF}) in the DC branches within the MT-HVDC link is presented in Figure 3.10. From this figure, it is clearly observed that there is an increase in P_{PF} at DC lines 1 to 3 compared to the basecase. Active power control results in an increase in P_{PF} at DC line 1, whilst P_{PF} decreases at DC lines 2 and 3. Contrary, when droop control is activated, P_{PF} at DC line 1 becomes the lowest among the cases because most of the P_{PF} is diverted to DC lines 2 and 3. These results demonstrate that the VSC control strategies are capable of effectively managing P_{PF} in the MT-HVDC link integrated with OWFs. On the other hand, P_{PF} across the DC lines 4, 5 and 6 remain the same for all cases because the power at these lines are injected by the wind farms (i.e., WFA, WFB and WFC).

Table 3.8: Reactive power flow result.

Branch	Basecase (MVAR)		Control					
			DC Voltage (MVAR)		Active power (+20%)- (MVAR)		Droop control (MVAR)	
	Q_f	Q_t	Q_f	Q_t	Q_f	Q_t	Q_f	Q_t
VSC1	0	-13.7	0	-13.3	0	-16.57	0	1.05
VSC2	0	-9.22	0	-3.9	0	-6.18	0	4
VSC3	0	-8.46	0	-6.32	0	-7.58	0	-25
DC line 1	0	0	0	0	0	0	0	0
DC line 2	0	0	0	0	0	0	0	0
DC line 3	0	0	0	0	0	0	0	0
DC line 4	0	0	0	0	0	0	0	0
DC line 5	0	0	0	0	0	0	0	0
DC line 6	0	0	0	0	0	0	0	0

Table 3.8 presents the reactive power flow (Q_{PF}) results for the scenarios, where the values in

the Q_f column are all zeros, indicating that there is no Q_{PF} across the DC branches. The only Q_{PF} observed is at the VSC's AC terminal, as seen in the Q_t column. This is because the VSC only allows P_{PF} within the DC system due to the activation of the zero constraint, as discussed in the OPF-FUBM formulation in (3.10) in section 3.2. This is clearly shows that the VSC in-model is able to maintain zero reactive power flow in the DC branches, by compensating the Q_{PF} at one of its terminal only as discussed detail in the section 3.1.1.

3.5 Chapter summary

This chapter presents a comprehensive overview of the concepts, elements, and formulations related to hybrid AC/DC networks, with a particular emphasis on the advanced topology of the MT-HVDC link. The focus of this thesis is on the VSC technology due to its suitability as a candidate for forming MT-HVDC links used to integrate large-scale OWF generation capacity to future AC networks and its superior capability in introducing additional flexibility of operation both in terms of voltage and power flow control. To model the VSC device efficiently and compactly, the FUBM is utilised because it offers greater freedom and flexibility, making it feasible to solve the entire hybrid AC/DC network within the single frame of reference for purposes of steady-state computation. The VSC in-model, which is one of the models in the FUBM, is explained in detail in section 3.1.1, covering the mathematical model and the OPF formulation structure (i.e., OPF-FUBM). In the OPF-FUBM formulation, an additional set of equality constraints is discussed that represents the controls in the VSC in-model within the FUBM. Then, the control strategies based on three types of controls (i.e., DC voltage control, active power control and droop control) are subsequently divided into two primary types of controls (i.e., conventional control and droop control), which are discussed in detail in section 3.3. A case study is presented to demonstrate the flexibility of the advanced hybrid AC/DC network topology, specifically with the model of the MT-HVDC link using these control strategies. The results demonstrate that VSC control strategies are effectively capable of managing the active power flow in the MT-HVDC link, whilst preventing reactive power flow in the DC system. Furthermore, the case study highlights how the VSC is able to regulate the voltage in the DC system and ensure that all voltages are within the acceptable limits. The SCOPF problem, particularly corrective control actions have received attention due to their pivotal role in developing greater flexibility in the power system, which is incorporated into the development of multiple scenarios and periods that will be discussed in the next chapter.

Chapter 4

Short-term Optimum Operational Planning for Hybrid AC/DC Networks used for Offshore Wind Integration

Short-term operations planning forms the key component with which the Transmission System Operator (TSO) manages the operation of the power system guaranteeing a seamless, reliable and economic operation of the system. Short-term operations planning can therefore be used as a key tool to maintaining operational security at all times and under all operating conditions [167]. Typically within a short-term operations planning framework a set of decisions (actions) such as a generation schedule are outlined ahead of real-time operation [78]. Such actions can often be complimented by a specific set of control decisions taken under different operating conditions thereby guaranteeing security of operation even at instances of loss of generation or excess demand (i.e., contingencies). Short-term operational planning studies therefore serve as a vital stage of the decision making process by the system operator to maintain a reliable and secure Electric Power System (EPS), whilst identifying operating bounds that meet all reliability criteria, which adhere to all technical and environmental constraints [168]. The initial objective of the operational planning is to minimise the cost of generation over a specific planning time horizon aligning with the load duration curve (i.e., graphical representation that are curves, illustrating the relationship between the time and demand by showing the percentage of time the demand is greater than or equal to a certain level. It is simply information on how electricity is used over time [169]). Nevertheless, this aim has been customised to take consideration for advancement in technology, driven by the transition energy sources from fossil fuels to renewable energy sources.

The integration of renewable energy resources, particularly wind, in the EPS creates technical and economic challenges related to short-term operational planning, which will require more operational flexibility (i.e., the ability to provide control and load-following over a larger operating range) in the power system to respond to the uncertainty (i.e., prediction error) and variability (i.e., changes in the renewable generation related to time variables) due to the random and inherently variable nature of the renewable energy resource [170] [171]. Within the renewable energy sector, wind power has emerged as a prominent source of electricity generation, due to the cost effectiveness and reliability of wind technology. However, wind power does have certain challenges including high uncertainty, low dispatchability, non-storability, high variability and limited predictability. Since wind farms can only reduce their output power, they are unable to increase the production in response to demand, hence wind power cannot be directly regulated either. These drawbacks have a significant impact in the power system operations, making it difficult to maintain a minimum cost of electricity whilst balancing supply and demand [172]. Given this, the need of accurate short-term operational planning with high penetration level of the wind power is crucial, not only for reliable and secure operation in the power system, but also for the commitment to end reliance on fossil fuel generation to achieve the net-zero carbon emission.

In the past the operational planning only had to consider the demands and discrete events (e.g., generator or line failures, equipment malfunctions or natural disasters) as uncertainties and variability [173]. Nonetheless, with the wind integration, the TSOs have to incorporate these factors (i.e., uncertainty and variability) in the generation side of operational planning, which requires the TSOs to evaluate and plan ahead flexibility (i.e., ability of the power system to adapt to a variety of uncertain scenarios by taking an alternative strategy of actions within an acceptable cost-limit and time-frame [174]). In contrast, the inaccurate short term operational planning (i.e., without incorporation of these factors) may lead to insufficient flexibility in the real time operation, inadequate power capacity and potential to undesirable circumstances (e.g., load shedding, wind curtailment or blackout). Therefore, modern short-term operational planning processes for systems with high levels of variable renewable energy penetration need to take into account the uncertainty and variability factors with various scenarios to ensure feasible and economical operation [175].

This chapter discusses short-term operational planning for hybrid AC/DC networks used for offshore wind integration, beginning with a brief explanation of short-term operations planning. The remainder of this chapter contains the following: Section 4.1 provides a full explanation of the single-period worst-case scenarios and the associated SCOPF formulation structure. Section 4.2 explains the two elements of multi-period operational planning that are utilised in the multi-period Security Constrained Optimal Power Flow (SCOPF). Sections 4.3 and 4.4 present the discussion of contingency analysis and the remedial action scheme. Section 4.5 provides a modified SCOPF formulation based on the incorporation of two elements discussed in section 4.2. Section 4.6 presents the case study and the discussion of results. Finally, Section 4.7 summarises this chapter.

4.1 Single Period Operational Planning

In the context of steady state analysis, the Economic Dispatch (ED) problem (or its counterpart, the Optimal Power Flow (OPF) problem) is viewed as a straightforward single period problem, which aims to find an optimal generator dispatch schedule that satisfies a specified demand whilst minimising the total cost [176] of operation incurred to the system operator. The term "single period" describes the process of planning and making decisions that concentrate on a single, specific time period (i.e., a snapshot) such as an hour or a day within the planning timescale. The ensuing decision problem need not be an economic dispatch and could also be formulated as unit commitment, or outage scheduling and can include a number of control actions such as voltage/VAR control and power flow control if appropriate. In this context, a deterministic problem formulation is used to execute a single deterministic scenario, which has a fixed set of input data and variables to optimise the operation of the system. The decisions determined by solving the single-period deterministic problem however should extend not only to instances of normal operation but also to abnormal, contingency, operation conditions as well. To this end, different scenarios are generated for which a unique solution is obtained deterministically (i.e., multi-scenario solutions). This approach is particularly useful if there are variables with uncertainty in the original power system operational planning problem for example in case of offshore wind or wind resource forecast [177].

4.1.1 The worst-case scenarios

As discussed at the beginning of this chapter, the primary issue associated with wind-based production is the uncertainty and variability, due to the variable nature of wind resources. These problems present major obstacles for the TSOs in controlling and managing this energy, since they need to accurately forecast the amount of energy generated by wind farms over a given planning timescale in which they are required to generate an optimum schedule for conventional generating units to ensure a balanced supply and demand equilibrium while minimising costs [178]. This becomes more crucial in the presence of high levels of wind power penetration, as this challenge is exacerbated in extreme contingency scenarios which may increase the risk of introducing unforeseen operational conditions further compromising the ability of the system to maintain balance between generation and demand.

In this context, many simulations have been conducted to examine and provide valuable information on the static security of the wind-dominated power system [179]. However, their lack of modelling tools for the multiple worse-case scenarios (i.e., multiple worse-case scenarios for winds and demands at the same time as the occurrence of an outage) hinders the TSO's ability to analyse and improve decision-making, particularly when considering grid security (i.e., the ability to balance generation and demand even after the occurrence of faults). The worst-case scenarios represent the extreme outcomes that could potentially occur, which TSOs need to manage in addition

to having a flexible operational plan (e.g., contingency plan or operational flexibility) to address. The consideration of these scenarios is vital especially for wind-dominated power systems, since the intensity of extreme wind speeds (i.e., high or low) are causing the wind farms to shut down (i.e. curtailment). Furthermore, projections from regional climate models are anticipated to indicate changes in the frequency and intensity of wind events that are expected to occur in the future [180].Therefore, in this research, incorporating a broader range of worst-case wind energy scenarios (i.e., High wind (HW) and Low wind (LW)) and worst-case demand scenarios (i.e., High Demand (HD) and Low Demand (LD)) with N-1 contingency (i.e., equipment outage) criterion has been investigated for a single period short term operational planning framework formulated as a SCOPF problem. These simulation scenarios have been thoroughly investigated, as demonstrated by the comprehensive case study presented in Section 4.6.1 of this chapter.

4.1.2 Security-constrained Operational Planning with Worst Case Scenarios

The traditional SCOPF formulation (as detailed in section 2.5.3 in Chapter 2) has been modified in order to manage and optimise power system operation under the adverse operating conditions (i.e., the worst-case scenarios (S)). The following is the mathematical expression for the basecase (i.e.,normal operating condition in the MT-HVDC system) optimisation for the worst-case scenarios without consideration of any contingencies (i.e., focusing only on extreme variations of demand and wind resource as outlined above).

$$\min_{x,u} \quad F(x,u) = \sum_{s \in S} f_0^s \left(x_0, u_0\right) \tag{4.1}$$

$$g_0^s \left(x_0, u_0\right) = 0, \quad \forall s \in S \tag{4.2}$$

$$h_0^s \left(x_0, u_0\right) \leq 0, \quad \forall s \in S \tag{4.3}$$

Within the set of numerous scenarios, $S = \{HW, LW, HD, LD\}$, the variable s represents the worst-case scenario, and f_0^s denote for function of total generation cost with $C = 0$. The worst-case scenario equality and inequality constraints, g_0^s and h_0^s are based on the same constraints as traditional SCOPF (i.e., nodal power balance constraints and limits on power flow through transmission lines). The x_0 and u_0 are the state and control variables for the worst-case scenario without contingency. Moreover, to include contingencies based on the $N-1$ reliability criterion (i.e., one outage at a time), the problem presented in (4.1) - (4.3) have been modified to include constraints explicit to contingencies as well as any additional controls from the RAS-FUBM control scheme.

The SCOPF problem formulation considering both contingencies and worst-case scenarios with

RAS-FUBM control scheme is expressed as below:

$$\min_{x,u} \quad F(x,u) = \sum_{s\in S}\sum_{c\in C} f_c^s\left(x_0, u_0, x_c, u_c\right) \tag{4.4}$$

$$g_c^s\left(x_c, u_c\right) = 0, \quad \forall c \in C, \forall s \in S \tag{4.5}$$

$$h_c^s\left(x_c, u_c\right) \leq 0, \quad \forall c \in C, \forall s \in S \tag{4.6}$$

$$|u_r - u_0| \leq \Delta u_r, \quad \forall r \in R \tag{4.7}$$

The function f_c^s, which represents the total generation has been extended to incorporate the contingency case and applied across multiple worst-case scenarios, which are consistent with the set of scenarios discussed previously. The variable c refers to the specific contingency case, where $c \in C$ and C is the set of all contingency indices (i.e., $C = \{1, 2, \ldots, N_c\}$, where N_c is the number of contingencies). The equality and inequality constraints g_c^s and h_c^s refer to the specific binding constraints for contingency case c - notice that these contingencies may not necessarily be same as the contingencies for the pre-contingency case where $c = 0$. The state variable x_c refers to the contingency and the state control in the RAS-FUBM action is denoted by symbol u_r. The constraint of RAS-FUBM control (r) in the set of permitted control in the RAS-FUBM (R) corresponds to equation (4.7).

A probability reliability assessment needs to be considered while analysing the integration of wind power within the power system analysis, since wind energy exhibits constrained and intermittent characteristics [181]. This probability consideration is crucial, as the inherent variability and uncertainty of wind generation could have an adverse impact on the overall reliability of power system, particularly in the worst-case scenario. The SCOPF formulation given above can therefore be modified to take into consideration the probabilistic nature of the wind resource, which is presented below again considering an $N-1$ reliability criterion:

$$\min_{x,u} \quad F(x,u) = \sum_{s\in S}\sum_{c\in C} w_s f_c^s\left(x_0, u_0, x_c, u_c\right) \tag{4.8}$$

$$g_c^s\left(x_c, u_c\right) = 0, \quad \forall c \in C, \forall s \in S \tag{4.9}$$

$$h_c^s\left(x_c, u_c\right) \leq 0, \quad \forall c \in C, \forall s \in S \tag{4.10}$$

$$|u_r - u_0| \leq \Delta u_r, \quad \forall r \in R \tag{4.11}$$

where variable w_s refers to the probabilities associated with scenario $s \in S$. For example, the probability of the high wind scenario (w_{HW}) can be defined as, w_{HW}=0.5 if the likelihood of high wind is 50%, and the probability of the low wind scenario (w_{LW}) can be defined as w_{LW}=0.25 if the likelihood of low wind is 25%. In this case, the objective function calculates an expectation of the cost of operation across all scenarios. However, in the worst-case scenario case study presented, the probability has been fixed for all worst-case scenarios, with w_s=1 assigned a value of 1.

The aims of the SCOPF with multiple worst-case scenarios is:

(a) To conduct a comprehensive risk assessment by identifying and analysing various worst-case scenarios of wind generation and demand variations

(b) To address a potential range of contingencies (i.e., outages of transmission lines or generators) and develop control strategies to mitigate the negative outcome of such contingencies (e.g. to alleviate network congestion and/or voltage profile variation)

(c) To ensure the EPS has appropriate plans and actions to cope with multiple extreme scenarios.

(d) Allow more thorough preparation and development of a robust contingency plan.

4.2 Multiple Period Operational Planning

Predicting demand behaviour is crucial, as daily demand is constantly changing due to a variety of contributing factors such as: a) consumption of electricity in a residence or industry; b) price of electricity; c) seasons; and d) economic conditions [182] [183]. Meanwhile, the wind power generation fluctuates over time, resulting in an increased level of uncertainty, because wind forecasts are influenced by dynamic weather conditions and the inherently intermittent nature. The simulations in many of the current research on wind power integration studies are predominantly using a single time period, which makes it challenging to analyse the variability and uncertainty within this time frame. However, in practical real-world applications, demands and wind forecasts are continuously updated within a multi-temporal framework, and any forecast errors will, consequently, impact the EPS in multiple aspects including reliability and economic performance [184]. Furthermore, the aim of power systems operational planning is to properly plan the operation of the system, including planning any control actions to deploy flexibility, given the hourly pattern of electricity demand and wind power forecasts to ensure the flexibility. In the context of multi-period operational planning, the term flexibility refers to the ability of the power system to deal with uncertainty and variability for both generation (i.e., wind power) and demand, while still adequately maintaining a reliable (i.e., stable and secure) system operation even as disturbances or unexpected situations occur, at an economical cost over a specific planning time horizon [185]. Therefore, the necessity to predict both demand and wind energy has driven the development of multi-period models within short term operational planning of power networks.

The need for the multiple time period modelling is to provide a detailed planning road map, which can capture the variability and uncertainty of wind generation and demand projections. This enables the operational planning framework (including any control actions to deploy additional flexibility if needed) to be easily and seamlessly implemented in real-time control actions, which is a critical consideration for modern power system with growing levels of wind integration. This integration has led to intricate impacts on EPS operation, particularly for the TSOs, who now carry

the vital responsibility of effectively scheduling the energy production from diverse generation units (i.e., conventional generators will typically be taken into consideration once wind power has been fully dispatched to its maximum output) [186], in order to achieve an optimal balance between generation and demand. The multi-period modelling approach can substantially mimic the hourly pattern of power system operation, which can offer significant advantages in terms of cost effectiveness, system reliability [187] and operational security as compared to the model of single period operational planning. However, developing multi-period operational planning framework requires modifications of mathematical formulation of the single-period planning framework, which makes the process more complicated, especially for larger-scale power system. This increasing complexity also directly affects the computational expenditure of solving the ensuing multiple period (multi-period) problem, especially for larger systems. Therefore, faster computing speed and higher efficiency on the computer hardware are required to provide insight, which is necessary for understanding how real time operation operates under different time horizons through a variety of assumptions.

To incorporate hourly variability of demand and wind resource into the multi-period planning framework presented in this thesis, a scaling factor has been used which scales randomly a given basecase demand/wind profile for all buses/wind generators respectively across all planning time periods. Furthermore, the partitioning concept of power systems has been applied in multi-period planning, simplifying the operation and management of power systems by breaking them down into manageable smaller subsystems or zones. Together, these two elements, scaling factor and partitioning, will be explained in more detail in the following section.

4.2.1 Scaling Factor

In a single period deterministic OPF, the demands modelled are constant and represented as a specified quantity of real and reactive power consumed at a particular bus. These standard demands are formulated as follows:

$$S_d^i = P_d^i + jQ_d^i = D_d^i \tag{4.12}$$

With i is the bus index, S is the complex power (MVA), P is the demand active power (MW), and Q is the demand reactive power (MVAR). The matrix size representing complex demands at all buses is N_b x 1, which N_b refers to the number of buses.

A standard non dispatchable wind generator is represented by a complex power injection at a specific bus (modelled essentially as negative demand), and the formulation for this power at generator k is as below:

$$S_g^k = P_g^k + jQ_g^k = W_g^k \tag{4.13}$$

Where S is the complex power (MVA), P is the generator active power (MW), and Q is the

generator reactive power (MVAR). The size of the vector containing all wind generators is $N_w \times 1$, where N_w is the number of all wind generators (a subset of all generators) [176]. In a single period problem, the vectors D_d^i and W_w^k in equations (4.12) and (4.13) can be represented in the following form:

$$D_d = \begin{bmatrix} d_1 & d_2 & d_3 \cdots\cdots d_i \end{bmatrix}^{\mathrm{T}}_{N_b \times 1} \tag{4.14}$$

$$W_w = \begin{bmatrix} w_1 & w_2 & w_3 \cdots\cdots w_i \end{bmatrix}^{\mathrm{T}}_{N_w \times 1} \tag{4.15}$$

Where N_b and N_w are numbers of buses and wind generators respectively. To extend this single-period formulation to multiple periods, scale factors (α) are introduced that are sampled from a uniform (u) distribution (i.e., $\alpha \sim u(0,1)$), which can be defined for each time period $t \in [1, \ldots, N_t]$. This will yield a $1 \times N_t$ row vector as seen in (4.16). The scale factors for wind and demand in the vector form can be expressed as shown below:

$$\alpha = \begin{bmatrix} \alpha_1 & \alpha_2 & \alpha_3 \cdots\cdots \alpha_t \end{bmatrix}_{1 \times N_t} \tag{4.16}$$

From equations (4.14), (4.15) and (4.16) the demand and wind models for the multiple period scenarios at time t at bus j and wind k are represented by matrices S_d^t and S_w^t:

$$S_d^t = D_j \alpha_d^{\mathrm{T}} \tag{4.17}$$

$$S_d^t = \begin{bmatrix} \alpha_1 d_1 & \alpha_2 d_1 & \cdots & \cdots & \alpha_t d_1 \\ \alpha_1 d_2 & \alpha_2 d_2 & \cdots & \cdots & \alpha_t d_2 \\ \alpha_1 d_3 & \alpha_2 d_3 & \cdots & \cdots & \alpha_t d_3 \\ \vdots & \vdots & \ddots & \ddots & \vdots \\ \alpha_1 d_j & \alpha_2 d_j & \cdots & \cdots & \alpha_t d_j \end{bmatrix} \tag{4.18}$$

The demand matrix of S_d^t is represented by equation (4.18), which is D_j multiplied by α_d^{T}. On the other hand, the wind generator matrix form of S_w^t is represented by equation (4.20), which is W_k multiplied by α_w^{T}.

$$S_w^t = W_k \alpha_w^{\mathrm{T}} \tag{4.19}$$

$$S_w^t = \begin{bmatrix} \alpha_1 w_1 & \alpha_2 w_1 & \cdots & \cdots & \alpha_t w_1 \\ \alpha_1 w_2 & \alpha_2 w_2 & \cdots & \cdots & \alpha_t w_2 \\ \alpha_1 w_3 & \alpha_2 w_3 & \cdots & \cdots & \alpha_t w_3 \\ \vdots & \vdots & \ddots & \ddots & \vdots \\ \alpha_1 w_j & \alpha_2 w_j & \cdots & \cdots & \alpha_t w_j \end{bmatrix} \tag{4.20}$$

The proposed scaling factor is able to modify standard demands and wind generations, enabling variability in both profiles across different time periods. This factor can be higher or lower depending on its application in the network analysis, representing a range of wind/demand profiles.

4.2.2 Partitioning Technique

In load flow analysis, wind generators are represented as negative loads in the power system. Furthermore, some literature models these non-dispatchable generators as a PQ bus [188] [189], by specifying an active power and a given power factor, with calculated reactive power consumption. However, in the multiple-period operational planning model developed in this thesis, the wind generator is represented as a PV bus (a type of bus described in section 2.4.2 of Chapter 2), where the active power is specified. Furthermore, this multi-period model incorporates the partitioning technique to facilitate the scalability of active power for demand and wind generation. This technique is implemented by grouping several buses into zones and the scale factor allows for the increment and decrement of active power. The partitioning technique is a method that divide a large power system into smaller subsystem or zones, which can be classified into different types such as geographic partitioning, operational partitioning or hierarchical partitioning. The advantages of this method include reducing computational burden (e.g., memory usage, energy consumption and processing time) and achieving faster simulation speed [190] for the optimisation problems.

This thesis utilises the operational partitioning to divide the hybrid AC/DC network into multiple zones, employing a load zone concept within the power system model. The load zone is a conceptual framework used to aggregate and manage the demand within a specific area of the power system. Each bus in the power system is represented by a value in a vector. In this vector, each value can either be:

- A number (index): This indicates the specific load zone that the bus belongs to.
- Zero: This means the bus does not belong to any load zone.

Let consider Z as a load zone consisting of multiple buses (b), which can be defined as:

$$Z = \{b_1, b_2, b_3, \ldots, b_n\}, \quad \forall n \in N \cup W \tag{4.21}$$

where n refers to the number of buses, N represents a set of demands and W represents a set of wind generations. It can be stated that n can either be the set of demands, the set of wind generations or belongs to both sets. Once the load zone has been defined, the total active power for demand, wind generation or a combination of both in that load zone, represented by P_z, can be increased or decreased using a scaling factor (β), where the value must be a positive integer ($\beta \geq 0$). This statement can be mathematically express as:

$$P_z^{\text{scale}} = \beta \sum_{n=1}^{N_b} P_z, \quad \forall n \in N \cup W \tag{4.22}$$

Where P_z^{scale} is the total scale active power either for demand or wind generation and N_b is the number of buses. If the load zone (Z) is set to zero, the active power at both demand and wind generation will not be modified.

In summary, the load zone concept allows for efficient management and analysis of power system operations within clearly defined operational boundaries. By aggregating demand and wind generation using the operational partitioning technique based on the load zone concept, this approach enables more streamlined adjustments to active power, allowing for increases and decreases to be made collectively rather than on an individual basis.

4.3 Contingency Analysis

The loss of equipment can cause changes in power flow and voltage, potentially leading to voltage drops or thermal overloads that may have a huge impact on the EPS. Predicting which outages are critical is challenging, as the simulations are performed simultaneously. Therefore, it is necessary to perform a security assessment by evaluating the effects of individual equipment outages. The most common approach utilised by researchers and TSO to anticipate the consequences of equipment failures is known as Contingency Analysis (CA) [191]. The CA is crucial in operational planning of modern power systems, due to the undergoing structural changes in the power generation (i.e., increased integration of renewable energy sources) and electricity demand (i.e., growth of smart devices and electric cars). The CA procedure involves modelling single failure events (N-1) and multiple failure events (N-k) in sequence, evaluating each scenario until all credible outages have been examined. The process in the CA verifies that all EPS voltages and thermal limits are within their respective bounds for every outage examined. However, the most challenging aspect of CA is the accuracy of the method [192] in selecting the most credible outages that have the most severe impact on the EPS . Additionally, there are a large number of contingency possibilities, which

would make this analysis time consuming, computationally burdensome and costly. In practice, TSOs only select a small number of contingencies that may be critical to the security and reliability of the power system. Once these critical contingencies have been identified, only these contingencies will be analysed to determine their effect. The process of identifying these critical contingencies is known as Contingency Ranking, where the contingencies are ranked in terms of severity [193].

4.3.1 Contingency Ranking

Contingency Ranking methods can be divided into two categories: Performance Index (PI) (i.e., in this research known as Severity Index (SI)) and screening. The screening method relies on approximating network order, such as the local outage distribution factor. On the other hand, the PI method is based on the severity of outages using either a rapid automated method, human assessment (i.e., years of operating experience) or combination of both [194]. In this research, the focus is only on PI technique, which is used to evaluate the EPS state after certain disturbances, and therefore, estimate the severity of each contingency. The SI analysis is crucial for identifying the most critical lines or generators in the EPS, which addresses how the EPS variables (e.g., voltage and power) deviate from their rated values. The higher the SI number means the more severe the impact of contingency to the EPS [195]. This makes the SI method well-suited for evaluating different contingencies relative to each other, because it ranks the contingencies based on how the relevant system or indicator reacts to the changes brought by those contingencies [196]. The general formulation for the SI is:

$$F = \sum f_i \tag{4.23}$$

where f_i refers to the function representing the overloading condition at ith outage, which can be related to the current, active power, reactive power, or bus voltage. The most common SI formula is shown in (4.24) with small x represents the overloading condition, whilst X^{max} refers to the upper limit of that condition. W is a weighting factor and n is the penalty factor, which should be a positive integer.

$$F = \sum W \left(\frac{x}{X^{\max}}\right)^{2n} \tag{4.24}$$

In this research the SI focus is solely based on the active power flow (loading in each line), and it is formulated as follows:

$$SI = \sum_{k=1}^{n} W \left(\frac{P_k}{P_k^{\max}}\right)^{2n} \quad k = 1, 2, 3 \ldots\ldots, N_l \tag{4.25}$$

Where P_k is the power flow from line k, P_k^{max} is the upper thermal limit for line k, and N_l is the number of branches. The ranking list was then determined by calculating the severity of each scenario (i.e., HW Low Demand (HWLD), HW High Demand (HWHD), LW Low Demand (LWLD), and LW High Demand (LWLD)). The sum of the severity of each scenario gives the

Contingency Ranking Index (CRI) values, through ranking the following formulation:

$$CRI = \sum_{i=1}^{N_s} S_i, \quad i = 1, \ldots\ldots N_s(\text{ i.e.number of scenario}) \tag{4.26}$$

Based on these equations (4.25) and (4.26) , the severity of contingencies can be ranked from the highest to the lowest, providing valuable information for TSOs to identify congested lines and take necessary measures to mitigate them.

4.4 Remedial Action Scheme

The management of the power transmission system refers to not merely the balancing of supply and demand, but also the requirement to uphold security of operation (i.e., the ability to withstand and alleviate the impact of any contingencies under a given reliability criterion). In order to ensure the overall security and reliability of the transmission system, as well as to meet regulatory compliance standards, the Remedial Action Scheme (RAS) has frequently been regarded as an attractive mitigation approach. This is primarily due to its straightforward design, easy implementation and economical control strategies, as compared to other alternative solutions [197]. The definition of RAS as per [198], is *a scheme designed to detect predetermined system conditions and automatically take corrective actions.* The aims of this scheme are to [199]:

(a) Maintain system stability.

(b) Maintain appropriate voltage levels.

(c) Maintain appropriate power flows (i.e., thermal limits).

(d) Minimise the impact of contingencies, congestion, catastrophic or cascading events (e.g., overloading thermal, voltage instability, transient instability, hidden failures in protection system).

In the process of developing the RAS, a number of important criteria have to be taken into account [200]:

(a) Compliance with regulatory reliability.

National Grid ESO in the UK has outlined system defence plan related to the system protection scheme aka RAS, which must adhere to the Network Code on Emergency and Restoration (NCER). The accordance in NCER Article 15 has a guideline for an automatic under frequency control scheme and an automatic low frequency demand. Whilst Article 16 and Article 17 underlines the automatic over frequency control scheme and automatic schemes against voltage collapse, respectively [201].

(b) Severity of violations.

The implementation action depends on the severity of the violations. If the violations are severe such as voltage collapse or cascading, the RAS actions should be implemented instantaneously. If the violations less severe including slight overloading thermal or voltage violations, the RAS actions may take delayed action to coordinate with other components or nearby protective relays. The RAS action also include the redispatch or reduce the loads or generations for the alleviation of violations.

(c) Security and dependability of RAS.

The security is related to the response of RAS actions in certain degree of certainty, which means that when there are no disturbances present there will be no actions taken. A number of precautions are also made to prevent mis-operation caused by measurement or communication errors. The RAS design and implementation should include failure analysis followed by risk mitigation measures such as voltage monitoring and control, power flow management, increased redundancy or more reliable components. Dependability of this scheme has to do with how certain the RAS actions will respond to the disturbances, such as independent DC supply system, control coordination, independent communication system, coordination and back up of the two RAS systems or consideration of components failures such as breakers or switching system.

(d) The feasibility of implementing RAS.

In the technical feasibility related to the infrastructure and system capabilities need to be feasible to initiate the RAS responses. This includes having software capabilities to solve the computational challenges (i.e., numerical solutions), control devices to enable fast and reliable RAS actions and available communication systems. Additionally, the scalability and expandability of RAS are important factors. The RAS design should be able to handle the increasing system complexity and allow expansion as the grid evolves over time.

The utilisation of RAS is often considered as a cost-effective alternative for transmission planning optimisation, particularly in scenarios where the capital expenditure associated with transmission system expansion is prohibitively high. However, this approach has drawbacks in the implementation that add complexity to the transmission system problem and require careful design to ensure all possible events are captured and the system is not prone to false triggering [202]. The RAS can be categorised into two types: conventional RAS related to current implementing actions and the RAS-FUBM that has been developed as part of this research. Both types of actions will be explained in detail in the following section.

4.4.1 Conventional RAS

The conventional RAS is related to a range of corrective action interventions that can be performed based on the following categories [203]:

(a) **Event-based approach**: This approach is activated during contingencies to identify outages or faults in the EPS and performs pre-planned targeted action to alleviate the problem. Furthermore, this approach is also designed to reactively respond to specific situations such as overloading transmission line.

(b) **Response-based approach**: This approach is designed to be activated in response to detected instability or abnormal operating conditions (i.e., disturbances) within the EPS, including frequency drops or voltage drops. Additionally, this approach is programmed to reactively respond based on measurement of various system variables.

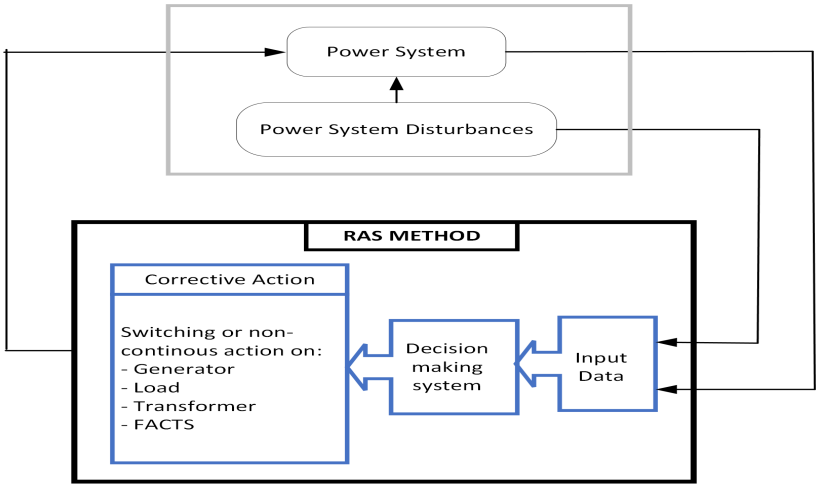

Figure 4.1: Standard RAS structure.

Figure 4.1 shows the standard RAS conventional structure with the corrective actions. When there is a disturbance in the EPS, all the input data (e.g., information related to the components and discrete events) is collected and sent through to RAS scheme that has been designed. Then, the scheme analyses all the data and provide an appropriate decision-making plan for the TSO. Finally, the corrective actions (i.e., switching or non-continuous actions) are performed on components such as load shedding, generation rescheduling, FACTs devices, Transformer (i.e., utilisation of on load tap changers) [204].

4.4.2 RAS-FUBM

The development of the 'VSC in model' by [205] has allowed for incorporating the additional controllability features of the VSC within a typical operational planning framework. In this thesis, taking advantage of the modelling flexibility of the FUBM, which was previously presented in

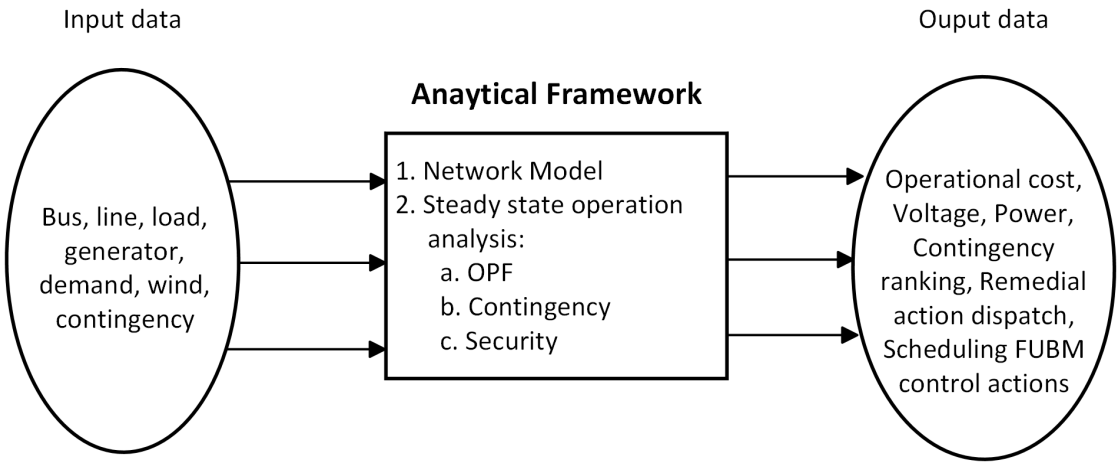

Figure 4.2: RAS-FUBM Framework

section 3.1 of Chapter 3, a new RAS scheme is introduced which can be used within any short-term operational planning framework to plan and deploy additional flexibility control actions promised by the VSC. This modelling capability is even more critical for security-constrained planning frameworks for networks with large-scale offshore wind generation capacity because it will allow the TSO to make use of the additional control actions available by the VSCs, which are often used to integrate large-scale offshore wind generation capacity to the network (in form of for example MT-HVDC links).The RAS-FUBM control, which is based on an event-based approach can therefore be considered as a novel approach to extend the conventional RAS and can be used in hybrid AC/DC networks. Mathematically, the RAS-FUBM scheme is an improved optimisation model for modelling the operation of various control strategies for the VSCs within any network that has converter-interfaced resources such as offshore wind turbines. The framework is illustrated in Figure 4.2. By incorporating multiple control mechanisms, the RAS-FUBM control is designed to:

(a) Alleviate the congestion in transmission lines within a hybrid AC/DC network.

(b) Reduce the security risk posed by uncertainty in the wind power in systems with high penetration of offshore wind generation capacity.

(c) Enhance the security and stability of hybrid AC/DC systems which have embedded MT-HVDC links.

Figure 4.3 illustrates the detail outline of the RAS-FUBM framework, which consists of three main parts: input data, analytical framework and output data. The input data is a data collection process that can be sourced from historical records, measurements, and simulation studies. It contains an information either from the components (e.g. buses, transmission lines or generators), scenarios (e.g., demands or wind powers) or discrete events (e.g., malfunction or failure equipment).

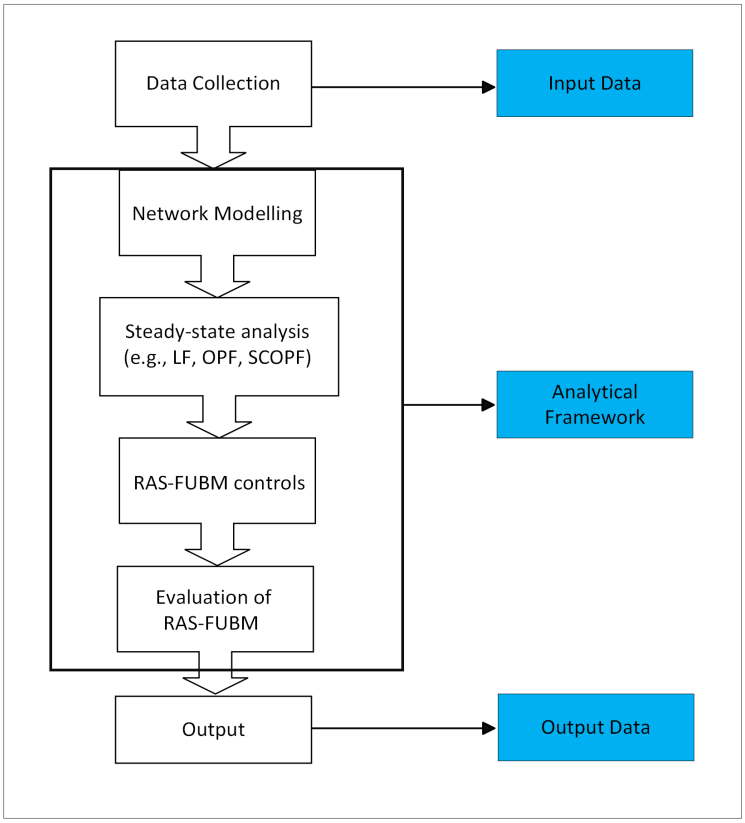

Figure 4.3: Detail outline of the RAS-FUBM framework

The second part is an analytical framework, which involves network modelling, steady-state operations and RAS-FUBM actions. The development of network modelling is to capture connectivity and physical characteristics of the system, which aims to simulate and analyse the behaviour of power system components. Some key points that need to be considered in the network modelling are:

(a) Network elements (i.e., characteristics and parameters of each component).

(b) Topology such as connection points and paths for the power flow.

(c) Impedance and admittance.

(d) Power flow equations such as Kirchoff's Law, Ohm's Law or Newton Raphson.

(e) Bus representation (i.e., slack bus, load or generator buses).

Third step in this framework is the steady-state analysis that involves running the simulations based on the scenarios (e.g., basecase, contingency or multiple period), analysing the results, making necessary adjustments and repeating the process again to achieve the desired outcome. The simulations are performed using software tools such as MATPOWER, AIMMS or CPLEX. The aim of this process is to solve the power system optimisation problem that can be either OPF,

SCOPF or contingency analysis. The system is assessed on critical variables such as voltages, powers or currents to identify potential issues related to stability and security. The RAS-FUBM controls to identify critical system conditions and trigger appropriate actions, to mitigate the contingencies or congestions. The last process in the analytical framework is evaluation of the RAS-FUBM performance, which measures how well the RAS-FUBM meets the defined objective during different scenarios. The final part is the output data that represents the production of satisfactory results, which is intended to ensure the power system's performance meets its objectives, whilst it operates in a secure and reliable manner.

4.5 Security Constrained Multi Period Optimal Power Flow Formulation

The time-dependent in presence of emergent flexibility resources should be included in a comprehensive SCOPF problem, in order to effectively manage wind energy's uncertainty and variability [206]. Furthermore, power system is dynamic by nature; therefore, conducting a SCOPF based on a multi-period strategy is necessary, due to the fluctuations exhibited by electricity demand and wind power generation over time. Managing these fluctuations is essential, as they significantly influence the variables in the power system (e.g., voltage, power flows and cost). In order to replicate the real-world operation of the power system, the standard single period SCOPF has been expanded in this research to a multiple period operational planning, incorporating RAS-FUBM scheme. The following is the mathematical formulation of the new SCOPF problem that includes time-dependent variables:

$$\min_{\substack{x_{0t},u_{0t}.....\\ x_{ct},u_{ct}.....\\ x_{rt},u_{rt}}} f\left(x_{0t}u_{0t}\right) \tag{4.27}$$

subject to:

$$g_{n,c,r,t,t}\left(x_{c,r,t}u_{cc,r,t}\right) = S^{g}_{(n,c,r,t)} - S^{d}_{(n,c,r,t)} + S^{bu}_{(n,c,r,t)}, \quad n \in N, c \in C, r \in R, t \in T \tag{4.28}$$

$$h_{n,c,r,t}\left(x_{c,r,t}u_{c,r,t}\right) \leq S^{\max}_{(n,m),c,r,t} \quad (n,m) \in L, c \in C, r \in R, t \in T \tag{4.29}$$

$$x_{\min(n,g)} \leq x \leq x_{\max(n,g)}, \quad n \in N, g \in G \tag{4.30}$$

$$|u_{ct} - u_{0t}| \leq \Delta u_{c}, \quad c \in C \tag{4.31}$$

$$|u_{rt} - u_{ct}| \leq \Delta u_{rt}, \quad r \in R, t \in T \tag{4.32}$$

The variable t indicates the time periods, whilst x_{rt} and u_{rt} represent the state and control variables for the RAS-FUBM control strategy actions, which are in the form of:

$$(x_{rt}, u_{rt}) = \begin{pmatrix} P^g & Q^g & VM & \theta & B_{eq} & \theta_{sh} & m_a & G_{sw} \end{pmatrix}^{\mathrm{T}}$$

The variables B_{eq}, θ_{sh}, m_a and G_{sw} refer to the following: susceptance, shift angle of the VSC, tap changer ratio for the Controlled Tap-Changing Transformers (CTT) and VSC switching losses, respectively. The variable θ is the voltage angle refers to the phase angle of the nodal voltages at different buses. On the other hand, θ_{sh} denotes the phase angle of the VSC, which functions similarly to the phase angle of the Phase Shifter Transformer (PST) in controlling the active power flow between two nodes to maintain the quality of the power supply. In this research, both variables are expressed in degrees. The coupling constraint in equation (4.32), which is included in the multiple period SCOPF formulation, establishes the maximum allowable action controls in the RAS-FUBM following post-contingency states. These control actions refer to the corrective measures that need to be implemented during contingency scenarios to ensure the network system always remains secure and reliable.

4.6 Case Study

Both single-period and multi-period operational planning are included in the case study. The single period analysis takes into account several worst case scenarios with contingency, whilst multi-period analysis looks at a 24-hour time horizon and account for contingencies as well.

4.6.1 Simulation: Single Period Operational Planning

Optimisation scenarios presented in this case study involve the approach described in section 4.1. The worst-case scenario (i.e., HW, LW, HD, LD) is applied to the modified IEEE30 bus system (refer to Figure 4.4) integrated with three wind farms to perform the SCOPF simulations and evaluate the RAS-FUBM application. The bus, branch, and generator data for the IEEE 30-bus AC system are provided in Appendix B. The DC parameters and converters data utilised in this case are consistent with Table 3.4, which was presented in the case studies (section 3.4) in Chapter 3. Multiple scenarios, both with and without contingency (i.e., contingency case follow the N-1 rule, which is an outage at branch 38) have been considered as a critical case, which requires RAS actions to restore a secure operational state. The simulation program is executed on the MATLAB platform, and the contingency simulation did not create any islands.

Result and Discussion

The results of the SI calculations for the various worst-case scenarios have been plotted in the graph shown in Figure 4.5, in accordance with the SI formulation as outlined in equation (4.24). From this graphical illustration, it can be observed that the case without contingency has the lowest CRI values relative to the whole contingency case. On the other hand, as can be seen from the

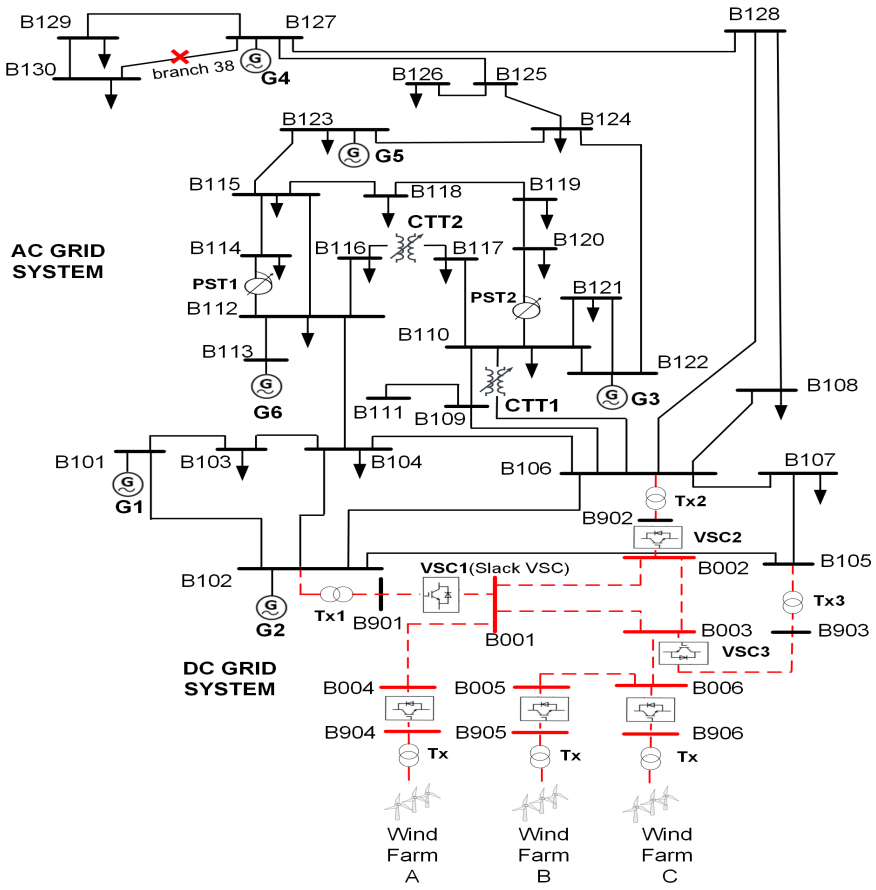

Figure 4.4: MT-HVDC network model

graph, the thermal stress within the system escalates across all worst-case scenarios (i.e., HWLD, HWHD, LWLD, LWHD), when an outage occurs at branch 38. It is noteworthy to point out that the CRI rises in proportion to the elevated levels experienced by the demand situations, for cases HWHD and LWHD. In contrast, the CRI dramatically drops when the demand scenarios hit their lowest points, as observed in cases HWLD and LWLD.

In the basecase, the congestion is not severe as observed in the SI numbers (i.e.,4.2982 (HWLD), 6.0687 (HWHD), 3.2635 (LWLD), 5.2258 (LWHD)) which show the lowest values compared to the other cases. Nonetheless, when branch 38 is disconnected the severity worsen for all scenarios (i.e., HWLD, HWHD, LWLD, LWHD) as can be seen from the SI values (i.e.,4.9559 (HWLD), 6.8679 (HWHD), 3.9022 (LWLD), 6.0223 (LWHD), as also displayed in Figure 3. In order to alleviate these congestions, particularly during worst-demands scenarios (i.e., HD and LD), control actions have to be implemented, and in these cases, voltage controls (i.e., high and low) have been utilised in the simulations at the reference VSC, which is VSC1. When the VSC is configured to a high voltage setting (i.e., near the upper limit), it is notable that both control schemes exhibit elevated SI values: for the CC = 5.0244 (HWLD), 7.0134 (HWHD), 3.9211 (LWLD) and 6.1383 (LWHD); and for the VDC = 5.0858 (HWLD), 7.045 (HWHD), 3.8336 (LWLD), 6.05 (LWHD). As opposed to

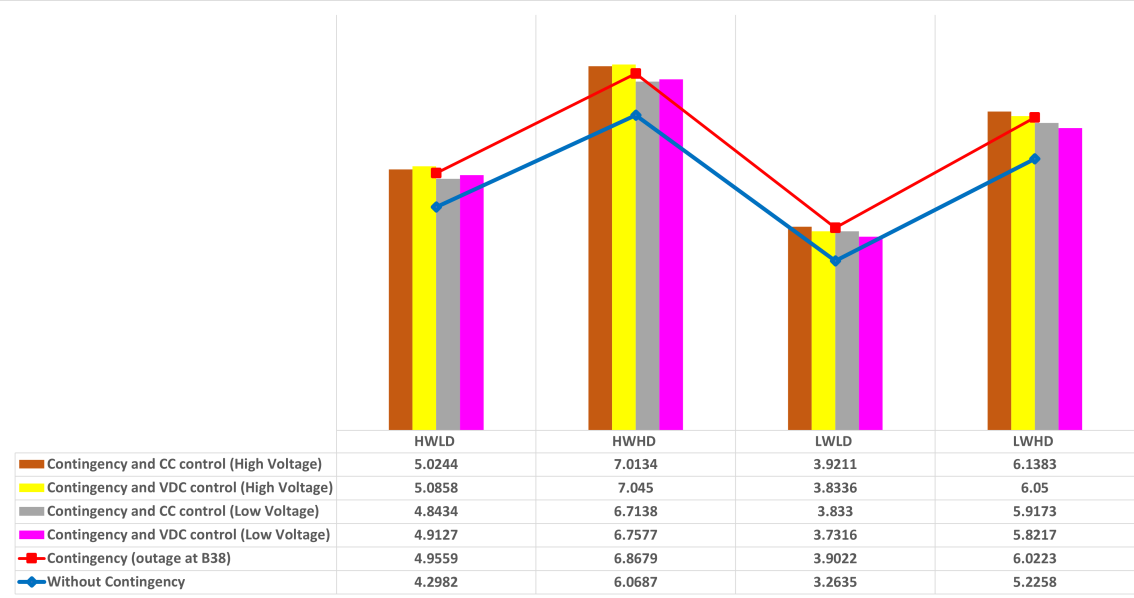

	HWLD	HWHD	LWLD	LWHD
Contingency and CC control (High Voltage)	5.0244	7.0134	3.9211	6.1383
Contingency and VDC control (High Voltage)	5.0858	7.045	3.8336	6.05
Contingency and CC control (Low Voltage)	4.8434	6.7138	3.833	5.9173
Contingency and VDC control (Low Voltage)	4.9127	6.7577	3.7316	5.8217
Contingency (outage at B38)	4.9559	6.8679	3.9022	6.0223
Without Contingency	4.2982	6.0687	3.2635	5.2258

Figure 4.5: Contingency Ranking Index (CRI) for all scenarios based on SI Value

the high voltage setting (i.e., VSC is set to a low voltage setting, which is near the lower limit), the SI values are decreased for both control schemes: for the CC = 4.8434 (HWLD), 6.7138(HWHD), 3.833 (LWLD) and 5.9173 (LWHD)); and for the and VDC = 4.9127 (HWLD), 6.7577 (HWHD), 3.7316 (LWLD) and 5.8217 (LWHD)).

The results from these simulations demonstrated that the ranking in the CRI can be purposefully adjusted, either increased or decreased, depending on the specific DC voltage configuration at the reference VSC. This ranking is considered a valuable guideline for TSOs to maintain vigilance regarding any abnormalities, which may arise within the EPS, particularly when numerous worst-case scenarios happen in the system. Additionally, this allows TSOs to take appropriate corrective actions right away, especially in the case of an unforeseen event. The implementation of necessary control actions is paramount to restoring the power system to a secure state after a contingency, even in the face of multiple concurrent worst-case scenarios. Furthermore, these control interventions have the capability to prevent a cascade of events that might eventually lead to a blackout, or the collapse of the entire system.

Figure 4.6 illustrates the active power generation by the conventional generators for both high voltage and low voltage configurations at the reference VSC, under worst case scenarios with a contingency (i.e., an outage at branch 38). Figures 4.6a illustrate the conventional control with high voltage configuration and Figure 4.6b displays the conventional control with low voltage setting. A closer inspection of graph 4.6a shows that when the voltage setting at the reference VSC is configured to a higher voltage, the active power generation is lower in the cases HWHD (i.e., generators 1, 2) and HWLD (i.e., generators 3, 4, 5 and 6), whilst the active power generation is higher in the cases LWLD (i.e., generators 1, 2) and case HWHD (i.e., generator 4). In Figure 4.6b, there is a slight increase in the active power generation in the cases HWHD (i.e., generators

1, 2) and case LWHD (i.e., generator 4). Figures 4.6c and 4.6d plot the results of the droop control implementation for both high voltage and low voltage configurations at the reference VSC. These results demonstrate a similar pattern of correlations (i.e., relationships) analysis performed under the conventional control conditions. From this statistical analysis of the graphical data, it can be summarised that generators located in close proximity to the DC system, are capable of reducing their active power generation during high voltage configuration, for both the conventional control and droop control under high wind (i.e., HW) conditions. These findings will assist TSOs in selecting appropriate sort of control techniques to mitigate the congestion, especially when considering voltage setting at reference VSC under worst-case scenarios.

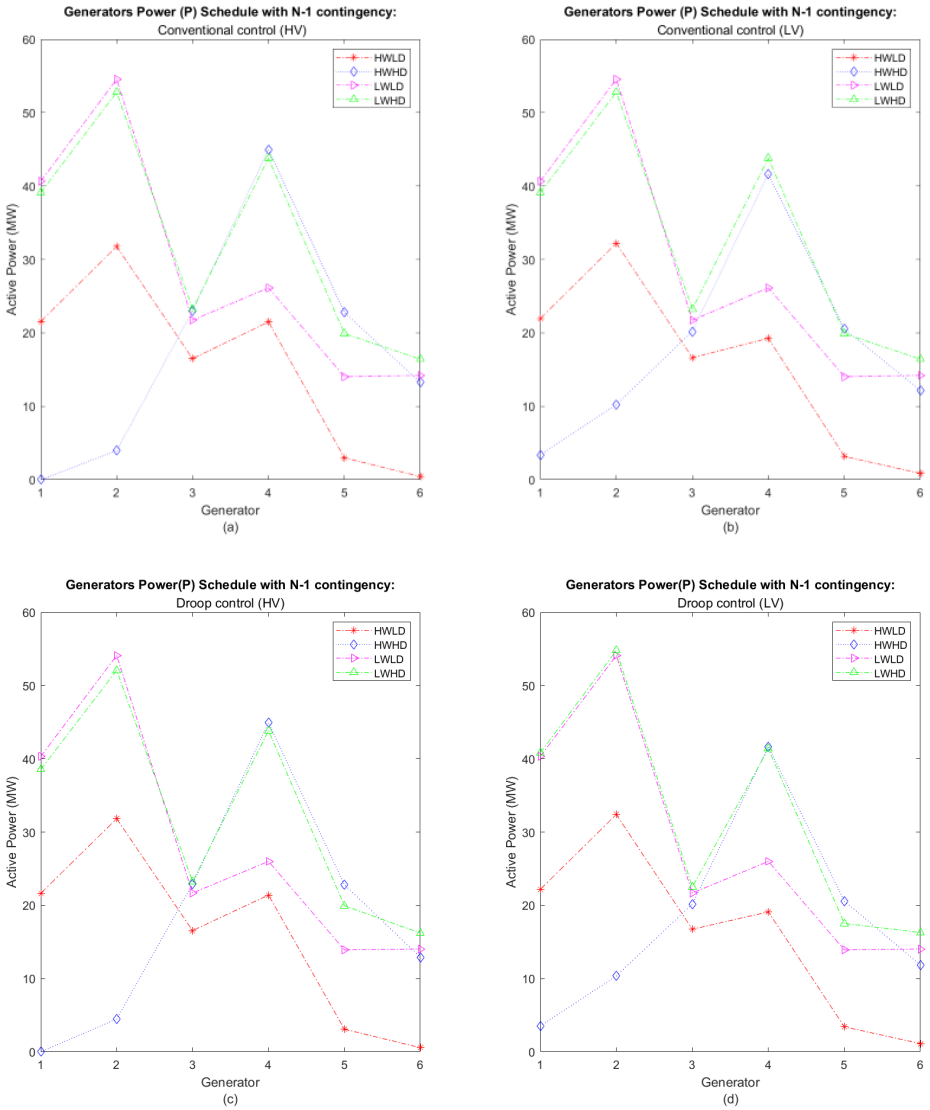

Figure 4.6: Generation optimal active power flow profile for the contingency scenarios with control strategies.

4.6.2 Simulation: Multiple Period Operational Planning

The performance of the proposed multi-period planning model, which is based on the scaling factor technique, is evaluated on the modified IEEE30-bus system. The topology of the modified network system is illustrated in Figure 4.14 that has been divided into two areas employing partitioning technique discussed in section 4.2.2. This partitioned system comprises a DC system with three wind farms located in partition 2, whilst partition 1 contains an AC system. The DC system consists of six DC lines, three converters (i.e., VSC1, VSC2 and VSC3) and three transformers (i.e., Tx1, Tx2 and Tx3), whilst the AC system has six conventional generators (i.e., G1, G2, G3, G4, G5 and G6), 30 buses, 41 transmission lines, and 18 demands. The simulations are performed in Matlab open-source programming language on laptop equipped with an Intel (R) Core (TM) i5-10210U CPU running at 1.60GHz (2.11 GHz), a 64-bit processor and 8.00 GB of RAM. All cases are successfully converged in the MATPOWER platform. The data for IEEE30 bus can be found in Appendix B, and the parameters related to the DC system (i.e., converter and DC grid) are the same as in the single period operational planning model. Table 4.1 provides detailed control settings of the VSCs for the basecase, and also the control settings for both conventional and droop control modes.

Table 4.1: Power Converter Characteristics

Scenario	Converter	Type	Mode	Control Constraint
a) Basecase	VSC1	II	4	$V_r = 1.0 p.u.$
	VSC2	I	3	$P_r = 25MW$
	VSC3	I	3	$P_r = 15MW$
Types of control				
b) Conventional Control				
i. DC Voltage	VSC1	II	4	$V_r = 0.98 p.u.$
ii. Active Power	VSC2	I	3	$P_r = 27.5MW$
	VSC3	I	3	$Q_r = 12MW$
c) Drop Control				
	VSC1	II	7	$V_r = 0.98 p.u.$
				$P_r = 27.5MW$
				$k_{dp} = -0.1$
	VSC2	I	3	$P_r = 12MW$
	VSC3	I	2	$Q_r = -25MVAR$

Three scenarios have been carried out in the multi-period operational planning that are: a) basecase; b) conventional control (i.e., combination control of DC voltage control and active power control); and c) droop control. For all cases, VSC1 is designated as the reference VSC, while the

Table 4.2: Contingency scenario

Contingency scenario	Lines	Generator
Outage 1	Branch 15	-
Outage 2	Branch 31	-
Outage 3	-	Generator 2
Outage 4	-	Generator 6

other VSCs operate according to the control types specified in Table 4.1. In case a (basecase) and b (conventional control) both VSC2 and VSC3 are assigned to active power control, as for case c (droop control) the VSC2 is set to active power control and VSC3 is set to reactive power control. The cases also considered a contingency event that adhered to the N-1 rule (i.e. outage occur one at a time, where only one branch or generator experiences as an outage at a time, as specified in Table 4.2), with 10% probability without creating an island. This probability approach is essential to be included in the steady state analysis, as it enables a more reliable estimation of the risk in the power system [207].

Result and Discussion

The objective function presented in (4.27) is a function related to the total generation cost of conventional generators over a period of 24 hours. From this function the costs for the basecase and contingency cases (i.e., outage at branch 15 and generator 2) are plotted in the graph as presented in Figure 4.7. It can be observed from the graph that the costs for the basecase vary over the 24-hour horizon, with the highest generation cost occurring at hour 20 and the lowest generation cost happening at hour 6. There is an unusual pattern where the costs are negative at hours 2 and 18, likely due to the majority of electricity generation coming from wind farms, as the wind generation costs in this research are set to zero. These costs increase in the event of a contingency (i.e., outages at branch 15 and generator 2) as opposed to the basecase, and it is obvious that these costs rise dramatically when the outage occurs at generator 2. The overall cost generation within 24 hours for the basecase is 6366.62$/MWh, whilst the contingency costs associated with outages at branch 15 and generator 2 are 6390.09$/MWh and 7257.05$/MWh, respectively. This corresponds to a 0.37% increase for the branch 15 outage scenario, whilst the generator 2 outage result in substantially higher cost increase of approximately 14% in respect to the basecase.

The comparison of the increment cost for 24 hours period between branch 15 outage and generator 2 outage is clearly shows in Figure 4.8. From this graph, it is apparent that when the outage happens at generator 2 the total generation becomes higher as compared to the outage at branch 15, especially at hour 20 (i.e., the highest cost) and hour 6 (i.e., the lowest cost). At hour 20 the cost for contingency branch 15 (contingency B15) is 557.58$/MWh and the cost for

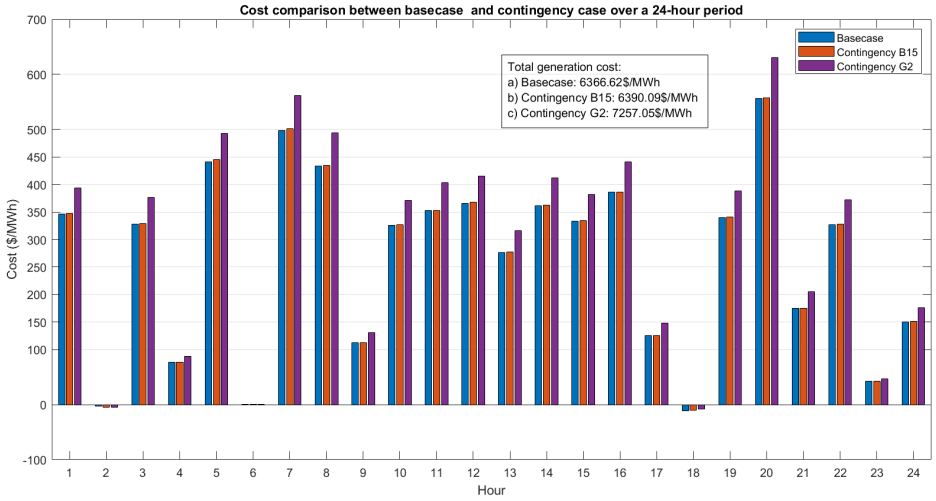

Figure 4.7: Total generation cost over 24-hour period for basecase and contingency case

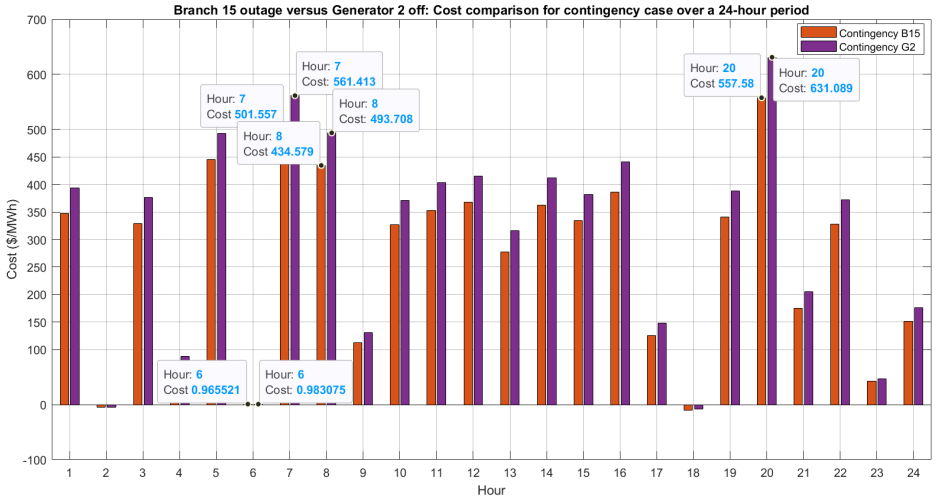

Figure 4.8: Cost comparison: Contingency B15 versus contingency G2

contingency at generator 2 (contingency G2) is 631.09$/MWh, and the difference between both cost is 73.51$/MWh. Further analysis at hour 7 shows that the costs for both contingency B15 and contingency G2 are 501.56$/MWh and 561.41$/MWh, respectively. The difference between both costs is 59.86$/MWh. At hour 8 the contingency B15 cost is 434.58$/MWh and the cost for contingency G2 is 493.71$/MWh, and the difference between them is 59.13$/MWh. As for the lowest cost that occurs at hour 6, the contingency B15 cost is 0.97$/MWh and the contingency G2 cost is 0.98$/MWh, the difference between both costs are relatively small, which is 0.018$/MWh. The observation from these results could be summarised as follow: an outage at the generator would result in higher production costs (i.e., 53.18% from overall cost for both contingencies) for electricity generation from the conventional generators as opposed to the branch outage costs (i.e., 46.82% from overall cost for both contingencies).

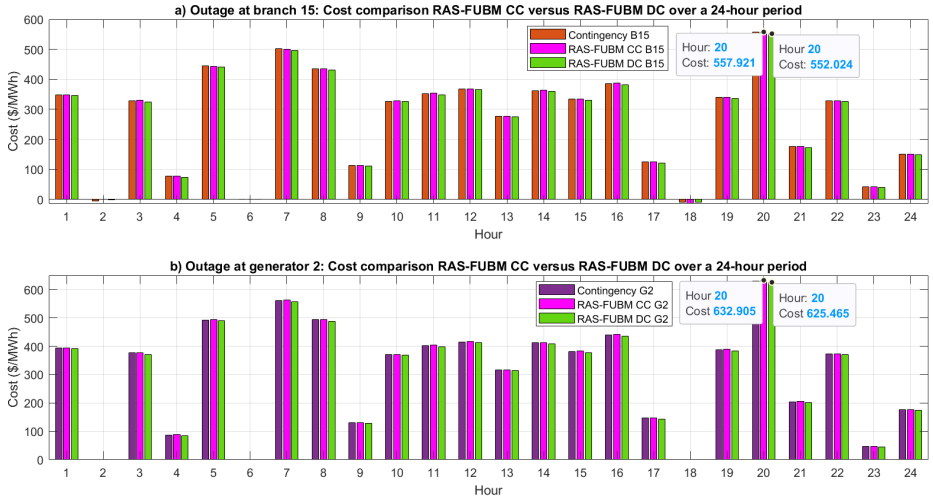

Figure 4.9: Contingency versus RAS-FUBM actions. a) Outage at branch 15 b) Outage at generator 2

As depicted in Figure 4.9, the execution of RAS-FUBM actions shows minimal cost savings for both control methods in terms of the hourly total generating expense when RAS-FUBM actions are executed, when considering the hourly total generating expenditure for electricity within a day. The costs comparison between contingency B15 (i.e., outage at branch 15) and RAS-FUBM actions. (i.e., the RAS-FUBM actions consist of the RAS-FUBM CC and RAS-FUBM DC, which are the conventional control and droop control, respectively, incorporated within the RAS-FUBM approach. Both the conventional control and droop control employ VSCs within the FUBM model, which have been discussed in detail in Section 3.3 of Chapter 3.) is displayed in Figure 4.9a, whilst Figure 4.9b illustrated the contingency G2 (i.e., outage at generator 2) in relation to both RAS-FUBM actions. Analysing the data presented in Figure 4.9a (i.e., Outage at branch 15), reveals that at hour 20, which exhibits the highest cost in the overall period, the cost for the contingency B15 is 557.58$/MWh, whilst RAS-FUBM CC and RAS-FUBM DC are 557.92 and 552.02 respectively. This translates to a saving cost of 0.341$/MWh for RAS-FUBM CC and 5.556$/MWh for RAS-FUBM DC compared to the contingency B15. Examining Figure 4.9b (i.e., Outage at generator 2) at the same hour, the cost for the contingency G2 is 631.09$/MWh. The RAS-FUBM CC cost is 632.91$/MWh, whilst the RAS-FUBM DC cost is 625.47$/MWh. Consequently, the cost saving in relation to the contingency G2 are 1.816$/MWh for RAS-FUBM CC and 5.623$/MWh for RAS-FUBM DC. These calculations clearly show that compared to the RAS-FUBM CC, the RSA-FUBM DC has had smaller effect on the overall generation cost. Both graphs, which demonstrate that the RSA-FUBM DC cost is less than the RAS-FUBM CC cost almost every hour, confirm the result of this investigation. Overall, these outcomes show that both RAS-FUBM action can reduce the total cost of generation, with the RAS-FUBM providing a small further savings in the event of a contingency, such as generator or branch outage.

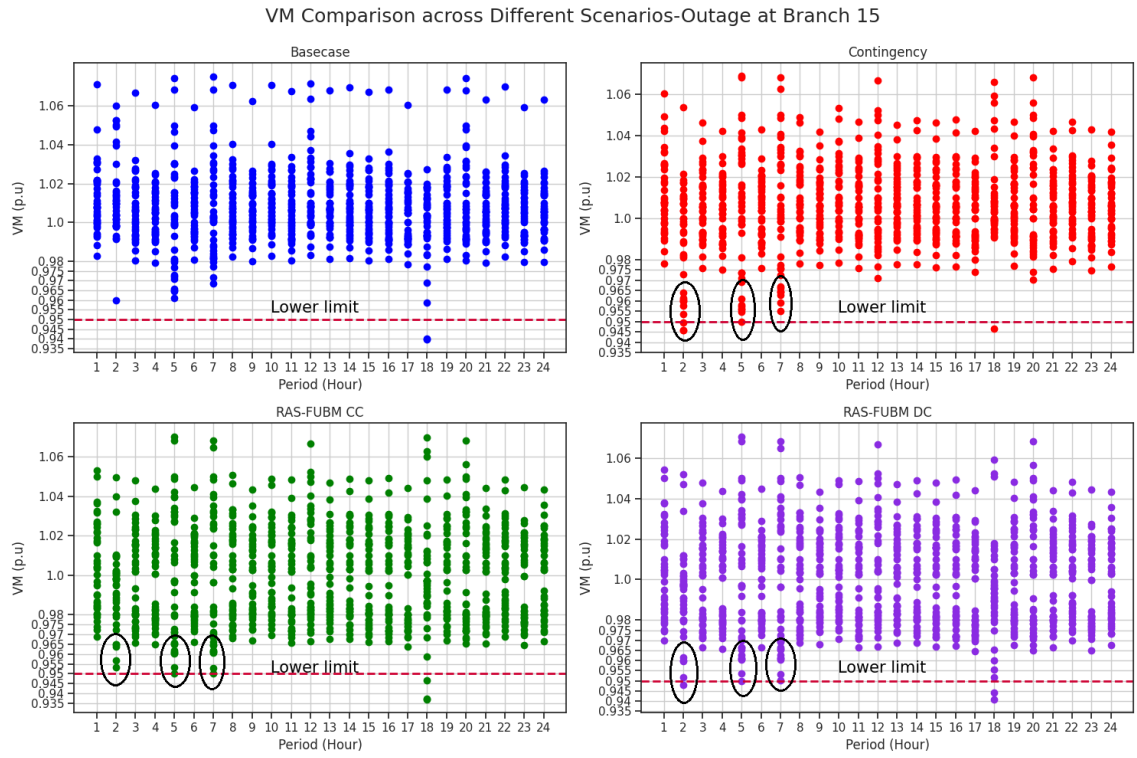

Figure 4.10: VM for all cases across 24-hour period for outage at branch 15

Difference Voltage Magnitude (VM) limitations are applied to an AC and DC systems, with the AC system having two upper limits in particular. The lowest bound for the AC system is 0.95p.u, whilst the upper bounds are set at 1.1p.u for the generator bus and 1.05p.u for the demand bus. The upper and lower limits for the DC system are 1.15p.u and 0.95p.u, respectively. Figure 4.10 depicts the voltage profile outcomes (i.e., basecase, contingency, RAS FUBM CC and RAS-FUBM DC) over a 24-hour period in the event of an outage at branch 15. All VM in the basecase lies within the ranges allowed on both AC and DC systems. However, when branch 15 disconnected (i.e., contingency B15), there is a significant voltage drop below the threshold, as shown by the contingency graph. The voltage drops to 0.94p.u at period 2, and many voltages are lower at periods 5 and 7 compared to the basecase, which is considered an unstable voltage condition. If this voltage instability continues,the power system may not be secure and significant losses could occur, potentially leading to power shutdown or a blackout. RAS-FUBM has been implemented to reduce the risk since it is vital to conduct suitable control in order to mitigate the risk of this situation deteriorating further. When the RAS-FUBM measures are activated, the voltages are increased as illustrated in the RAS-FUBM CC and RAS-FUBM DC graphs at hours 2, 5 and 7.

The effect of voltage instability also occurs when there is a generator outage as shown in Figure 4.11. Even though the voltages are within the permitted range during the basecase, they decrease when generator 2 is turned off. What stands out in this Figure compared to Figure 4.10 is that the number of voltage drop is less, as opposed to the branch outage scenario, where the voltage drop

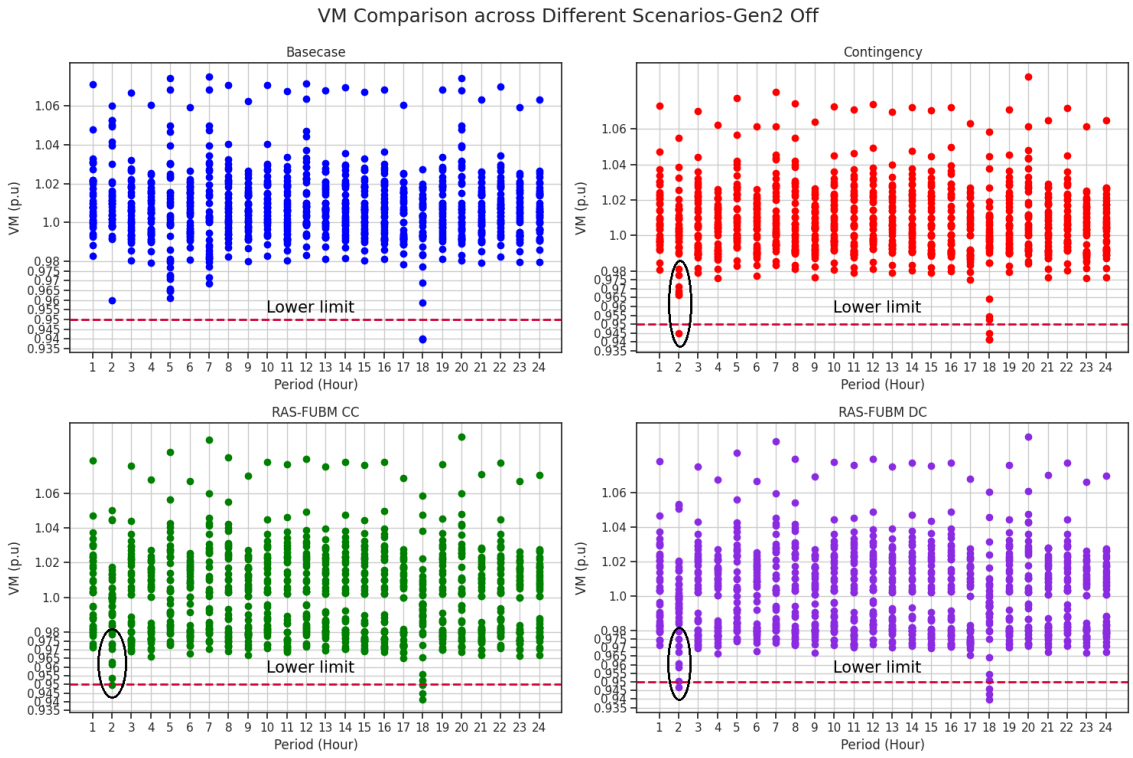

Figure 4.11: VM: Generator 2 off

only occurs at period 2 (i.e., approximately 0.945p.u). These voltages are raised to the allowed levels at the same hour by the RAS-FUBM control actions (refer to the Figure RAS-FUBM CC and RAS-FUBM DC), allowing the power system to operate in a secure and stable manner. The observations drawn from Figures 4.10 and 4.11 provide credibility to the theory that effective controllability can improve voltage stability, which is crucial for strengthening the power system's ability to operate more reliably, securely and stably. Based on these outcomes, when a contingency scenario, such as a branch or generator loss, happens in the system the implementation of RAS-FUBM measures considerably delivers a healthy voltage profile over a 24-hour period. Adopting RAS-FUBM can restore the voltages to an acceptable limit for a steady state operation, particularly in the event of a contingency.

In order to assess the degree of congestion in the MT-HVDC system under several scenarios (i.e., basecase, contingency case, RAS-FUBM CC and RAS-FUBM DC), the contingency ranking approach, as outlined in section 4.3.1, has been applied to the multi-period operational planning model. The Severity Index (SI) for active power flow has been calculated as per equation (4.25). Subsequently, the SI for each branch has been added together using equation 4.26, yielding the overall SI value for each scenario over a 24-hour period, and these values are then ranked and presented on a heatmap. The branch 15 outage is depicted graphically in Figure 4.12, whilst the generator 2 outage is illustrated in Figure 4.13. From the heatmap presented in Figure 4.12, it can be observed that hour 20 exhibits the highest SI value of 0.9418, indicating it represents the

most critical scenario in terms of thermal overloading over the 24-hour period for the basecase. The next most severe thermal overloading occurs at hours 16 and 8, with SI values of 0.7909 and 0.7729, respectively. The lowest SI value on the list is 0.3228, which occurs at hour 6.

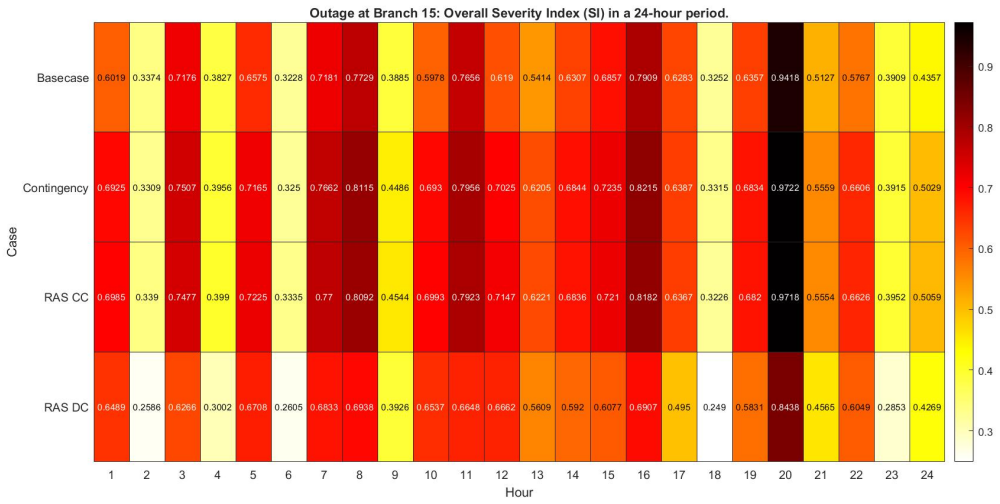

Figure 4.12: SI for outage at branch 15

The list of SI remains unchanged when the contingency occurs (i.e., outage at branch 15), however, the heatmap's SI number indicates level of congestion has intensified. The SI value at hour 20 remains the highest at 0.9722, followed by 0.8215 at hour 16 and 0.8115 at hour 8 in descending order. For the respective hours of 20, 16 and 8, the contingency severity exhibits an incremental percentage of 3.2%, 3.9% and 5% in comparison to the basecase. At hour 6, the lowest SI value in the contingency scenario is 0.325, representing a 0.7% increase higher than the basecase. To alleviate the congestion during contingency scenario, the RAS-FUBM controls (i.e.,RAS-FUBMM CC and RAS-FUBM DC) have been implemented. The application of these control measures has resulted in a significant reduction in system severity, as evidenced by the SI values presented on the heatmap. For the RAS-FUBM CC, the higher SI values are observed in decreasing order: 0.9718 at hour 20, 0.8182 at hour 16 and 0.8092 at hour 8. In comparison, hour 6 has the lowest SI number of 0.3335. The percentage of RAS-FUBM CC decrements relative to the contingency case is 0.04%, 0.40% and 0.28% for hours 20, 16 and 8, respectively. In contrast, the lowest SI value demonstrates a 2.62% increase percentage from the contingency scenario. The RAS-FUBM DC result is similar to the RAS-FUBM CC, nevertheless, the severity in the system is less congested as evidence by the SI number exhibited on the heatmap. The SI values are significantly lower at the same hours as previously described (i.e. hours 20, 16, 8 and 6) than the RAS-FUBM CC, which are 0.8434, 0.6907,0.6938 and 0.2605. Comparing the RAS-FUBM CC with the hours 20, 16, 8 and 6, the SI values in this form of control are decreasing at 13.2%, 15.92% and 14.5% and 19,85%, respectively. The results presented suggest that, in comparison to the RAS-FUBM CC, the RAS-FUBM DC is a more effective control for mitigating congestion. Taken together, the

outcomes of RAS-FUBM CC and RAS-FUBM DC lend credibility to the concept that RAS-FUBM measures are able to alleviate power system congestion, particularly in the event of a contingency strike such as a branch outage.

The heatmap representation from the total SI calculations based on equation 4.26 for the generator 2 outage is presented in Figure 4.13, and the SI ranking list for this contingency matches the outcome of the branch 15 outage. Although the ranking list remains identical with the outage at branch 15, the severity of the congestion appears more severe when generator 2 is disconnected. The contingency SI values for the third highest ranks are 1.22, 0.9504, and 0.9409, observed at hours 20, 16 and 8, respectively. The aforementioned data, when converted to percentage relative to the basecase SI values (i.e., hour 20 is 0.9418, hour 16 is 0.7909 and hour 8 is 0.7729), shows that the relative increments are 29.5% for hour 20, 20.2% for hour 16 and 21.7% for 8. The SI values of 1.226 at hour 20, 0.9536 at hour 16 and 0.9455 at hour 8, demonstrate that the activation of RAS-FUBM CC has resulted in slightly more severe congestion than the contingency case. These values, when converted to percentages, are 0.49%, 0.34% and 0.49%. The lowest SI values for RAS-FUBM CC is 0.3318, which is 2.79% higher than the contingency scenario (i.e., SI value for the contingency is 0.3228, which is the same as basecase). The results for the RAS-FUBM DC are somewhat counterintuitive compared to the RAS-FUBM CC, even though the ranking list is still the same. Referring to the SI values on the heatmap for hours 20, 16 and 8, which are 1.056, 0.7875 and 0.791, respectively, there has been a decrease in congestion for 13.44%, 17.14% and 15.93% of the time. The heatmap's most notable discovering in RAS-FUBM DC case is that the lowest SI value (i.e., 0.2566) has dropped by 20.51% compared to the lowest SI contingency value. Overall, these results indicate that RAS-FUBM DC is more effective to alleviate the congestion in the power system network compared to the RAS-FUBM CC, when there is a generator outage.

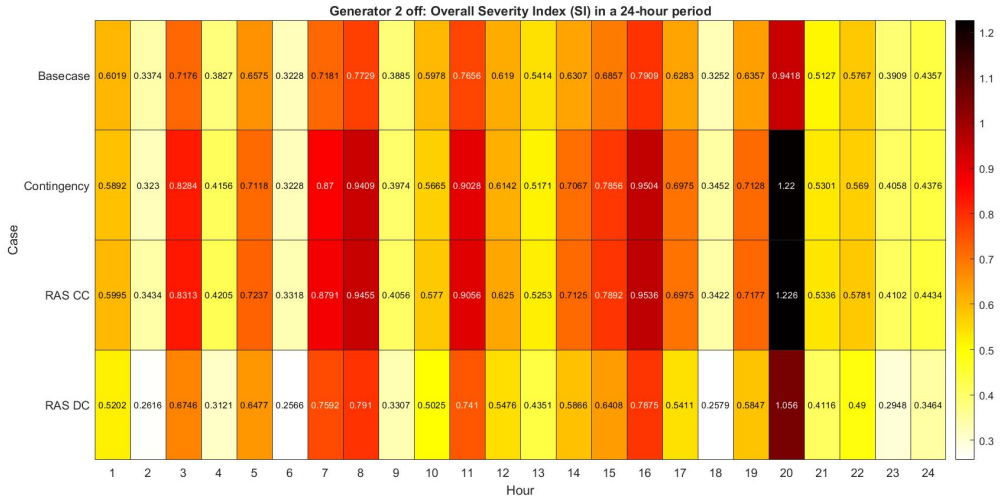

Figure 4.13: SI for outage at generator 2

In summary, several simulations have shown the effectiveness of RAS-FUBM controls (i.e.,

RAS-FUBM CC and RAS-FUBM DC), which is demonstrated by the voltage profile and SI results. Furthermore, these methods can alleviate congestion effects from the branch or generator outages by restoring the healthy voltage and minimising congestion as presented on the discussion results. As observed from the SI values, the RAS-FUBM DC is more efficient that the RAS-FUBM CC at alleviating congestion during the generator outage. The RAS-FUBM controls are effective at restoring the network system to a secure and reliable state. Additionally, the TSOs can use the RAS-FUBM controls to develop an optimal operational profile for a system incorporating large scale converter interfaced wind integration, before implementing it into practice in a real time operation.

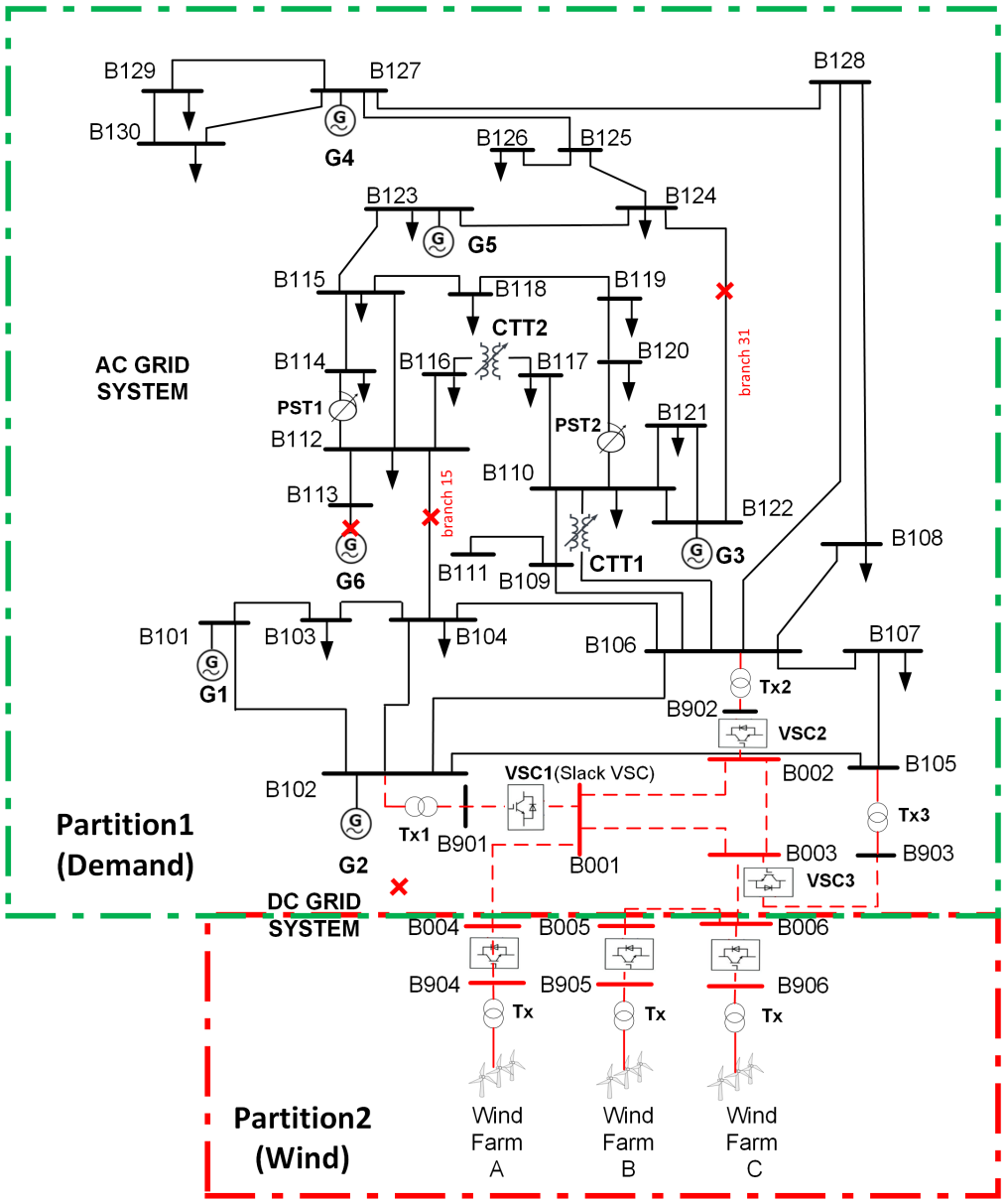

Figure 4.14: MT-HVDC system with two zones

4.7 Chapter summary

This chapter presents a comprehensive overview of the short-term operational planning related to the hybrid AC/DC networks used for offshore wind integration, which can be divided into single period operational planning and multiple period operational planning. The single period planning discussed in section 4.1 introduces the modelling tools to simulate multiple worst-case scenarios, associated with wind energy generation (i.e., high and low) and demand (i.e., high and low)), whilst concurrently simulating the possibility of an outage (i.e., complying with the N-1 rule) in the power system during a steady-state analysis. These scenarios are important considerations for TSOs to plan and develop robust contingency plans for operational flexibility. However, in real-world application, demand and wind energy are continuously changing due to various factors. Therefore, it is crucial to investigate the hourly pattern of demand and wind energy. To incorporate hourly variability in demands and wind resources, two elements have been introduced (i.e., scaling factor and partitioning technique) to modify the standard SCOPF formulation and enable variability in both demand and wind profiles across different time periods, which are covered in section 4.2. A novel approach for the RAS scheme (i.e., RAS-FUBM) is introduced in section 4.4, which can be utilised in a short-term operational planning framework to plan and deploy flexibility actions within hybrid AC/DC networks and mitigate contingency. To replicate the real-world operation planning, this thesis has modelled the multi-period SCOPF incorporating the RAS-FUBM scheme in section 4.5, in order to conduct dynamic analysis in the power system related to the fluctuations exhibited by electricity demand and wind power generation over time.

Two case studies are presented to demonstrate both single-period and multiple-period short-term operational planning. The results for the single period case highlighted that the contingency can be mitigated by taking prompt corrective actions, especially when the system experiences multiple worst-case scenarios. Meanwhile, the results in multiple-period operational planning demonstrate that the RAS-FUBM scheme is effective at restoring the hybrid AC/DC network integrated with offshore wind to a secure and reliable state. Furthermore, this scheme can assist TSOs in developing an optimal operational profile for a system incorporating large-scale converter-interfaced wind integration before implementing it in real-time operations. Further discussion of alleviating congestion in long-term planning associated with the multi-objective optimisation problem and the deployment of the VSC will be presented in the next chapter.

Chapter 5

Long-term Planning of Hybrid AC/DC Networks with Multi-terminal HVDC Links for Offshore Wind Integration

The infrastructure of the power system is aging [208], wherein transformations and upgrading are required to accommodate the growing integration of variable renewable energy output, particularly from Offshore Wind Farms (OWFs). These transformative and upgrading aspects are related to the long-term planning of the energy system, which requires comprehensive forward planning. In this context, long-term planning normally focuses on the development paths for the energy system that takes into account the infrastructure and long-lived technology investment cycle [209] such as expansion of generation through procurement planning and transmission, policy development and investment decision-making. The investment-planning model, which is intrinsically linked to the investment decisions made by the private sector and government's policies, represents a crucial aspect of long-term planning of energy systems. This model serves as a valuable analytical tool, enabling the assessment and guidance of investment and policy decisions pertaining to the development of the energy system [210]. However, modern power systems are undergoing a transition towards higher levels of renewable energy, and the unpredictable and variable nature of the renewable sources are making the overall power generation levels increasingly difficult to forecast [211]. The main obstacles during this transition period are the reliable delivery of electricity [212] and effectively managing the variability and uncertainty associated with the power balance between generation and demand. Practically, the traditional long-term planning approach is inadequate or not designed to meet this challenge and needs to be updated to be sufficiently flexible to keep

up with the rapid changes occurring during this transitional phase. The flexibility in the context of operational planning [213] is the ability of wind generation to be deployed within a certain timeframe to respond to changes in the additional demand and reduce the conventional generation outputs. Therefore, the power system needs to be transformed to ensure flexibility, particularly in the transmission system, which requires investment in the long- term investment planning focusing on transmission infrastructure that is suitable for maximising integration and deployment of variable renewable generation output.

Within the very paradigm of new enabling transmission technologies, the Multi-Terminal HVDC (MT-HVDC) system is the transformative concept in power systems that has great potential in addressing the obstacles of forthcoming transmission systems, particularly for enabling large OWFs with hundreds of MWs of generation capacity and located in farther distances from the shore [214]. The MT-HVDC systems could also potentially accelerate and facilitate the realisation of the European supergrid concept [215]. The supergrid is an extension of the existing transmission grid that is a combination of an AC and DC topology with either fully meshed or alternative topologies [216]. Its purpose is to transmit larger amounts of electricity and offers greater flexibility (i.e., improving the performance of AC system by regulating voltage, active power, reactive power, or current [217]). Given the higher levels of flexibility and control promised by MT-HVDC links, particularly those that are based on Voltage Source Converters (VSC), such a transmission technology may become a feasible solution for enabling higher flexibility of operation in future power systems with high levels of variable renewable generation output. However, this could present new challenges for the Transmission System Operators (TSO) [218], including the need to manage complex and varied control strategies, complex HVDC system topologies and infrastructure (e.g., FACTS and DC cables), and different requirements for each AC system terminal (i.e., cable ratings, capability of each AC node to inject and absorb a large amount of power (e.g., in the gigawatt range), protection and grounding, pylon size and space, and standard operability) [219] [14] [220]. In this chapter, the focus is on developing a new methodology with which a MT-HVDC link can be designed with optimum placement of VSC stations.

The rest of this chapter contains the following: section 5.1, explains the optimal VSC placement within the MT-HVDC transmission planning. Section 5.2 describes the Multi Objective -OPF (MO-OPF) in detail, considering overall generation, congestion and VSC capital/operation costs. The next section provides an overview of the congestion management techniques. In the next section, this thesis studies the DC voltage at the reference VSC node, deploying the VSC placement along with statistical analysis, to provide insightful understanding of the VM variables characteristics. Finally, the most important aspects of this chapter are summarised in the chapter summary.

5.1 MT-HVDC Transmission System Planning with Optimum VSC Placement

Installation of new components, in particular plug-in VSC stations into an existing transmission system (i.e., VSC placement), is expensive and requires careful consideration of various factors that influence the decision criteria. The identification of component needs to take into account three main steps [221]:

(a) **Scenario:**

Potential future scenarios to evaluate infrastructure requirements and projects.

(b) **System needs:**

Identify which scenarios would benefit from new system assets.

(c) **Project assessment:**

Cost-benefit evaluation of the projects for transmission, generation and storage in each scenario.

Given the economic constraints [222], the optimal number of VSC stations within a particular power system can be determined through the identification of components need analysis. This analytical stage would yield valuable insight and resolve the limitations of VSC stations (e.g., costs, availability of space for the VSC station, demand for the VSC stations, policy requirements, etc) by meticulously weighing the benefits of deploying these VSC converters and their associated costs. The VSC is considered as a feasible option for utilising transmission line assets to their maximum potential [223], as they provide for the new flexibility (i.e., controlling power system parameters such as voltage and power) that can increase the system's reliability, stability and operations security [224], particularly for hybrid AC/DC networks (e.g., AC systems with embedded MT-HVDC links). The integration of the VSC can increase power transfer capability from one location to another location that most require it, without necessitating procurement of additional generation capacity or topological changes that require costly grid expansion investment [225]. Hence, embedded MT-HVDC links, whilst requiring high initial investment costs can reduce the overall cost of operation of the power system in the long-term by introducing additional flexibility into the system and deferring or avoiding costly grid expansion and/or generation procurement in the long-term to account for growing demand and/or growing variable renewable generation output.

In order to optimise the VSC placement within a typical long-term planning problem, the optimisation tools need to incorporate the multiple decision criteria, namely the VSC station initial installation costs as well as operation and congestion, both from cost perspective and from grid steady-state performance perspective. These multiple criteria may be introduced mathematically

as different objective functions, which will make the ensuing long-term planning problem mathematically expresses a multi-objective optimisation problem. The trade-off principle [226], which competes one objective against another, is not the focus of this thesis. Instead, the multi-objective analysis in this chapter focuses more on the advantages of integrating VSC in the power system under study, which will be covered in more detail in the following section.

5.2 Multi-Objective OPF (MO-OPF) Problem Formulation

The OPF is the most significant tool in the context of power system planning and is extensively studied as a viable optimisation tool for power systems, as covered in-depth in Chapter 2. However, real-world optimisation problems require the solution of numerous objective functions to be considered, especially when dealing with critical problems such as reducing carbon emissions, reducing losses, etc, making single-objective optimisation problems impractical. In this chapter, a general Multi-Objective OPF (MO-OPF) problem formulation is developed for purposes of long-term transmission planning of hybrid AC/DC networks with MT-HVDC links. The MO-OPF problem can be mathematically expressed in (5.1):

$$\text{Minimise} \quad \mathbf{F}(x,u) = \sum_{j \in J} f_j(x,u) \tag{5.1}$$

subject to:

$$g_e\,(x,u) = 0, \qquad \forall e \in E \tag{5.2}$$

$$h_f\,(x,u) \leq h_f^{\max} \qquad \forall f \in I \tag{5.3}$$

In (5.2) and (5.3) sets E and I are defined as sets of indices associated with equality and inequality constraints in the MO-OPF problem. Equality constraints are the power balance equations and inequality constraints pertain to the physical limits of the transmission lines as well as all other devices, including VSC stations in the system under study.

Function f_j, where $j \in J$ is the number of objective functions, is referred to as the total objective function associated with the MO-OPF problem, which can be explicitly expressed as follows:

$$\text{Minimise} \quad \mathbf{F} = [f_1, f_2, f_3, \ldots, f_T]\,, \qquad \forall j \in J$$

where 'T' denotes the total number of objective functions and '$\mathbf{F}$' is the sum of all objective functions as $\sum_{j \in J} f_j$, where j represents the number of objective function for all $\forall j \in J$ in a set of all objective function indices, J. The MO-OPF problem can be extended to incorporate the following objectives: a) minimising the combined cost of overall generation (f_g) and congestion cost (f_c); and b) minimising the combined cost of overall generation cost (f_g), congestion cost

(f_c), and VSC placement cost (f_p) in an MT-HVDC system integrated with OWFs. The modified MO-OPF formulation related to both objectives can be expressed as below:

$$\text{Minimise} \quad \mathbf{F}_{\mathrm{T}} = f_g + f_c + f_p \tag{5.4}$$

Subject to:

$$g_e\left(x,u\right) = 0, \qquad \forall e \in E \tag{5.5}$$

$$h_f\left(x,u\right) \leq h_f^{\max}, \qquad \forall f \in I \tag{5.6}$$

In (5.4), f_g, f_c and f_p are the overall generation cost, congestion cost and VSC placement costs, respectively. In the case where VSC is not considered, the objective function of placement f_p will be omitted and this will be further elaborated in the section 5.2.2 and 5.2.3. The following section will provide an explanation of each objective function.

5.2.1 Objective function

There are three objective functions in this section, which are all associated to the costs of overall generation, congestion and VSC placement. The MO-OPF takes all objective functions simultaneously to be solved, in order to find an optimal solution for all objective function, with each objective function explained in detail in the following section.

1. Objective function 1: Minimise overall generation cost for conventional generator.
   The standard generation cost function's objective is to minimise the total generation cost, and related to the fuel cost, operation and maintenance costs that mathematically expressed as below:
   $$f_{(g,i)} = \sum_{i \in G} a_i + bP_i + cP_i^2, \qquad \forall i \in G \quad (\$/h) \tag{5.7}$$
   Where $f_{(g,i)}$ is the quadratic function that represents the total generation cost of the $i-th$ generation unit with $i \in G$ and G set of all generator indices. The variables a, b, and c are the cost coefficients related to that conventional generator unit, which are given in the units of \$, $\$/MWh$ and $\$/MWh^2$, respectively. In (5.7), P_i represents the active power generated by the $i-th$ generator.

2. Objective function 2: Congestion cost.
   The second objective is the cost of congestion pertaining to the sum of all Severity Index congestion (SI_c) and the associated congestion cost (α). This objective is formulated as:
   $$f_c = \sum_{c \in C} \alpha \mathbf{SI_c}, \qquad \forall c \in C \quad (\$) \tag{5.8}$$

where C is defined as the set of all congestions with c being indexed over this set. The Severity Index (SI) for each line is calculated as follows:

$$SI = \sum_{k \in K} W \left(\frac{P_k}{P_k^{\max}} \right)^{2n}, \qquad \forall k \in K \tag{5.9}$$

where K is defined as the set of all line congestions with k being indexed over this set. In (5.9), P_k is the power flow from line k, and P_k^{max} is the upper limit for line k. The variables W and n are the weighting factor and the penalty factor that have to be positive, respectively.

3. Objective function 3: VSC placement cost.
   The third objective function is associated to the VSC placement cost (f_p), which is the sum of the VSC's capital investment cost (f_p^{CAPEX}) and the operating costs (f_p^{OPEX}) multiplied by the number of VSC (N_{vsc}). This expression can be mathematically formulated as:

$$f_p = \sum_{p \in P} \left(f_p^{\text{CAPEX}} + f_p^{\text{OPEX}} \right) N_{\text{vsc}}, \quad \forall p \in P \quad (\$/MW) \tag{5.10}$$

   where P is defined as the set of all VSC placements with p being indexed over this set. The variable N_{vsc} refers to the number of VSCs, and the capital investment cost (f_p^{CAPEX}) as well as the operation cost (f_p^{OPEX}) for the VSCs are described further below:

   (a) CAPEX cost: capital investment cost

$$f_p^{\text{CAPEX}} = c_p P_p, \quad \forall p \in P \tag{5.11}$$

   Where f_p^{CAPEX} is the capital expenditure per VSC, which is calculated as the product of two scalar values: the cost of the initial VSC (i.e., component only) denoted as c_p and expressed in dollars ($), and the capacity of the VSC, denoted as P_p and expresses in megawatts (MW).

   (b) OPEX cost: Operation cost

$$f_p^{\text{OPEX}} = n \sum_{y=1}^{N_{\text{year}}} \frac{f_p^{\text{CAPEX}}}{(1 + \text{dr})^y} \quad \forall p \in P \tag{5.12}$$

   Where f_p^{OPEX}, is the *Net Present Value* of the incurred operating costs of maintaining the VSC stations, and the variables n, dr and y refer to the normal utilisation rate, the discount rate and the project lifetime in years per VSC station, respectively. The utilisation rate is the effective equipment life cycle [227] of the VSC, which is expressed as a percentage value.

5.2.2 Multi-objective function without VSC

The multi-objective function without VSC is a function consisting of two objectives ($j = 2$). These objectives are the summation of the generation cost (f_g) and the congestion cost (f_c), within a standard HVAC system that consists of conventional generators only. The purpose of this function is to minimise the overall generation cost in conjunction with the total congestion cost across each transmission line in the standard HVAC system (i.e., IEEE30 bus system) without the presence of wind generation. The expression of this function is determined by below:

$$\text{Minimise} \quad \mathbf{F}_{\mathrm{T}} = f_g + f_c \tag{5.13}$$

$$g_e^0(x,u) = 0, \quad \forall e \in E \tag{5.14}$$

$$h_f^0(x,u) \leq h^{\max} \quad \forall f \in I \tag{5.15}$$

Function $\mathbf{F}_{\mathrm{T}}$, is the sum function of two objective functions: overall generation cost (f_g) and congestion cost (f_c), as shown detail in (5.7) and (5.8). The (g_e^0) is the equality constraint that represents the basecase scenario, and E is the set of all equality constraints with e being indexed over this set. The (h_f^0) refers to the inequality constraint for the basecase scenario, with I is the set of all inequality constraints with f being indexed over this set. Both constraints follow the same constraints as the single OPF constraints, as discussed in Chapter 2.

5.2.3 Multi-objective function with VSC placement

The multi-objective function in the presence of VSC is a function that has three objectives (j=3), which is the summation of generation cost (f_g), congestion cost (f_c) and VSC placement cost (f_p), within a MT-HVDC system consisting of combination generation of conventional generators and wind generators. This function F_T has the same expression as in the (5.4) except the index (p) has been added into the equality and inequality constraints, which refer to the VSC placement in the MT-HVDC system. The MO-OPF in this scenario is expressed as:

$$\text{Minimise} \quad \mathbf{F}_{\mathrm{T}} = f_g + f_c + f_p \tag{5.16}$$

$$g_e^p(x,u) = 0, \quad \forall e \in E, \quad \forall p \in P, \tag{5.17}$$

$$h_f^p(x,u) \leq h^{\max}, \quad \forall f \in I, \quad \forall p \in P \tag{5.18}$$

$$|u_r - u_0| \leq \Delta u_r, \quad \forall r \in R \tag{5.19}$$

where (g_e^p) is the equality constraint in the MT-HVDC system, whilst E and P are defined as the set of all equality constraints and VSC placements, with e and p being indexed over these sets, respectively. As for the inequality, it is denoted by (h_f^p), where I is the set of all inequality constraints, and f being indexed over this set. The last equation has been introduced in the

presence of the VSC, which refers to the maximum allowable control permitted in the RAS-FUBM control (Δu_r), as explained in detail in Section 4.4.2] of Chapter 4. The VSC device, when placed within the grid system, is capable of controlling the voltages and power flows on both the AC and DC sides, particularly during contingency events. The variable u_r refers to the RAS-FUBM control action taken during the post-contingency state, and u_0 refers to the base case action (i.e., without the presence of VSC). The set 'R' is defined as the set of all control actions in the RAS-FUBM, with r being indexed over this set.

5.3 Congestion management in the power system

Congestion refers to a situation where the transmission line capacities are exceeded (i.e., overloaded thermal limits) due to higher demands, operational limitation (i.e., physical limit in the infrastructures or components) or contingency cases (i.e., outages or failures equipment such as transmission line or generator). The congestion may result in economically sub-optimal operation (i.e.,a state where the power system is not operating in the most cost-effective manner, despite still being able to meet the requisite power delivery demands in a consistent and reliable service [228]), stability issues (i.e., voltage and frequency), or in severe cases cascading blackout events. Therefore, implementing a congestion management technique is vital to mitigate any severe risks of congestion and maintain the security and reliability of power system. There are many congestion management methods developed over the years [229] [230], and they can be divided into two groups: technical and non-technical as illustrated in Figure 5.1. There are two approaches on the technical: a) generation-centric (e.g., rescheduling generation or Distribution Generation (DG) including smart grid DG, location or sizing the DG); and b) transmission-centric (e.g. Flexible AC transmission systems (FACTS) integration, FACTS location or placement, HVDC integration, Security Constrained Optimal Power Flow (SCOPF), and contingency analysis). On the other hand, the non-technical side can be divided into: a) Market-centric approaches encompassing nodal pricing, zonal pricing and auctioning; and b) customer-centric involving demand response analysis and load curtailments. The main focus of this research on congestion management techniques is a transmission-centric approach related to the FACTS/HVDC grid integration.

FACTS devices, which are based on power electronic devices have seen increasing utilisation in the power transmission system. These devices have the ability to control line impedance, nodal voltage magnitude and phase angle, as well as active and reactive powers [231], thereby alleviating transmission congestion and enabling improvement in the grid infrastructure, together with other benefits. Optimising the return on investment from the FACTS integration is necessary because of the high cost of these components. This is particularly important when it comes to the control settings, which directly affect the generators and loads in the power system [232], and also could mitigate the congestion in the transmission lines. Considering the importance of these control settings and their ensuing impact on the operation of the power system, within the context of

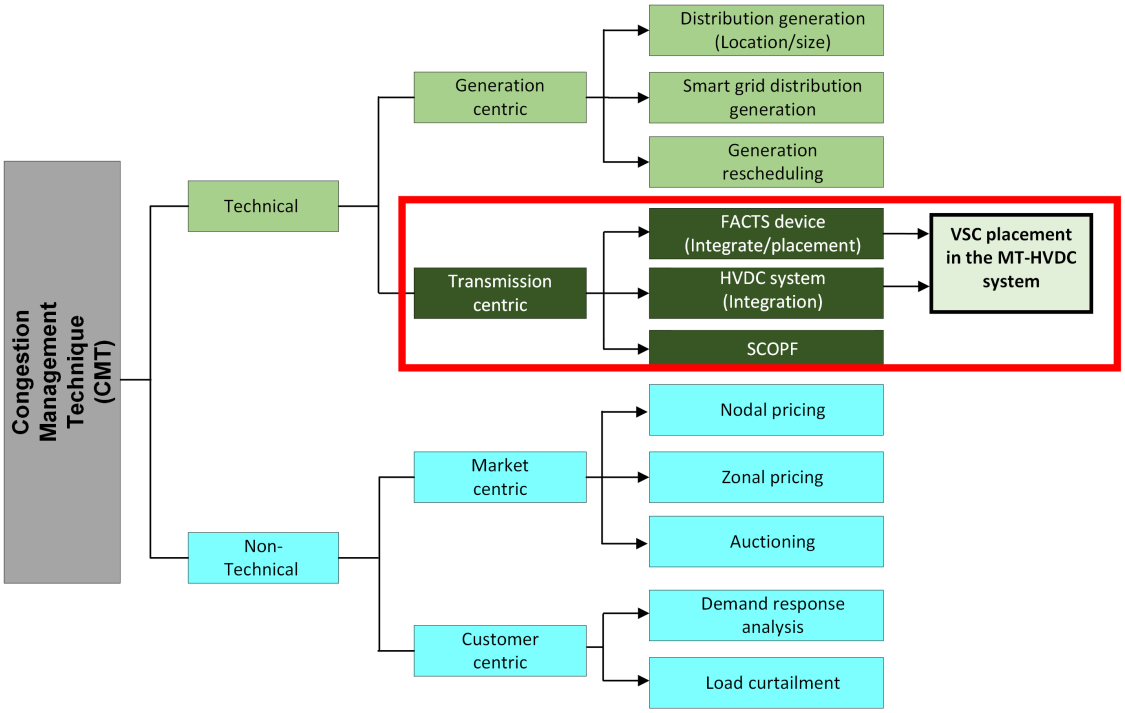

Figure 5.1: Congestion Management Technique

hybrid AC/DC systems, this research investigates the role and impact of DC voltage control at the reference VSC station within a MT-HVDC transmission system, which is designed to integrate offshore wind farm generation capacity to an existing AC power system. The first problem to consider is the optimal placement of VSC converter stations within the MT-HVDC system, followed by an analysis of the impact of DC voltage control at the VSC reference node for the purpose of alleviating any congestion impacts within the entire AC/DC system.

5.4 Control of DC voltage at Reference VSC node

One of the important state variables characterising the operation in a power system is Voltage Magnitude (VM), which normally exhibits variations due to the factors such as load changes, generator output (e.g., wind and solar), network topology changes and disturbances. Maintaining VM levels at every bus is paramount for both normal operation and in the event of disturbances. Within an MT-HVDC system, the reference VSC plays a pivotal role in regulating the entire voltage profile, ensuring that the total active power entering the power system equals the total power leaving, inclusive of the losses [233] incurred across the hybrid AC/DC network. The chosen DC voltage setpoint at the reference VSC influences the severity of voltage variations and the distribution of balancing power at both the AC and DC sides. By applying precise control of the DC voltage at the VSC reference, it ensures the healthy voltage (i.e., VM that is maintained within the range limit), which could prevent abnormal voltages (i.e., overvoltage or undervoltage

scenarios) that could disrupt power transmission. Existing research on DC voltage control has primarily focused on controlling DC voltage deviation through simulation of DC link dynamics associated with the VSCs connected to weak grids [234], implementing voltage droop control in MT-HVDC system [235] [236], applying distributed DC voltage control in two-terminal HVDC systems [237] and regulating DC voltage in a point-to-point VSC-HVDC system [238].

The operations of VSC in the MT-HVDC system integrating large-scale OWFs presents two primary control challenges namely, active power sharing and voltage regulation. Despite the fact that both active power control and voltage regulation are relatively important to ensure the reliability of the hybrid AC/DC networks, the analysis of these controls depends on the operational requirements, either to regulate the voltage or transmit the power flow. The most typical control structure layout in the MT-HVDC system consists of many buses that integrate with VSC to regulate the active power injected into the AC system, one bus as a reference bus (i.e., the slack bus) for an AC system and one VSC (i.e.,reference VSC) assigns to control the DC voltage to maintain the voltages within the whole MT-HVDC system. [233]. For the power system to be stable and resilient [239], DC voltage regulation has therefore higher control priority, particularly in the weak grid conditions such as OWF connections. Furthermore, the power fluctuations in the OWFs, resulting from weather-related variations in wind energy supply leads to voltage variations that have an impact on the operation of the power system and subsequently reliability of supply to consumers [240]. Uncontrolled voltage variations could lead to tripping converters, blackouts or potential damage to equipment. Given the importance of maintaining stable DC voltage in an MT-HVDC system used to integrate large-scale OWF generation capacity, it is crucial to analyse the variations of DC voltage control setting at the reference VSC within such systems. This is necessary to achieve a balance between supply and demand, control power flow through the entire AC/DC network, minimise losses, and effectively manage any contingencies or disturbances that may arise. There has not been extensive research conducted regarding DC voltage control in reference VSC node within an MT-HVDC system specifically suited for power systems planning (long-term and short-term) studies which are the context of this thesis. Determining the optimal placement for the VSCs is highly important, since it affects not only the economy aspects (i.e., capital and operation cost as explained in Section 5.2.1 under objective function 3) but also the efficiency and reliability of the future power system, particularly in the MT-HVDC system. Furthermore, the VSC placement has an impact on voltage profiles, power flow and overall power system performance, due to the VSC ability to control power system parameters such as power and voltage. However, there are not many research studies related to the DC voltage control, particularly at the reference VSC within the MT-HVDC system. Given this, the main focus of this thesis is the investigation of this specific type of control (i.e., DC voltage control at the VSC reference node) within the context of the VSC placement in the MT-HVDC system. Studying the DC voltage at the VSC reference node may help understand the voltage characteristics within the MT-HVDC system, as well as maintain all

node voltages within acceptable limits even during unforeseen events such as varying demands and winds or transmission congestion. Furthermore, comprehending the DC voltage control at the VSC reference can help ensure the control approach is designed and operated to maintain the security of the power system, and meet future demand scenarios for any given operating conditions [241]. This insight can be very valuable in the long-term transmission strategies.

The characteristic of VMs with the DC voltage control at the VSC reference node can be analysed using a statistical model approach. This approach involves data collection, preprocessing and the implementation of applicable statistical techniques, which in this thesis focuses on probability distribution function. Firstly, all the data (i.e., VM values) from every simulation are compiled, capturing all operating conditions. Then, a probability distribution analysis (i.e., on discrete or continuous variables) is performed to analyse the probability distribution of the data. This probability analysis can help in determining the fundamental statistical properties of the variations in the VM variables, which includes the process of descriptive statistics (i.e., calculation of mean, variance, standard deviation, etc.) to understand the characteristics of these variables. The results of this statistical analysis would then be presented through appropriate visualisations (e.g., density plots, histograms, scatter plots, or box plots) and summarised in a report, which would provides valuable insight for the operation, control and long-term planning of the MT-HVDC system utilising the DC voltage control at the VSC reference node. Therefore, studying the DC voltage control at VSC reference node within the MT-HVDC system deploying the VSC placement can be highly beneficial for long-term planning.

In this thesis, the VM behaviour, as it varies with the voltage settings at the reference VSC in the MT-HVDC system, is examined using the normal probability distribution. This distribution has been chosen because it can accurately represent how variations in demand and generation produces changes in voltage. Furthermore, the probability distribution model has been applied to characterise the randomness in the demand [242], wind energy assessment [243], solar radiation [244], and the power system reliability analysis [245].Considering unpredictability at the demand and generation sides typically causes voltage changes, modelling the VM values becomes essential in an effort to understand the volatility in the voltages for all nodes (i.e., both AC and DC systems). In this thesis, the normal distribution has been utilised to model the VM values to comprehend the voltage profiles across all nodes, within the variation voltage settings at reference VSC. Analysing and presenting the VM values in a more informative way is necessary to provide a better understanding of this variable (i.e., VMs). The normal distribution (i.e., known as Gaussian distribution) is widely used in many engineering fields, as it allows for accurate representation of a broad range of random phenomena, such as electrical parameters [246]. Numerous studies have been conducted on the normal distribution in regard to power system analysis, including randomness of load data based on historical data [247], wind power prediction in relation to wind speed [248], and monitoring the harmonic current based on abnormal data [249]. In this chapter the normal

distribution assumption is used to statistically model and visualize VM variations to help better understand the inherent relation between line congestion and VM variation. This is explained in more detailed in Section 5.4.1.

The key challenge in the hybrid AC/DC network is effectively managing transmission line congestion, which arises due to the contingency events (e.g., the outage system components or abrupt increases in demands and wind generations). This congestion can be mitigated following the initial stage of Contingency Analysis (CA) framework. This framework involves identifying and ranking transmission lines according to their level of severity. The CA is crucial in operational planning of modern power systems, due to undergoing structural changes in the power generation (i.e., increased integration of renewable energy sources) and electricity demand (i.e., growth of smart devices and electric cars). The ranking in the CA is calculated based on the level of severity in the measured variables (e.g., bus voltage, current, active power or reactive power) using a performance index (in this research it is called a Severity Index (SI)). The advantages of evaluating these two variables through SI, providing a comprehensive overview of the changes in the transmission lines across a specific scenario [250]. Generally, there are two variables measured in the SI namely, active power and bus nodal VM. The focus variable in this research pertaining to the SI is active power, and the formulation of this SI as presented in section 4.3.1 of Chapter 4. Furthermore, the effect of changing the VSC set point has been covered through SI analysis, including the implementation of two control methods: RAS-FUBM CC (i.e., conventional control) and RAS-FUBM DC (i.e.,droop control), which are covered in-depth in section 4.4.2 of the same chapter. From the SI formula, the congestion of each voltage control setting for each scenario (as presented in the case study in this chapter) can be ranked and analysed. This will assist the Transmission System Operators (TSOs) in taking measurable and appropriate actions to ensure the stable and secure operation of the EPS.

5.4.1 Statistical Modelling of Voltage Magnitude Variations

In this section, a simple but effective statistical model for analysing and visualising the VM variations is given. The descriptive statistics are a method to process and present different types of data, such that the data can be more informative [251]. These statistics can be classified into two major categories [252]:

(a) Measures of Central Tendency (MCT) describe the center point of a data set using a single value. There are three types of measurements in MCT: mean or average, median and mode. The mean, which is the most common measurement in the normal distribution, can be calculated by summing all the values in the data set (x_j) and dividing this result by the number of observations (k). The formula for the sample mean (μ) is expressed as follows:

$$\mu = \frac{\sum_{j=1}^{k} x_j}{k} \tag{5.20}$$

(b) Measures of Dispersion (MD) describe the extent to which individual data values deviate from the mean. There are three methods for assessing MD: range, variance and standard deviation. The range is computed by subtracting the lowest value from the highest value in the data set. The variance (v) represent the relative dispersion of data points from the mean, and it is denoted by:

$$v^2 = \frac{\sum_{j=1}^{k} (\bar{x} - x_j)^2}{n-1} \tag{5.21}$$

Where '$\bar{x}$' is the sample mean, '$(\bar{x} - x_j)$' is the deviation from the mean for each value in the data set and k is the size of the sample (i.e., the number of data values). The last method is the standard deviation (σ) is simply the square root of the variance, which formulated as per below:

$$\sigma = \sqrt{\frac{\sum_{j=1}^{k} (\bar{x} - x_j)^2}{n-1}} \tag{5.22}$$

The graph in Figure 5.2 illustrates the normal distribution, commonly known as a bell curve, with the x-axis representing the two categories in the descriptive statistics. In this graph, the data symmetrically distributed around its mean, whilst the width of the curve is determined by the standard deviation.

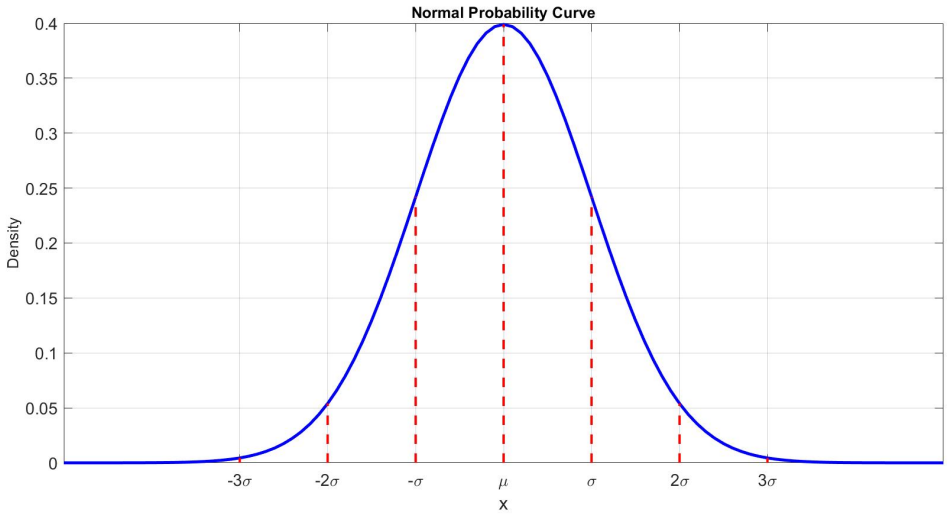

Figure 5.2: Probability Density Function for Normal Distribution

A probability distribution can be defined for both discrete and continuous random variables. In this thesis, it is assumed that voltage magnitude variations are represented as a continuous random variable. For any random variable X defined as a function from sample space Ω to the real numbers (representing the outcome in Ω) a Probability Density Function (PDF) [253] can be defined as $f_X(x)$. The PDF is often characterised by a set of parameters Θ. The Cumulative Distribution Function (CDF) is defined as the probability measure of $x \leq X$ as $F(x) = P(x \leq X) = \int_{-\infty}^{x} f_X(x)dx$. In this context, the PDF gives a density measure of the random variable

distribution.

For a normal probability distribution the PDF is characterised by its mean (μ) and standard deviation (σ), and can be mathematically expressed as follows for any continuous random variable X:

$$f_X(x) = \frac{1}{\sigma\sqrt{2\pi}} e^{\frac{-(x-\mu)^2}{2\sigma^2}} \tag{5.23}$$

In this thesis, the voltage magnitude variable has been treated as a continuous random variable, VM, following a normal distribution assumption with a density function given in (5.23). The random distribution of different VM values are then visualised using this assumption of normal distribution using figures similar to the one shown in Figure 5.2.

5.5 Hybrid AC/DC Network Planning - Case Studies

There are two case studies that have been performed to understand the impact of VSC placement within the hybrid AC/DC network. The first case study (Case One) explores a multi-objective function incorporating into the standard OPF formulation which has three objective costs as explained in section 5.2. The second case study (Case Two) delves into the relationship between DC voltage control at the reference VSC node within the MT-HVDC system in relation to VSC placement, analysing a scenario involving four VSCs. Collectively, these case studies aim to provide a comprehensive analysis of the implications of VSC placement within a hybrid AC/DC network, considering both the economic and operational aspects of an optimum placement of VSCs within an MT-HVDC system. It therefore provides a holistic techno-economic framework for planning and designing such systems precisely aimed at integrating large-scale OWF generation capacity into existing AC power networks.

5.5.1 Case One: Hybrid AC/DC Network Planning using Multi-Objective OPF

The proposed formulation of the MO-OPF problem is tested in two systems, which are a purely AC system (HVAC) and a hybrid AC/DC network with embedded MT-HVDC link. Two different topologies for the MT-HVDC link have been considered for the case of the hybrid AC/DC network namely, one topology with three VSCs and a second topology with four VSCs. Each topology is simulated once in the ensuing MO-OPF model. The HVAC system is based on the IEEE30-bus system and the data of this system can be found in Appendix B. The MT-HVDC system with three VSCs is the same as the case study in section 4.1 in Chapter 4, but without any contingency (refer to Figure 4.4), whilst for the second MT-HVDC topology with four VSCs, there is one additional VSC connected to bus 123 on the HVAC side as shown in Figure 5.6. The VSC1 is assigned as the reference VSC for both topologies in the relevant MT-HVDC link. The control settings of the other VSCs can be found in Table 4.1 for MT-HVDC topology 1 and Table 5.6

for MT-HVDC topology 2. Details of the VSC parameters for different MT-HVDC topologies are given in Table 5.1. The simulations for the case studies are executed using MATPOWER version 7 run on MATLAB (R2021b) on a laptop equipped with an Intel(R) Core (TM) i5- 10210U CPU running at 1.60GHz (2.11 GHz), a 64-bit processor and 8.00 GB of RAM.

Table 5.1: VSC parameters for different MT-HVDC topologies

VSC parameters	
Cost component ($)	10,000
Project lifetime (years)	25
Normal utilisation	0.75
VSC capacity (MW)	50
Discount rate	0.09
No. of VSCs (MT-HVDC Topology 1)	3
No. of VSCs (MT-HVDC Topology 2)	4

Table 5.2 shows the results of the different objective functions following the solving of the MO-OPF model for the basecase (i.e., purely AC system), MT-HVDC topologies 1 and 2 cases. The basecase cost is 5,113.54$/MWh, whilst the MT-HVDC topologies 1 and 2 cases are 1,635,626.12$/MWh and 2,179,426.10 $/MWh, respectively. The difference in cost between topology 1 and basecase is 1,630,512.58 $/MWh and the difference between topology 2 and the basecase is 2,174,312.56 $/MWh. The differences in these values demonstrate the significant cost for VSC integration into the purely AC power system, thus this integration requires a careful analysis, such as the identification of system needs analysis that has been discussed in section 5.1. From the costs of topology 1, which has three VSCs, and topology 2, which has four VSCs, it can be seen that there is a 543,799.99 $/MWh cost difference between these different topologies, representing a 33% increase in cost. This cost indicates that an increased number of VSC will result in a higher overall cost in the objective function, as demonstrated by the percentage increase in cost between the two topologies. Despite the overall cost being higher for the integration of VSC based MT-HVDC systems compared to the basecase, the VSC placement demonstrates superior performance with respect to generation cost from conventional generators, an outcome that will be further discussed in the forthcoming result.

Table 5.2: Total cost for all cases

Total cost (F_T)-($/MWh)		
Basecase	Topology 1 (3VSCs)	Topology 2 (4VSCs)
$5,113.54$	$1,635,626.12$	$2,179,426.10$

The total generation cost for every case is displayed in Table 5.3, where it is obvious that

there is considerable cost reduction with the hybrid AC/DC network (i.e., AC system embedded MT-HVDC system) as opposed to the basecase (i.e., purely AC system). The overall generation costs for basecase, topology 1 and topology 2 are 576.8923 $/MWh, 470.7239 $/MWh and 476.136 $/MWh, respectively. Comparing the MT-HVDC topologies to the basecase, the cost reductions are 106.17 $/MWh and 100.76 $/MWh, respectively, and these reductions equate to 18% for topology 1 and 17% for topology 2. However, the reduction in cost between topologies 1 and 2 is not very significant, amounting to only a 1.15% saving, which equates to 5.4121 $/MWh in monetary terms. These findings provide support that the renewable energy could lower the total cost of generation from conventional generators. In the future scenario, all conventional generators (i.e., powered by fossil fuel) will be turned off, and electricity will only be generated from clean energy sources such as wind, enabling the achievement of net zero carbon emission by 2050.

Table 5.3: Overall generation cost for all cases

Generation cost (f_g)-($/MWh)		
Basecase	Topology 1 (3VSCs)	Topology 2 (4VSCs)
576.8923	470.7239	476.136

Contingency analysis has been conducted on the basecase, and severity of each line has been calculated as per equation 4.25 in section 4.3.1 in Chapter 4. The SI values are then presented in the graph shown in Figure 5.3. The ranking list from the graph shows that the highest rank occurs at line 35 with an SI value of 0.8737, followed by lines 10 and 33 with SI values of 0.5542 and 0.4882, respectively. These three lines are considered the critical lines that need to be monitored, particularly during contingencies related to N-1 scenarios (i.e., single component outage). This analysis provides a more accurate observation related to the congestion in the HVAC system, by utilising the SI ranking list to determine the most severe contingency on the lines. Given this information, the TSO will be able to monitor the critical lines and take the necessary actions to ensure the power system remains in a secure state in terms of lines overloading. The following results will demonstrate the performance of this SI ranking list in the modified IEEE30 bus system with the large- scale integration of converters with the generation from OWFs.

Figure 5.4 analyses the impact of line congestion severity for different number of VSC placements, with placement 1 having three VSCs and placement 2 having four VSCs. Figure 5.4a shows the SI ranking for the placement 1, it is apparent that the branch with the highest severity ranking is branch 35, exhibiting a SI 0.9432. This is followed by the second and third highest severity rankings of 0.5614 and 0.5556, occurring at branches 30 and 10, respectively. Comparing the SI values for branch 35 between placement 1 and the basecase, the difference is 0.0695, representing an 8% increase in severity in the system. For branch 10, the difference in SI value is 0.0674, which means there is an increase of 12% in severity on this line from the basecase. However, the SI ranking marginally changes when an additional VSC is plugged into the MT-HVDC system for

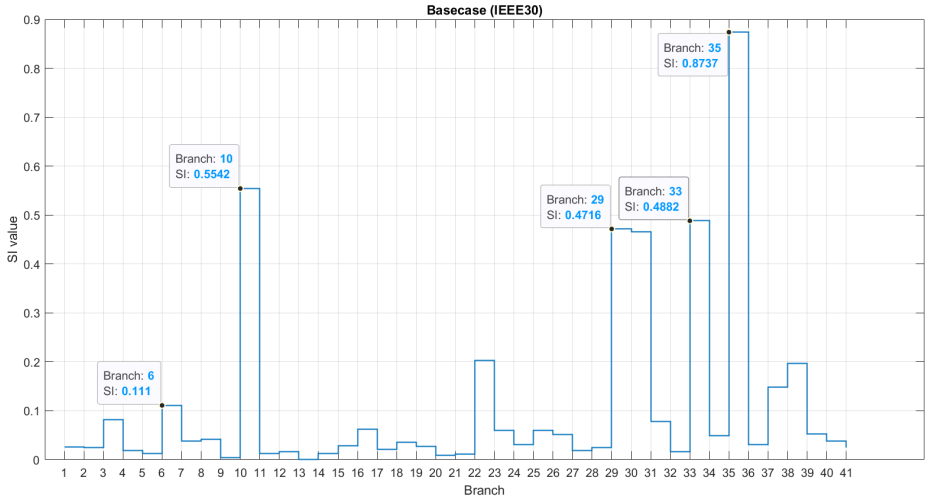

Figure 5.3: SI Basecase

the placement 2 case, as shown in Figure 5.4b. Branch 30 is presently in the highest ranking with a SI value of 0.9547, followed by branch 35 at 0.7406 and branch 10 at 0.5552. In comparison for placement 2 and the basecase, the difference in SI value is -0.1331 for branch 35 and 0.067 for branch 10. This represents a 15% decrease in severity for branch 35 and a 12% increase in severity for branch 10. For branches 30, 35 and 10, the comparison of SI value between placement 1 and placement 2 is 0.0115, 0.1792 and -0.0004, which indicates a 1.22% and 31.92% rise in severity for branches 30 and 35 and a 0.07% decrease for branch 10. The difference in SI value between placement 1 and placement 2 is rather large when considering the impact of branch 52 (i.e., HVDC line). There is a 91% reduction in severity on that line (i.e., branch 52) with SI values of 0.015 (i.e., placement 1) and 0.0013 (i.e., placement 2). Overall, these results indicate that the VSC placement is able to increase and decrease the severity on each line and can modify the ranking list in the SI without any control actions. The implementation of the control action, which is a built-in element of the VSC, may cause the SI ranking to change, which could reduce the severity and mitigate the congestion in the hybrid AC/DC network.

The impact of the VSC placement not only can be seen at SI ranking list, but also in the active power generation as displayed in Figure 5.5. Generators 2 and 5 injected 55.402MW and 16.267MW active power, respectively, into the hybrid AC/DC network. However, the amount of these power injections changes when the VSCs are connected to the hybrid AC/DC network with the integration of three wind farms. During the placement 1 with three VSCs, the active power generation at generator 2 is 43.035MW and generator 5 is 15.726MW, indicating a 22% and 3% drop in injected power for both generators as compared to the basecase. As for the placement 2, with four VSCs, the injected active power generation for generator 2 is 48.559MW and 9.640MW for generator 5, representing a decrease of 12% and 41% for each generator. The difference between placements 1 and 2 for active power generation at generators 2 and 5 are 5.525MW and 6.087MW,

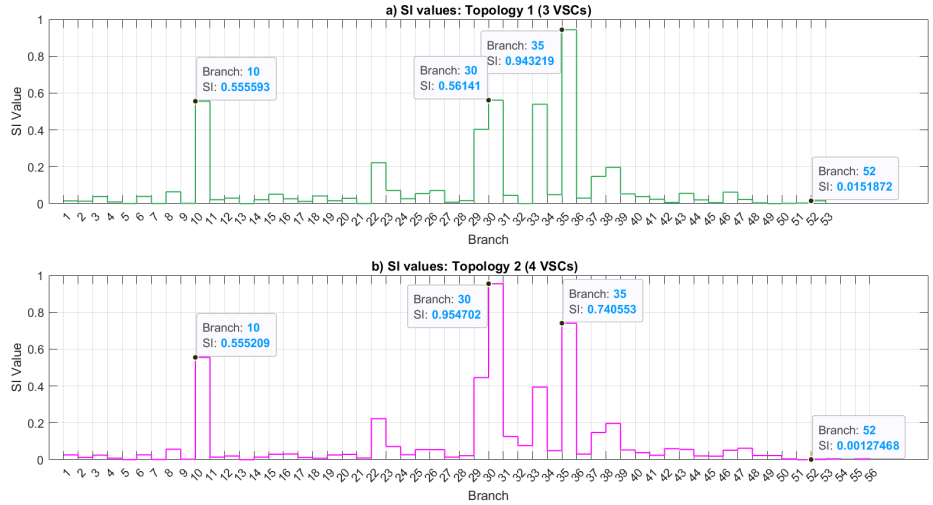

Figure 5.4: SI values with a) Toplogy 1 (3VSCs); and b) Topology 2 (4VSCs

respectively, representing a 13% and 39% proportional increase and decrease in comparison to placement 1. The VSC is plugged at same buses (i.e., bus B102 for generator 2 and bus 123 for generator 5) in the HVAC side, which is why the comparison only pertains to these generators. From these results, it can be summarised that the VSC placement can significantly reduce the active power generation from the conventional generators and is able to deliver power effectively from the three integrated wind farms into the hybrid AC/DC network.

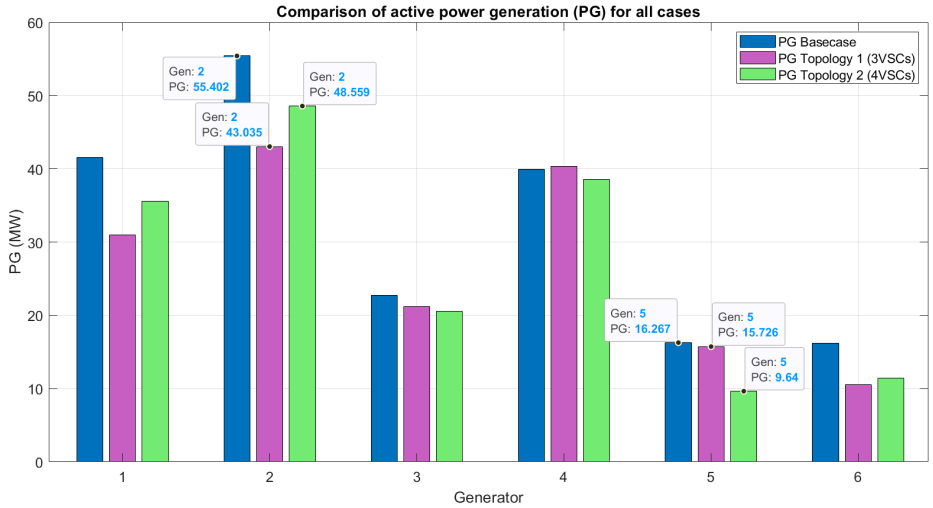

Figure 5.5: Active power generation (MW)

Table 5.4 shows the total losses for all cases: basecase, placement 1 with 3 VSCs and placement 2 with 4 VSCs, which have the values of 2.860MW, 3.106MW and 3.189MW, respectively. The difference losses between placement 1 and the basecase are 0.245MW, whilst the difference between placement 2 and the basecase is 0.328MW. This corresponds to increments of 8.6% and 11.5% in

losses for the respective placements compared to the basecase. The losses are larger in placement 2 by 2.7% or 0.083MW, as compared to placement 1. From these outcomes, it can be concluded that the VSC connection with HVDC lines has higher losses compared to the HVAC link, which supports the theory that the energy losses along the 50 km transmission lines for a VSC-HVDC link are 4.45%, whilst losses along the HVAC link are only 3.31% [43]. Furthermore, the higher the number of VSCs, the higher the losses in the hybrid AC/DC power system, as the VSC converters present higher losses due to the high switching frequency [254]. Therefore, the VSC integration requires careful consideration not just of the cost of installation, but also the higher losses. However, these drawbacks can be offset by the controllability features that VSC provides

Table 5.4: Total losses for all cases

Total lossess (MW)		
Basecase	Topology 1(3VSCs)	Topology 2(4VSCs)
2.86	3.105	3.188

5.5.2 Case Two: Hybrid AC/DC Network Planning - DC Voltage Control within the MT-HVDC Link

An MT-HVDC link as seen in Figure 5.6, which is a modified model based on IEEE30 bus system, integrated with Offshore Wind Farms (OWFs) has been simulated to evaluate the variations in voltage control at reference VSC node (i.e., VSC1) within the MT-HVDC link. The data pertaining to the HVAC network within the hybrid AC/DC system can be obtained from Appendix B. The MT-HVDC link consists of 7 DC lines, 4 VSC stations and 4 transformers. The system is simulated using MATPOWER version 7 run on MATLAB (R2021b) on a laptop equipped with an Intel(R) Core (TM) i5- 10210U CPU running at 1.60GHz (2.11 GHz), a 64-bit processor and 8.00 GB of RAM. The MT-HVDC grid and control parameters are the same as in the case study in Chapter 3, presented in Table 3.4. These parameters are used to solve the OPF for the proposed test system, and to evaluate the impact of using different voltage settings at the reference converter (i.e., reference VSC).

The VSC control settings (i.e., DC voltage settings at the DC side) have been configured as per Table 5.5. In all cases, VSC1 is assigned as a reference VSC, while the other VSCs operate in accordance with their chosen control type, as per detailed in Table 5.6. There are four scenarios to be considered in this study: a) Basecase; b) Demand and Wind Increased (DWI) by 5% (DWI +5%); c) conventional control; and d) droop control. The parameters of the standard demand and demand increased by 5% are shown in Table 5.10, whilst the parameters of the standard wind generation and wind increased by 5% are displayed in Table 5.11. In cases (a), (b) and (c) the active power is assigned for the VSC2, VSC3 and VSC4. As for the case (d), VSC2 and VSC 4 are assigned for active power control, whilst VSC3 controlled the reactive power.

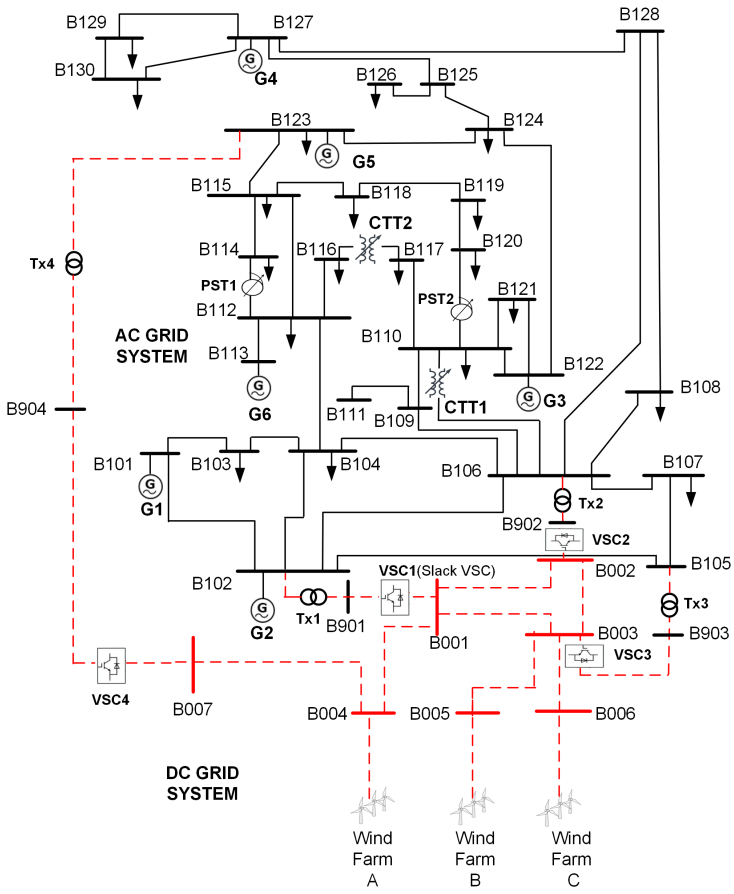

Figure 5.6: MT-HVDC system integrated with OWFs

Table 5.5: DC Voltage Set Points at VSC1

DC voltage set points at VSC1	
Set 1	0.9555
Set 2	0.96
Set 3	0.97
Set 4	0.98
Set 5	0.99
Set 6	1.005
Set 7	1.01
Set 8	1.01
Set 9	1.02
Set 10	1.03
Set 11	1.04
Set 12	1.05
Set 13	1.06

Figure 5.7 illustrates the Probability Density Function (PDF) for the Voltage Magnitude (VM) at all buses for a particular voltage setting (i.e., 0.955, 0.96, 0.98, 0.99, 1.005, 1.01, 1.02, 1.04 and 1.06) at the reference VSC. The green and red curves represent the VM for the basecase and increased all demands and winds by 5% (i.e., DWI (+5%)). Whilst the RAS-FUBM CC and RAS-FUBM DC control curves are depicted by blue and pink, respectively. The CC refers to the

Table 5.6: VSC setting

No	Type of control	Converter	Type	Mode	Control constraint
1	Basecase and DWI (+5%)	VSC2	I	3	$P_f = 25$MW
		VSC3	I	3	$P_f = 15$MW
		VSC4	I	3	$P_f = 15$MW
2	Conventional Control	VSC2	I	3	$P_f = 27.5$MW
		VSC3	I	3	$P_f = 12$MW
		VSC4	I	3	$P_f = 13.5$MW
3	Droop control	VSC1	III	7	$P_f = 27.5$MW, $k_{dp} = -0.1$
		VSC2	I	3	$P_f = 12$MW
		VSC3	I	2	$Q_t = -20$MVAR
		VSC4	I	3	$P_f = 13.5$MW

conventional control and DC refers to the droop control, which employ VSC within the FUBM model, each have been discussed in detail in Section 3.3 of Chapter 3. These control strategies have subsequently been incorporated into the RAS-FUBM approach, as further elaborated upon in Section 4.4.2 of Chapter 4. The dotted lines in the graphs represent the VM mean values. It can be observed that when the voltage settings are set below 1.0 p.u. (i.e., the base case), the probability curves for VMs at both controls (i.e., RAS-FUBM CC and RAS-FUBM DC) are underneath the basecase and the DWI +5% case curves. Furthermore, the VM mean values during these settings are noticeably less than 1.0p.u, except for the voltage setting at 0.99p.u, where the VM mean for the RAS-FUBM CC is slightly above 1.0p.u (i.e., 1.0016), which span from approximately 0.95p.u at the lower end to 1.08p.u at the higher end.

However, these curve trends transition when the voltage settings are greater than 1.0p.u, as the density curves for VM values at both controls lie on top of both the basecase and DWI +5% case curves. The values of VM during these voltage settings range from 0.96 at the lower end to beyond 1.08p.u at the upper end. An anomalous pattern emerges when the voltage is set to 0.9555, exhibiting a higher probability of occurrences for VM (i.e., the bell shape curve lies above the basecase and DWI +5% case) in the case RAS-FUBM DC control compared to RAS-FUBM CC control. The exhibited anomalous pattern when the voltage is set to 0.955p.u indicates that this specific VSC setting point is not recommended. The lower limit of the VM for the AC system is 0.95 p.u, whilst DC system is 0.9p.u, which implies that the VSC setting should not be configured in close proximity to the lower limit of these respective systems. Analysing the pattern (i.e., density) curve for the VM from the PDF is crucial, as it provides insight into how this variable behaves under different voltage settings. Observing this pattern can detect occurrences where the voltage significantly deviates from the nominal values, which can help detect the potential voltage stability issues or abnormal pattern as shown in the case voltage setting 0.9555p.u.

The SI based on active power (P) flow is calculated at each transmission line to identify congestion along the lines. Then each SI is summed together to obtain the overall SI. The overall SIs are

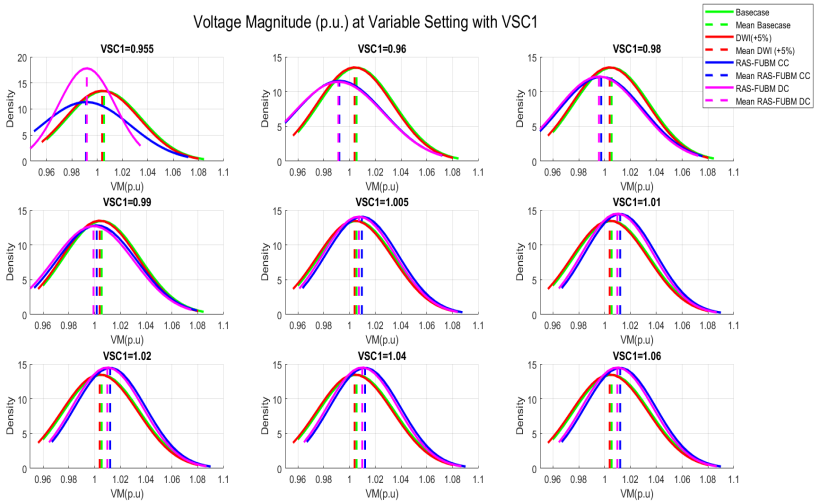

Figure 5.7: Voltage profile for all DC voltage settings

then visualised using a heatmap, showing the results for all cases across the different voltage settings at reference VSC, as depicted in Figure 5.8. The heatmap reveals that the SI values increased by 2.84% (i.e., the value is 0.8327) across all voltage settings compared to the basecase value of 0.8097. This indicates that the network congestion within the MT-HVDC system becomes severe when the demand consumption and wind injections are increased by just 5%. In order to mitigate this congestion, two controls are implemented (i.e. RAS-FUBM CC and RAS-FUBM DC). Analysing the performance of these two types of controls, it can be observed that RAS-FUBM CC demonstrates the lowest SI numbers, indicating it is more effective at alleviating the severity of congestion across variable voltage settings. The RAS-FUBM CC, which is a combination control of DC voltage control and an active power, provides an improvement in the overall EPS stability. In the RAS-FUBM CC, one VSC is assigned for the voltage control and others VSC are assigned for an active power control, which provides better distribution among active power in the transmission lines. This in turn can help mitigate congestion in the overall or specific transmission lines. To the contrary, the SI numbers for the RAS-FUBM DC are higher and continue to increase as the voltage setting is raised. Once the voltage reaches a certain setting (i.e., ≥ 1.05) the SI number is higher compared to the DWI +5% case. The RAS-FUBM DC is a distributed control technique, by which the proportion of power sharing among converters is determined by the droop gain. Each VSC adjusts its power independently based on the droop characteristic. This characteristic depicted in Figure 3.7 in section 3.3.2 of Chapter 3 consists of a negative slope in the regulation curve. The steeper slope in the droop curve is a drawback, as it corresponds to a poorer regulation voltage [255], which can potentially impact the overall stability of the power system. This limitation is inherent to linear control scheme, as they tend to be less robust against the proportional power sharing requirements.

Maintaining voltage stability within acceptable limits is a critical aspect in power system op-

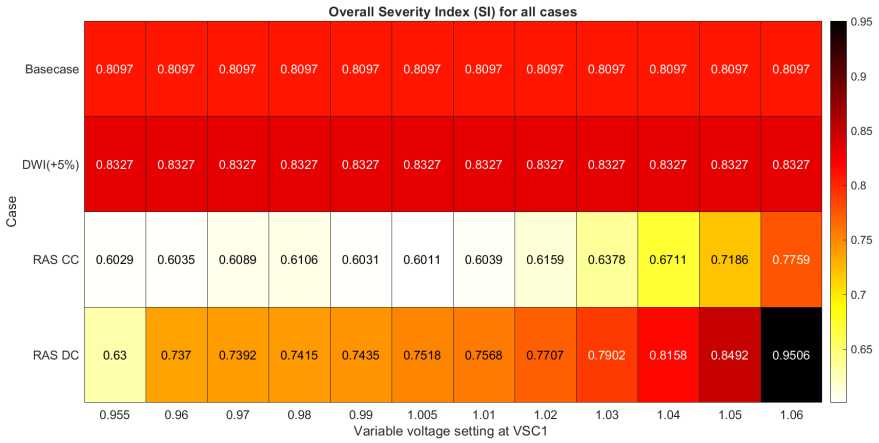

Figure 5.8: Severity Index for all DC voltage settings

eration. In order to evaluate the feasibility of VM values under different scenarios (i.e., basecase, DWI +5%, RAS-FUBM CC and RAS-FUBM DC for different DC voltage setting at DC side), the probability of VM ranges are measured using the CDF. Table 5.8 and Table 5.9 show the probability of specific ranges of VMs (i.e., $P(0.96 \leq x \leq 0.98), P(0.98 \leq x \leq 1.02), P(0.97 \leq x \leq .04), P(1.03 \leq x \leq 1.04) and P(1.06 \leq x \leq 1.08)$) for the basecase and DWI +5%. For the basecase and DWI+5% cases, which have the same standard deviation (σ) of 0.0296, but different mean (μ) values (i.e., basecase at 1.0054 p.u. and DWI +5% case at 1.0039 p.u.), the analysis of the data from these tables reveals that the VM values exhibit the highest probability of falling within the 0.97 p.u. to 1.04 p.u. range for both scenarios. The CDF indicates that the probability of the VM values within these acceptable ranges is 0.7623 (76.23%) for the basecase and 0.7632 (76.32%) for the DWI +5% case. The probability of the VM values falling within the interval between 0.98p.u -1. 02p.u is 0.4930 (49.30%) for the basecase and 0.4976 (49.76%) for the DWI +5% case. Investigating the probability of the VM values nearing the lower limit (i.e., the voltage magnitude limits for AC and DC systems are displayed in Table 5.7) demonstrated that the probability is relatively low. For the basecase, the probability is 0.1329 (13.29%) for the VM range between 0.96 p.u. - 0.98 p.u., and for the DWI +5% case, the probability is 0.1407 (14.07%) for the same VM ranges. For the VM values close to the upper limit (with VM ranges 1.03p.u-1.04p.u), the data shows the probability for the basecase and DWI+5% are 0.0818 (8.18%) and 0.0776 (7.76%), respectively. The probability for the VM values near the upper limit is 0.0818 (8.18%) for the basecase and 0.0776(7.76%) for the DWI +5%, where the VM ranges from 1.03p.u to 1.04p.u. The percentage probability of VM values beyond the upper limit for the AC system (i.e., the upper limit for the load bus is 1.05p.u), specifically in the range of 1.06p.u – 1.08p.u, is approximately 2% for both cases. The calculated probabilities are 0.0268 (2.68%) for the basecase and 0.0238 (2.38%) for the DWI +5% case.

Table 5.12 compares the results obtained from the probability analysis for two types of RAS-

Table 5.7: Voltage Magnitude Limits

Voltage Magnitude Limits	Lower limit	Upper limit
AC system		
Load bus :	1.05	0.95
Generator bus :	1.1	0.95
DC system		
All buses :	1.15	0.95

FUBM controls (i.e., RAS-FUBM CC and RAS-FUBM DC), which has the DC voltage setting at VSC1 is set to 0.98p.u, that has been implemented within the MT-HVDC system. The means and standard deviations for RAS-FUBM CC are 0.9973p.u and 0.0329, respectively, whilst for RAS-FUBM DC are 0.9956p.u and 0.0328, respectively. From the data in Table 5.12, it is apparent that the highest probability occurred for both RAS-FUBM actions within VM range 0.97p.u -1.04p.u, which is approximately 70%. The exact probability calculations are 0.6994 (69.94%) for the RAS-FUBM CC and 0.6949 (69.49%) for the RAS-FUBM DC. The likelihood of VM variance between 0.98p.u and 1.02p.u for the two RAS-FUBM actions is around 45% (i.e., RAS-FUBM CC is 0.4553 (45.53%) and RAS-FUBM DC is 0.4547 (45.47%)). As for the VM values near to the upper limits (i.e., 1.03p.u – 1.04p.u) the probability for RAS-FUBM CC is 0.0630 (6.30%) and RAS-FUBM DC is 0.0591 (5.91%). Whilst for the VM values near to the lower limits (i.e., 0.96p.u- 0.98p.u) the probabilities for RAS-FUBM CC and RAS-FUBM DC are 0.1710 (17.10%) and 0.1785 (17.85%), respectively. The likelihood of VM values lying in the range beyond the limit of 1.06p.u – 1.08p.u is relatively low, with RAS-FUBM CC at 0.0224 (2.24%) and RAS-FUBM DC at 0.0196 (1.96%). In summary, the results demonstrate that the VM values remain within acceptable operating limits, even when the DC voltage setting at the DC side has been configured to a lower value than the basecase (i.e., VSC1 parameter at basecase is set at 1.0p.u)

Table 5.13 displays the probability observations for the VM ranges between RAS-FUBM CC and RAS-FUBM DC actions at the higher DC voltage setting at DC side (i.e., VSC1 is set to 1.02p.u). Normal distribution for both control actions is defined by means and standard deviations at 1.0168p.u and 0.0264 for RAS-FUBM CC and 1.015p.u and 0.0261 for RAS-FUBM DC, respectively. The results obtained from the CDF calculation indicated that, approximately 77% (0.7726) of the VM values for the RAS-FUBM CC and 80% (0.7893) for the RAS-FUBM DC lie on the ranges of 0.97p.u-1.04p.u. Furthermore, almost 50% for both action (i.e., RAS-FUBM is 0.4667 and RAS-FUBM DC is 0.4866) of the VM values fall in the ranges of 0.98p.u – 1.02p.u. Contrary to when the VSC1 is set to the 0.98p.u, the probability of VM values close to the lower limits (i.e., 0.96p.u- 0.98p.u) is comparatively low, at about 6% (0.0656) for RAS-FUBM CC and 7% (0.0724) for the RAS-FUBM DC. It is noteworthy that there is a significant increase in the percentage of

likelihood for VM values close to its upper limits (i.e., 1.03p.u-1. 04p.u). For RAS-FUBM CC and RAS-FUBM DC, this corresponds to almost 12% (0.1190) and 11% (0.1136), respectively. The probability of VM ranges beyond 1.06p.u and less than 1.08p.u are relatively smaller, which is 4.24% for RAS-FUBM CC and 3.57% for RAS-FUBM DC. These percentages, however, are somewhat greater than those obtained with the VSC1 set to 0.98p.u. Overall, the results presented indicate that all VM values fall within the acceptable limits, regardless of whether the DC voltage setting at the DC side has been changed to a higher setting than the basecase (i.e., VSC1 parameter at basecase is set at 1.0p.u).

Table 5.8: Basecase

Basecase		
mean(μ) :	1.0054	
std (σ) :	0.0296	
	VM range (p.u)	Probability
$P(a \leq X \leq b)$	$0.96 - 0.98$	0.1329
	$0.98 - 1.02$	0.4930
	$0.97 - 1.04$	0.7623
	$1.03 - 1.04$	0.0818
	$1.06 - 1.08$	0.0268

Table 5.9: DWI +5%

DWI +5%		
mean (μ) :	1.0039	
std (σ) :	0.0296	
	VM range (p.u)	Probability
$P(a \leq X \leq b)$	$0.96 - 0.98$	0.1407
	$0.98 - 1.02$	0.4976
	$0.97 - 1.04$	0.7632
	$1.03 - 1.04$	0.0776
	$1.06 - 1.08$	0.0238

These results are particularly important, as these analyses show that the hybrid AC/DC network with the MT-HVDC link model offers greater flexibility, especially when demand and wind generation increase, and in this case study, it increases by 5% using DC voltage control. Furthermore, hybrid AC/DC networks are expected to become a prevalent form of network in the future, making it essential to develop planning scenarios that consider various types of control (i.e., DC voltage in this case study).

Table 5.10: Demand Data (P_d)

Bus	**Standard Demand** (P_d)	**Demand Increased by 5%** (P_d)
101	0	0
102	21.7	22.785
103	2.4	2.52
104	7.6	7.98
105	0	0
106	0	0
107	22.8	23.94
108	30	31.5
109	0	0
110	5.8	6.09
111	0	0
112	11.2	11.76
113	0	0
114	6.2	6.51
115	8.2	8.61
116	3.5	3.675
117	9	9.45
118	3.2	3.36
119	9.5	9.975
120	2.2	2.31
121	17.5	18.375
122	0	0
123	3.2	3.36
124	8.7	9.135
125	0	0
126	3.5	3.675
127	0	0
128	0	0
129	2.4	2.52
130	10.6	11.13
131	0	0
132	0	0
133	0	0
134	0	0
135	0	0
136	0	0
137	0	0
141	0	0

Table 5.11: Wind generator (P_g)

Wind Farm	**Standard Wind Generation** (P_g)	**Wind Increased by 5%** (P_g)
A	8	8.4
B	10	10.5
C	15	15.75

Table 5.12: Comparison of RAS-FUBM CC and RAS-FUBM DC for VSC1 = 0.98

VSC1 = 0.98					
RAS-FUBM CC			RAS-FUBM DC		
mean (μ) :	0.9973		mean (μ) :	0.9956	
std (σ) :	0.0329		std (σ):	0.0328	
	VM range (p.u)	Probability		VM range (p.u)	Probability
$P(a \leq X \leq b)$	$0.96 - 0.98$	0.1710	$P(a \leq X \leq b)$	$0.96 - 0.98$	0.1785
	$0.98 - 1.02$	0.4553		0.98 - 1.02	0.4547
	$0.97 - 1.04$	0.6994		0.97 - 1.04	0.6949
	$1.03 - 1.04$	0.0630		1.03 - 1.04	0.0591
	$1.06 - 1.08$	0.0224		$1.06 - 1.08$	0.0196

Table 5.13: Comparison of RAS-FUBM CC and RAS-FUBM DC for VSC1 = 1.02

VSC1 = 1.02					
RAS-FUBM CC			RAS-FUBM DC		
mean (μ) :	1.0168		mean (μ) :	1.015	
std (σ) :	0.0264		std (σ):	0.0261	
	VM range (p.u)	Probability		VM range (p.u)	Probability
$P(a \leq X \leq b)$	$0.96 - 0.98$	0.0656	$P(a \leq X \leq b)$	0.96 – 0.98	0.0724
	$0.98 - 1.02$	0.4667		0.98 - 1.02	0.4866
	$0.97 - 1.04$	0.7726		0.97 - 1.04	0.7893
	$1.03 - 1.04$	0.119		1.03 - 1.04	0.1136
	$1.06 - 1.08$	0.0424		1.06 – 1.08	0.0357

5.6 Chapter summary

This chapter presents a study for long-term planning to provide a holistic techno-economic framework for planning and designing the hybrid AC/DC networks with MT-HVDC link integrated with OWFs. The first aspect investigates incorporating multiple decision criteria through the MO-OPF problem formulation to optimise the VSC placement, considering overall generation, congestion and VSC placement (i.e., capital and operation costs) costs. The second aspect relates to the DC voltage control at the reference VSC node, deploying the VSC placement, which can benefit long-term planning to mitigate the MT-HVDC link congestion. Two case studies have been conducted to investigate the impact of VSC placement in hybrid AC/DC networks. The first case discovered the optimal VSC placement able to demonstrate superior performance, mitigating and reducing the congestion, despite relatively high integration costs of VSC within the MT-HVDC link. The second case study, utilised DC voltage control at the reference VSC node, along with statistical analysis to provide insightful understanding of the VM variables characteristics, which offers benefits for the operation, control and long-term planning of the MT-HVDC link. Overall, the findings from these two case studies provide a comprehensive understanding of techno-economic impacts of VSC placement within the hybrid AC/DC network.

Chapter 6

Conclusion

This final chapter synthesises the conclusions drawn from the research presented throughout the thesis. In line with the thesis aims and objectives, it explores the aspects of associated challenges, focuses on significant contributions, and addresses the crucial issues of problem transformation in the power system as stated in the research questions. Furthermore, it lays out a path forward for future directions in which this work can be extended at the end of this chapter.

6.1 Conclusion

The aim of this thesis has been to develop a model for reinforcement of transmission systems through the utilisation of Voltage Source Converter (VSC) technology, employing the Flexible Universal Branch Model (FUBM) to model the operation of a Multi-Terminal HVDC (MT-HVDC) link integrated with Offshore Wind Farms (OWFs). In order to achieve the reliability of a power system, which is related to the extensive analysis of the objectives outlined in section 1.2, a series of research questions has been identified in section 1.3 that further delves into the more challenging aspects of the research challenges presented in the same section. Chapter 3 presented a comprehensive mathematical modelling of the MT-HVDC link, utilizing the VSC in-model (one of the FUBM models) for OPF formulation, collectively referred to as OPF-FUBM. Chapter 4 introduced a modification of SCOPF formulation structures for short-term operational planning, specifically single-period and multi-period approaches, in the power systems to respond to the uncertainties and variability associated with the random and inherently variable nature of renewable energy resources, particularly offshore wind. Furthermore, the novel approach to the traditional Remedial Action Scheme (RAS), known as RAS-FUBM, was established to facilitate flexible actions aimed at mitigating contingencies within hybrid AC/DC networks. Chapter 5 presented a long-term planning approach associated with the multi-objective optimization problem related to OPF (i.e., MO-OPF) and the deployment of the VSC to alleviate the congestion with MT-HVDC link integrated with OWFs. This planning aims to provide a holistic techno-economic framework for

planning and designing the hybrid AC/DC networks with the MT-HVDC link. In summary, this thesis contributes to the development of reinforcement transmission models and control strategies, which can enhance the integration of renewable energy into existing power systems. The following subsection will provide a summary of the contributions made by this work.

6.2 Key outcome and contributions

The challenging aspects of this thesis in section 1.3 have contributed to the development of transmission reinforcement models through control strategies in VSC technology, thereby enhancing the integration of renewable energy into existing power systems. Further explanations of the contributions of this thesis can be summarized as follows:

(a) **A Mathematical Model for MT-HVDC links:**

MT-HVDC links, which typically consist of multiple converters forming a meshed DC link, are seen to be a feasible solution to integrate offshore wind resource capacity on a large scale and facilitate long-distance power exchange between different independent operating regions (e.g., countries). The mathematical modelling of these links for steady-state operational planning and analysis was discussed in Chapter 3. This modelling demonstrated the capability of converters, particularly focusing on VSC technology, to regulate voltage and power in both AC and DC systems, thereby providing greater freedom and flexibility within the power system and effectively enhancing reliability and operational security. This comprehensive modelling approach could yield critical insights into the design and operation of Supergrid infrastructures, which aim to enhance interconnectivity among power systems across regions. Furthermore, it could expedite the implementation of such infrastructures, facilitating energy trading and enabling efficient power system management.

(b) **A holistic operational planning framework:**

The control strategy discussed in Chapter 3 for MT-HVDC links using VSC technology represents an innovative modelling framework within the power system, especially for the hybrid AC/DC networks. Given its enhanced flexibility, the operation of the power system can be improved in terms of both voltage regulation and power flow control. The VSC is a suitable candidate for forming MT-HVDC links that also integrate large-scale OWFS generation capacity into future AC networks. The development of control strategies could enhance the resilience of the transmission system against disruptions, thereby improving reliability in the power system and reducing the impacts of outages. These contributions showcase the versatility of VSC technology in modern power systems, particularly in facilitating the transition to renewable energy sources and addressing future demand for technologies such as electric vehicles, energy storage, and smart grids. Furthermore, it could facilitate the integration of various renewable energy sources, such as wave, tidal and hydrogen into a unified energy hub.

This integration could encourage investment in renewable energy projects and contribute to national and global climate goals.

(c) **Application and impact assessment of additional control strategies in hybrid AC/DC networks with embedded MT-HVDC links:**

Modern power systems require a flexible operation approach. The implementation of the VSC control strategies framework in Chapters 4 and 5, which considers a range of scenarios (e.g., worst-case scenarios, multi-period scenarios, and multi-objective scenarios), has demonstrated the flexibility and reliability of the power system, particularly in mitigating contingencies and congestion within the MT-HVDC link. The application of these control strategies in operational planning (i.e., short-term and long-term considerations) in hybrid AC/DC networks has led to robust analyses based on scenario planning. These applications establish performance benchmarks based on multiple scenario analyses, enabling the comparison of different control strategies and identifying optimal practices in the operational planning. By providing Transmission System Operators (TSOs) with these analyses (i.e., scenario planning) throughout the operational planning phase, this approach will also help them make optimal decisions. In a broader context, the application of control strategies in the MT-HVDC link integrated with OWFs contributes to power grid modernisation initiatives, facilitating the transition of weather-dependent generation towards a smarter and more resilient power system, particularly within hybrid AC/DC networks.

6.3 Future works

The work presented in this thesis has established a comprehensive framework for reinforcing the transmission system in hybrid AC/DC networks of modern power system. It introduces new performance benchmarks for optimisation modelling problems based on multiple scenario assessments, thereby offering greater flexibility within power system and presenting highly realistic and flexible mathematical models for OPF and SCOPF. Nevertheless, there remain significant potential for further expanding the contribution of this work to the field of power system research, as outlined below:

(a) **Control strategy evaluation:**

Evaluate other control strategies in the FUBM under steady-state conditions, assessing their effectiveness in managing power flow and ensuring stability in hybrid AC/DC networks such as AC voltage control and reactive power control.

(b) **Loss assessment:**

Examine the trade-offs between different operating strategy configurations and analyse techniques for minimising losses in both AC and DC systems. Furthermore, when evaluating

losses in the DC system, characteristics of power electronics devices in the FACTS such as temperature and thermal should be given consideration.

(c) **Machine learning:**

Integrate machine learning with traditional OPF methodologies to optimise power dispatch in hybrid AC/DC networks, taking into account various operating strategies. Additionally, employ machine learning to improve stochastic optimisation models, thereby facilitating more informed decision-making under uncertainty in generation and demand.

(d) **Dynamic modelling:**

Develop dynamic models of hybrid AC/DC networks to accurately simulate the behaviour of MT-HVDC links under various operating conditions. Utilising real-time simulation to analyse the power system performance and optimise its operation effectively.

Bibliography

[1] U. DeSA, "World population projected to reach 9.7 billion by 2050," *United Nations Department of Economic and Social Affairs*, 2015.

[2] U. Nations, "For a livable climate: Net-zero commitments must be backed by credible action," *Climate Change*, 2022.

[3] X. Wu, Z. Tian, and J. Guo, "A review of the theoretical research and practical progress of carbon neutrality," *Sustainable Operations and Computers*, vol. 3, pp. 54–66, 2022.

[4] D. Tan and D. Novosel, "Energy challenge, power electronics & systems (peas) technology and grid modernization," *CPSS Transactions on Power Electronics and Applications*, vol. 2, no. 1, pp. 3–11, 2017.

[5] M. I. Henderson, D. Novosel, and M. L. Crow, "Electric power grid modernization trends, challenges, and opportunities," in *IEEE, Nov*, 2017.

[6] J. R. Aguero, E. Takayesu, D. Novosel, and R. Masiello, "Modernizing the grid: Challenges and opportunities for a sustainable future," *IEEE Power and Energy Magazine*, vol. 15, no. 3, pp. 74–83, 2017.

[7] D. Jigoria-Oprea, C. Barbulescu, S. Kilyeni, and M. Raduca, "Large wind farms integration in romanian power system. case study: Moldavia region," in *2011 6th IEEE International Symposium on Applied Computational Intelligence and Informatics (SACI)*. IEEE, 2011, pp. 565–570.

[8] A. Navon, G. Ben Yosef, R. Machlev, S. Shapira, N. Roy Chowdhury, J. Belikov, A. Orda, and Y. Levron, "Applications of game theory to design and operation of modern power systems: A comprehensive review," *Energies*, vol. 13, no. 15, p. 3982, 2020.

[9] O. Azeem, M. Ali, G. Abbas, M. Uzair, A. Qahmash, A. Algarni, and M. R. Hussain, "A comprehensive review on integration challenges, optimization techniques and control strategies of hybrid ac/dc microgrid," *Applied Sciences*, vol. 11, no. 14, p. 6242, 2021.

[10] H. Government, "The ten point plan for a green industrial revolution," *Tech. rep*, 2020.

[11] H. H. Alhelou and M. Golshan, "Decision-making-based optimal generation-side secondary-reserve scheduling and optimal lfc in deregulated interconnected power system," in *Decision making applications in modern power systems*. Elsevier, 2020, pp. 269–299.

[12] A. F. Abdin, A. Caunhye, E. Zio, and M.-A. Cardin, "Optimizing generation expansion planning with operational uncertainty: A multistage adaptive robust approach," *Applied Energy*, vol. 306, p. 118032, 2022.

[13] S. N. Sea, "Roadmap to the deployment of offshore wind energy," *windspeed*, 2005.

[14] D. Van Hertem, M. Ghandhari, and M. Delimar, "Technical limitations towards a super-grid—a european prospective," in *2010 IEEE International Energy Conference*. IEEE, 2010, pp. 302–309.

[15] D. Jovcic, L. Lamont, and K. Abbott, "Control system design for vsc transmission," *Electric Power Systems Research*, vol. 77, no. 7, pp. 721–729, 2007.

[16] M. Shafiullah, M. Abido, and A. Al-Mohammed, *Power system fault diagnosis: a wide area measurement based intelligent approach*. Elsevier, 2022.

[17] C. L. Lara, D. S. Mallapragada, D. J. Papageorgiou, A. Venkatesh, and I. E. Grossmann, "Deterministic electric power infrastructure planning: Mixed-integer programming model and nested decomposition algorithm," *European Journal of Operational Research*, vol. 271, no. 3, pp. 1037–1054, 2018.

[18] J. Á. González Ordiano, S. Waczowicz, V. Hagenmeyer, and R. Mikut, "Energy forecasting tools and services," *Wiley Interdisciplinary Reviews: Data Mining and Knowledge Discovery*, vol. 8, no. 2, p. e1235, 2018.

[19] L. Baringo and A. J. Conejo, "Transmission and wind power investment," *IEEE transactions on power systems*, vol. 27, no. 2, pp. 885–893, 2012.

[20] M. Mahdavi, C. S. Antunez, M. Ajalli, and R. Romero, "Transmission expansion planning: Literature review and classification," *IEEE Systems Journal*, vol. 13, no. 3, pp. 3129–3140, 2018.

[21] A. Kazerooni, *Methodologies and techniques for transmission planning under corrective control paradigm*. The University of Manchester (United Kingdom), 2012.

[22] M. Shahidehpour, H. Yamin, and Z. Li, *Market operations in electric power systems: forecasting, scheduling, and risk management*. John Wiley & Sons, 2002.

[23] M. Jadidoleslam, A. Ebrahimi, and M. A. Latify, "Probabilistic transmission expansion planning to maximize the integration of wind power," *Renewable energy*, vol. 114, pp. 866–878, 2017.

[24] Q. Li, J. Wang, Y. Zhang, Q. Wu, C. Gu, and Q. Yang, "Hierarchical market-based optimal planning of transmission network and wind-storage hybrid power plant," *International Journal of Electrical Power & Energy Systems*, vol. 153, p. 109328, 2023.

[25] M. A. Odhano, M. S. Jokhio, N. A. Unar, N. H. Mirjat, S. A. Khatri, and B. Aslam, "Modelling and analysis of power losses in transmission system of pakistan: a case study of matiari-lahore vsc-hvdc link," in *2021 6th International Multi-Topic ICT Conference (IMTIC)*. IEEE, 2021, pp. 1–5.

[26] I. M. De Alegría, J. L. Martín, I. Kortabarria, J. Andreu, and P. I. Ereño, "Transmission alternatives for offshore electrical power," *Renewable and sustainable energy reviews*, vol. 13, no. 5, pp. 1027–1038, 2009.

[27] A. Endegnanew, H. Svendsen, and R. Torres-Olguin, "Design procedure for inter-array electric design (d2. 2)," *EU FP7 EERA-DTOC Project*, 2013.

[28] G. F. Reed, H. A. Al Hassan, M. J. Korytowski, P. T. Lewis, and B. M. Grainger, "Comparison of hvac and hvdc solutions for offshore wind farms with a procedure for system economic evaluation," in *2013 IEEE Energytech*. IEEE, 2013, pp. 1–7.

[29] R. Ulsund, "Offshore power transmission: Submarine high voltage transmission alternatives," Master's thesis, Institutt for elkraftteknikk, 2009.

[30] B. Kirby and E. Hirst, "Ancillary service details: Voltage control," Oak Ridge National Lab.(ORNL), Oak Ridge, TN (United States), Tech. Rep., 1997.

[31] C. Wadhwa, *Electrical power systems*. New Age International, 2006.

[32] P. Kundur, "Power system stability," *Power system stability and control*, vol. 10, pp. 7–1, 2007.

[33] E. Acha, *Power electronic control in electrical systems*. Newnes, 2002.

[34] A. Alassi, S. Bañales, O. Ellabban, G. Adam, and C. MacIver, "Hvdc transmission: Technology review, market trends and future outlook," *Renewable and Sustainable Energy Reviews*, vol. 112, pp. 530–554, 2019.

[35] O. Gomis-Bellmunt, A. Egea-Alvarez, A. Junyent-Ferré, J. Liang, J. Ekanayake, and N. Jenkins, "Multiterminal hvdc-vsc for offshore wind power integration," in *2011 IEEE Power and Energy Society General Meeting*. IEEE, 2011, pp. 1–6.

[36] C. Li, K. Li, C. Ma, P. Zhang, Q. Tao, Y. Sun, and X. Wang, "Flexible control strategy for hvdc transmission system adapted to intermittent new energy delivery," *Global Energy Interconnection*, vol. 4, no. 4, pp. 425–433, 2021.

[37] R. Perveen, N. Kishor, and S. R. Mohanty, "Off-shore wind farm development: Present status and challenges," *Renewable and Sustainable Energy Reviews*, vol. 29, pp. 780–792, 2014.

[38] K. Meah and S. Ula, "Comparative evaluation of hvdc and hvac transmission systems," in *2007 IEEE Power Engineering Society General Meeting.* IEEE, 2007, pp. 1–5.

[39] A. Madariaga, J. Martín, I. Zamora, I. M. De Alegría, and S. Ceballos, "Technological trends in electric topologies for offshore wind power plants," *Renewable and Sustainable Energy Reviews*, vol. 24, pp. 32–44, 2013.

[40] D. Van Hertem, O. Gomis-Bellmunt, and J. Liang, *HVDC grids: for offshore and supergrid of the future.* John Wiley & Sons, 2016.

[41] A. Raza, A. Mustafa, K. Rouzbehi, M. Jamil, S. O. Gilani, G. Abbas, U. Farooq, and M. N. Shehzad, "Optimal power flow and unified control strategy for multi-terminal hvdc systems," *IEEE Access*, vol. 7, pp. 92 642–92 650, 2019.

[42] M. Abdelwahed, H. Sindi, and E. F. El-Saadany, "Power sharing control and wind power curtailing for offshore multi-terminal vsc-hvdc transmission," in *2016 IEEE Smart Energy Grid Engineering (SEGE).* IEEE, 2016, pp. 141–146.

[43] B. Van Eeckhout, D. Van Hertem, M. Reza, K. Srivastava, and R. Belmans, "Economic comparison of vsc hvdc and hvac as transmission system for a 300 mw offshore wind farm," *European Transactions on Electrical Power*, vol. 20, no. 5, pp. 661–671, 2010.

[44] Z. Wang, L. Yao, J. Wu, X. Cai, and G. Shi, "Large offshore wind power collection using dc grid technology," in *International Conference on Renewable Power Generation (RPG 2015).* IET, 2015, pp. 1–6.

[45] M. K. Bucher, R. Wiget, G. Andersson, and C. M. Franck, "Multiterminal hvdc networks—what is the preferred topology?" *IEEE Transactions on Power Delivery*, vol. 29, no. 1, pp. 406–413, 2013.

[46] G. K. Mishra and Y. Singh, "Performance analysis of various topologies in hvdc networks," *International Journal of Power Systems*, vol. 6, 2021.

[47] O. Gomis-Bellmunt, J. Liang, J. Ekanayake, R. King, and N. Jenkins, "Topologies of multiterminal hvdc-vsc transmission for large offshore wind farms," *Electric Power Systems Research*, vol. 81, no. 2, pp. 271–281, 2011.

[48] A. Raza, M. Younis, Y. Liu, A. Altalbe, K. Rouzbehi, and G. Abbas, "A multi-terminal hvdc grid topology proposal for offshore wind farms," *Applied Sciences*, vol. 10, no. 5, p. 1833, 2020.

[49] L. Q. Liu and C. X. Liu, "VSCs-HVDC may improve the Electrical Grid Architecture in future world," *Renewable and Sustainable Energy Reviews*, vol. 62, pp. 1162–1170, 2016. [Online]. Available: http://dx.doi.org/10.1016/j.rser.2016.05.037

[50] M. E. Montilla-DJesus, S. Arnaltes, E. D. Castronuovo, and D. Santos-Martin, "Optimal power transmission of offshore wind power using a VSC-HVdc interconnection," *Energies*, vol. 10, no. 7, 2017.

[51] A. Alassi, S. Bañales, O. Ellabban, G. Adam, and C. MacIver, "HVDC Transmission: Technology Review, Market Trends and Future Outlook," *Renewable and Sustainable Energy Reviews*, vol. 112, pp. 530–554, 2019.

[52] E. Karami, G. B. Gharehpetian, H. Mohammadpour, A. Khalilinia, and A. Bali, "Generalised representation of multi-terminal VSC-HVDC systems for AC-DC power flow studies," *IET Energy Systems Integration*, vol. 2, no. 1, pp. 50–58, 2020.

[53] B. Yang, B. Liu, H. Zhou, J. Wang, W. Yao, S. Wu, H. Shu, and Y. Ren, "A critical survey of technologies of large offshore wind farm integration: summary, advances, and perspectives," *Protection and Control of Modern Power Systems*, vol. 7, no. 1, 2022. [Online]. Available: https://doi.org/10.1186/s41601-022-00239-w

[54] E. Pierri, O. Binder, N. G. Hemdan, and M. Kurrat, "Challenges and opportunities for a European HVDC grid," *Renewable and Sustainable Energy Reviews*, vol. 70, no. October 2015, pp. 427–456, 2017. [Online]. Available: http://dx.doi.org/10.1016/j.rser.2016.11.233

[55] L.-q. Liu and C.-x. Liu, "VSCs-HVDC may improve the Electrical Grid Architecture in future world," *Renewable and Sustainable Energy Reviews*, vol. 62, pp. 1162–1170, 2016.

[56] M. P. Bahrman and B. K. Johnson, "The ABCs of HVDC transmission technologies," *IEEE power and energy magazine*, vol. 5, no. 2, pp. 32–44, 2007.

[57] C. Ng and P. McKeever, "Next generation HVDC network for offshore renewable energy industry," *IET Conference Publications*, vol. 2012, no. 610 CP, pp. 1–7, 2012.

[58] M. Belgacem, M. Khatir, M. A. Djehaf, R. Bouddou, and S. A. Zidi, "Modeling and Control of Multi-Terminal Direct Current with Voltage Margin Control Strategy," *Proceedings - 2019 4th International Conference on Power Electronics and their Applications, ICPEA 2019*, no. September, pp. 25–27, 2019.

[59] I. M. de Alegría, J. L. Martín, I. Kortabarria, J. Andreu, and P. I. Ereño, "Transmission alternatives for offshore electrical power," *Renewable and Sustainable Energy Reviews*, vol. 13, no. 5, pp. 1027–1038, 2009.

[60] E. P. Wiechmann, P. Aqueveque, R. Burgos, and J. Rodriguez, "On the efficiency of voltage source and current source inverters for high-power drives," *IEEE Transactions on Industrial Electronics*, vol. 55, no. 4, pp. 1771–1782, 2008.

[61] Y. Xue, "Modelling and control of hybrid LCC HVDC System," Ph.D. dissertation, University of Birmingham, 2016.

[62] K. RGAARD, S. MIKKELSEN *et al.*, "Bipolar operation of an HVDC VSC converter with an LCC converter [C]," in *CIGRE Colloquium on HVDC and Power Electronic Systems*, vol. 7, 2012, pp. 1–7.

[63] Hitachi Energy, "Dogger bank customer success story," 2023, accessed: 2025-02-27. [Online]. Available: https://www.hitachienergy.com/uk-ie/en/news-and-events/customer-success-stories/dogger-bank

[64] O. Sha and W. Zhang, "Optimal coordinated control of steady-state voltage stability in ac/dc systems incorporating vsc-hvdc," in *The 16th IET International Conference on AC and DC Power Transmission (ACDC 2020)*, vol. 2020, 2020, pp. 1420–1425.

[65] S. Liu, M. Miao, T. Shi, and J. Li, "Optimal power flow in hybrid AC/DC distribution network considering different control strategies of VSC stations," *China International Conference on Electricity Distribution, CICED*, no. 201804260000018, pp. 1380–1384, 2018.

[66] K. Peng, S. Eskandari, and E. Santi, "Analytical loss model for power converters with sic mosfet and sic schottky diode pair," in *2015 IEEE Energy Conversion Congress and Exposition (ECCE)*. IEEE, 2015, pp. 6153–6160.

[67] P. S. Jones and C. C. Davidson, "Calculation of power losses for mmc-based vsc hvdc stations," in *2013 15th European Conference on Power Electronics and Applications (EPE)*. IEEE, 2013, pp. 1–10.

[68] Q. Wang and S. Lu, "Power loss evaluation for sic mosfet-based isolated bidirectional dual active bridge dc-dc converter," in *2019 14th IEEE Conference on Industrial Electronics and Applications (ICIEA)*. IEEE, 2019, pp. 2457–2462.

[69] N. Prabaharan and K. Palanisamy, "A comprehensive review on reduced switch multilevel inverter topologies, modulation techniques and applications," *Renewable and Sustainable Energy Reviews*, vol. 76, pp. 1248–1282, 2017.

[70] J. Beerten, S. Cole, and R. Belmans, "Generalized steady-state VSC MTDC model for sequential AC/DC power flow algorithms," *IEEE Transactions on Power Systems*, vol. 27, no. 2, pp. 821–829, 2012.

[71] D. Chattopadhyay, "Operational planning of power system: An integrated approach," *Energy sources*, vol. 16, no. 1, pp. 59–73, 1994.

[72] J. D. McCalley, "Introduction to system operation, optimization, and control."

[73] Y. Ding, C. Singh, L. Goel, J. Østergaard, and P. Wang, "Short-term and medium-term reliability evaluation for power systems with high penetration of wind power," *IEEE Transactions on Sustainable Energy*, vol. 5, no. 3, pp. 896–906, 2014.

[74] Y. Li, L. Yu, and F. Zhang, "Technical and economic research on far coast wind power transmission based on ac transmission system," in *2024 7th International Conference on Energy, Electrical and Power Engineering (CEEPE)*. IEEE, 2024, pp. 1302–1306.

[75] J. Reneses, E. Centeno, and J. Barquin, "Coordination between medium-term generation planning and short-term operation in electricity markets," *IEEE Transactions on Power Systems*, vol. 21, no. 1, pp. 43–52, 2006.

[76] S. Mohseni, A. C. Brent, S. Kelly, and W. N. Browne, "Demand response-integrated investment and operational planning of renewable and sustainable energy systems considering forecast uncertainties: A systematic review," *Renewable and Sustainable Energy Reviews*, vol. 158, p. 112095, 2022.

[77] Y. Du, X. Shen, D. M. Kammen, C. Hong, J. Nie, B. Zheng, and S. Yao, "A generation and transmission expansion planning model for the electricity market with decarbonization policies," *Advances in Applied Energy*, vol. 13, p. 100162, 2024.

[78] S. R. Khuntia, B. W. Tuinema, J. L. Rueda, and M. A. van der Meijden, "Time-horizons in the planning and operation of transmission networks: an overview," *IET generation, transmission & distribution*, vol. 10, no. 4, pp. 841–848, 2016.

[79] D. Salman and M. Kusaf, "Short-term unit commitment by using machine learning to cover the uncertainty of wind power forecasting," *Sustainability*, vol. 13, no. 24, p. 13609, 2021.

[80] A. S. Gaur, P. Das, A. Jain, R. Bhakar, and J. Mathur, "Long-term energy system planning considering short-term operational constraints," *Energy Strategy Reviews*, vol. 26, p. 100383, 2019.

[81] A. J. Wood, B. F. Wollenberg, and G. B. Sheblé, *Power generation, operation, and control*. John Wiley & Sons, 2013.

[82] P. Kundur, J. Paserba, V. Ajjarapu, G. Andersson, A. Bose, C. Canizares, N. Hatziargyriou, D. Hill, A. Stankovic, C. Taylor *et al.*, "Definition and classification of power system stability ieee/cigre joint task force on stability terms and definitions," *IEEE transactions on Power Systems*, vol. 19, no. 3, pp. 1387–1401, 2004.

[83] E. Ciapessoni, D. Cirio, A. Pitto, M. Van Harte, and M. Panteli, "Power system resilience: definition, features and properties," *Cigré Science & Engineering Journal*, vol. 30, 2023.

[84] J. Osborn and C. Kawann, "Reliability of the us electric system–recent trends and current issues," *Nil*, 2002.

[85] E. A. Hailu, G. N. Nyakoe, and C. M. Muriithi, "Techniques of power system static security assessment and improvement: A literature survey," *Heliyon*, vol. 9, no. 3, 2023.

[86] J. Das, *Load flow optimization and optimal power flow*. Crc Press, 2017.

[87] J. D. McCalley, V. Vittal, and N. Abi-Samra, "An overview of risk based security assessment," in *1999 IEEE Power Engineering Society Summer Meeting. Conference Proceedings (Cat. No. 99CH36364)*, vol. 1. IEEE, 1999, pp. 173–178.

[88] D. Nguyen and M. Negnevitsky, "Probabilistic security assessment for power system operation with significant wind penetration," in *2012 IEEE International Conference on Power System Technology (POWERCON)*. IEEE, 2012, pp. 1–6.

[89] U. Shahzad, "Probabilistic security assessment in power transmission systems: a review," *Journal of Electrical Engineering, Electronics, Control and Computer Science*, vol. 7, no. 4, pp. 25–32, 2021.

[90] F. Capitanescu, M. Glavic, D. Ernst, and L. Wehenkel, "Applications of security-constrained optimal power flows," in *Modern Electric Power Systems Symposium, MEPS06*, 2006.

[91] E. Vaahedi, *Practical power system operation*. John Wiley & Sons, 2014.

[92] S. Kalyani and K. S. Swarup, "Classification and assessment of power system security using multiclass svm," *IEEE Transactions on Systems, Man, and Cybernetics, Part C (Applications and Reviews)*, vol. 41, no. 5, pp. 753–758, 2010.

[93] S. Kalyani and K. Swarup, "Static security evaluation in power systems using multi-class svm with different parameter selection methods," *International Journal of Machine Learning and Computing*, vol. 1, no. 2, p. 193, 2011.

[94] R. Fischl, "Application of neural networks to power system security: Technology and trends," in *Proceedings of 1994 IEEE International Conference on Neural Networks (ICNN'94)*, vol. 6. IEEE, 1994, pp. 3719–3723.

[95] J. Geeganage, U. Annakkage, T. Weekes, and B. A. Archer, "Application of energy-based power system features for dynamic security assessment," *IEEE Transactions on Power Systems*, vol. 30, no. 4, pp. 1957–1965, 2014.

[96] Y. Li, Y. Li, and Y. Sun, "Online static security assessment of power systems based on lasso algorithm," *Applied Sciences*, vol. 8, no. 9, p. 1442, 2018.

[97] R. Eichler, R. Krebs, S. Savulescu, and M. Wache, "Early detection and mitigation of the risk of blackout in transmission grid operation," in *Cigré International Symposium, Bologna, Italy*, 2011, pp. 13–15.

[98] C. Brochure, "Review of on-line dynamic security assessment tools and techniques," *CIGRE Working Group C*, vol. 4, p. 601, 2007.

[99] L. Wang and K. Morison, "Implementation of online security assessment," *IEEE Power and Energy Magazine*, vol. 4, no. 5, pp. 46–59, 2006.

[100] K. Morison, L. Wang, and P. Kundur, "Power system security assessment," *IEEE power and energy magazine*, vol. 2, no. 5, pp. 30–39, 2004.

[101] P. W. Sauer, K. L. Tomsovic, and V. Vittal, "Dynamic security assessment," *Power system stability and control*, vol. 5, pp. 421–430, 2007.

[102] A. N. Huda and R. Živanović, "Large-scale integration of distributed generation into distribution networks: Study objectives, review of models and computational tools," *Renewable and Sustainable Energy Reviews*, vol. 76, pp. 974–988, 2017.

[103] W. K. Chen, *The electrical engineering handbook*. Elsevier, 2004.

[104] P. Murty, *Power systems analysis*. butterworth-heinemann, 2017.

[105] A. Bretas, N. Bretas, J. B. London Jr, and B. Carvalho, *Cyber-physical power systems state estimation*. Elsevier, 2021.

[106] A. Von Meier, *Electric power systems: a conceptual introduction*. John Wiley & Sons, 2024.

[107] A. R. Bergen, *Power systems analysis*. Pearson Education India, 2009.

[108] M. Castro-Nunez and R. Castro-Puche, "Advantages of geometric algebra over complex numbers in the analysis of networks with nonsinusoidal sources and linear loads," *IEEE Transactions on Circuits and Systems I: Regular Papers*, vol. 59, no. 9, pp. 2056–2064, 2012.

[109] J. D. Glover, T. J. Overbye, and M. S. Sarma, *Power system analysis & design*. Cengage Learning, 2017.

[110] J. J. Grainger, *Power system analysis*. McGraw-Hill, 1999.

[111] K. M. Tenny and M. Keenaghan, *Ohms Law*. StatPearls Publishing, Treasure Island (FL), 2023. [Online]. Available: http://europepmc.org/books/NBK441875

[112] I. Nagrath, D. Kothari, and R. Desai, "Modern power system analysis," *IEEE Transactions on Systems, Man, and Cybernetics*, vol. 12, no. 1, pp. 96–96, 1982.

[113] N. Mbuli and W. Ngaha, "A survey of big bang big crunch optimisation in power systems," *Renewable and Sustainable Energy Reviews*, vol. 155, p. 111848, 2022.

[114] M. Gómez Sánchez, Y. M. Macia, A. Fernández Gil, C. Castro, S. M. Nuñez González, and J. Pedrera Yanes, "A mathematical model for the optimization of renewable energy systems," *Mathematics*, vol. 9, no. 1, p. 39, 2020.

[115] P. Y. Papalambros and D. J. Wilde, *Principles of optimal design: modeling and computation.* Cambridge university press, 2000.

[116] W. S. De Oliveira and A. J. Fernandes, "Optimization model for economic evaluation of wind farms-how to optimize a wind energy project economically and technically," *International Journal of Energy Economics and Policy*, vol. 2, no. 1, pp. 10–20, 2012.

[117] Y.-H. Song, *Modern optimisation techniques in power systems.* Springer Science & Business Media, 2013, vol. 20.

[118] W. Bukhsh, C. Edmunds, and K. Bell, "Oats: Optimisation and analysis toolbox for power systems," *IEEE Transactions on Power Systems*, vol. 35, no. 5, pp. 3552–3561, 2020.

[119] I. Ahmed, M. Rehan, A. Basit, S. H. Malik, K.-S. Hong *et al.*, "Multi-area economic emission dispatch for large-scale multi-fueled power plants contemplating inter-connected grid tie-lines power flow limitations," *Energy*, vol. 261, p. 125178, 2022.

[120] R. Chakrabarti, P. Chattopadhyay, and C. Panigrahi, "A review of recent advances in dynamic economic dispatch," *J. Inst. Eng. Electr. Eng. Div*, vol. 91, pp. 9–15, 2010.

[121] M. H. Hassan, S. Kamel, F. Jurado, and U. Desideri, "Global optimization of economic load dispatch in large scale power systems using an enhanced social network search algorithm," *International Journal of Electrical Power & Energy Systems*, vol. 156, p. 109719, 2024.

[122] J. Carpentier, "Optimal power flows: uses, methods and developments," *IFAC Proceedings Volumes*, vol. 18, no. 7, pp. 11–21, 1985.

[123] F. Capitanescu, "Critical review of recent advances and further developments needed in ac optimal power flow," *Electric Power Systems Research*, vol. 136, pp. 57–68, 2016.

[124] E. Acha, P. Roncero-Sánchez, A. De la Villa-Jaen, L. M. Castro, and B. Kazemtabrizi, *VSC-FACTS-HVDC: Analysis, modelling and simulation in power grids.* John Wiley & Sons, 2019.

[125] P. Pezzini, O. Gomis-Bellmunt, and A. Sudrià-Andreu, "Optimization techniques to improve energy efficiency in power systems," *Renewable and Sustainable Energy Reviews*, vol. 15, no. 4, pp. 2028–2041, 2011.

[126] M. Zhao, Z. Chen, and J. Hjerrild, "Analysis of the behaviour of genetic algorithm applied in optimization of electrical system design for offshore wind farms," in *IECON 2006-32nd Annual Conference on IEEE Industrial Electronics*. IEEE, 2006, pp. 2335–2340.

[127] M. R. Kalil, I. Musirin, and M. Othman, "Ant colony optimization for maximum loadability search in voltage control study," in *2006 IEEE International Power and Energy Conference*. IEEE, 2006, pp. 240–245.

[128] M. Ebeed, S. Kamel, and F. Jurado, "Optimal power flow using recent optimization techniques," in *Classical and recent aspects of power system optimization*. Elsevier, 2018, pp. 157–183.

[129] A. M. Nassef, M. A. Abdelkareem, H. M. Maghrabie, and A. Baroutaji, "Review of metaheuristic optimization algorithms for power systems problems," *Sustainability*, vol. 15, no. 12, p. 9434, 2023.

[130] R. D. Zimmerman, C. E. Murillo-Sánchez, and R. J. Thomas, "Matpower: Steady-state operations, planning, and analysis tools for power systems research and education," *IEEE Transactions on power systems*, vol. 26, no. 1, pp. 12–19, 2010.

[131] A. Alvarez-Bustos, B. Kazemtabrizi, M. Shahbazi, and E. Acha-Daza, "Universal branch model for the solution of optimal power flows in hybrid ac/dc grids," *International Journal of Electrical Power & Energy Systems*, vol. 126, p. 106543, 2021.

[132] S. S. H. Yazdi, S. H. Fathi, J. M. Monfared, and E. M. Amiri, "Optimal operation of multi terminal hvdc links connected to offshore wind farms," in *2014 11th International Conference on Electrical Engineering/Electronics, Computer, Telecommunications and Information Technology (ECTI-CON)*. IEEE, 2014, pp. 1–6.

[133] A. Monticelli, M. Pereira, and S. Granville, "Security-constrained optimal power flow with post-contingency corrective rescheduling," *IEEE Transactions on Power Systems*, vol. 2, no. 1, pp. 175–180, 1987.

[134] C. L. Borges and J. M. Alves, "Power system real time operation based on security constrained optimal power flow and distributed processing," in *2007 IEEE Lausanne Power Tech*. IEEE, 2007, pp. 960–965.

[135] D. Phan and J. Kalagnanam, "Some efficient optimization methods for solving the security-constrained optimal power flow problem," *IEEE Transactions on Power Systems*, vol. 29, no. 2, pp. 863–872, 2013.

[136] D. Layden and B. Jeyasurya, "Integrating security constraints in optimal power flow studies," in *IEEE Power Engineering Society General Meeting, 2004.* IEEE, 2004, pp. 125–129.

[137] M. M. Bhaskar, M. Srinivas, and S. Maheswarapu, "Security constraint optimal power flow(scopf)- a comprehensive survey," *Global Journal of Technology and optimization*, vol. 2, no. 11, 2011.

[138] F. Capitanescu, J. M. Ramos, P. Panciatici, D. Kirschen, A. M. Marcolini, L. Platbrood, and L. Wehenkel, "State-of-the-art, challenges, and future trends in security constrained optimal power flow," *Electric power systems research*, vol. 81, no. 8, pp. 1731–1741, 2011.

[139] F. Zhang, *Solving Large Security-Constrained Optimal Power Flow for Power Grid Planning and Operations.* Case Western Reserve University, 2020.

[140] H. Li, Z. Zhang, X. Yin, and B. Zhang, "Preventive Security-Constrained Optimal Power Flow with Probabilistic Guarantees," *Energies*, vol. 13, no. 9, 2020. [Online]. Available: https://www.mdpi.com/1996-1073/13/9/2344

[141] F. Capitanescu and L. Wehenkel, "Improving the statement of the corrective security-constrained optimal power-flow problem," *IEEE Transactions on Power Systems*, vol. 22, no. 2, pp. 887–889, 2007.

[142] ——, "A new iterative approach to the corrective security-constrained optimal power flow problem," *IEEE transactions on power systems*, vol. 23, no. 4, pp. 1533–1541, 2008.

[143] L. Huang, C. S. Lai, Z. Zhao, G. Yang, B. Zhong, and L. L. Lai, "Robust $N-k$ security-constrained optimal power flow incorporating preventive and corrective generation dispatch to improve power system reliability," *CSEE Journal of Power and Energy Systems*, vol. 9, no. 1, pp. 351–364, 2022.

[144] X. Wu, A. J. Conejo, and N. Amjady, "Robust security constrained acopf via conic programming: Identifying the worst contingencies," *IEEE Transactions on Power Systems*, vol. 33, no. 6, pp. 5884–5891, 2018.

[145] D. T. Phan and X. A. Sun, "Minimal impact corrective actions in security-constrained optimal power flow via sparsity regularization," *IEEE Transactions on Power Systems*, vol. 30, no. 4, pp. 1947–1956, 2014.

[146] Y. Xu, Z. Y. Dong, R. Zhang, K. P. Wong, and M. Lai, "Solving preventive-corrective scopf by a hybrid computational strategy," *IEEE transactions on power systems*, vol. 29, no. 3, pp. 1345–1355, 2013.

[147] W. Sun, C. C. Liu, and S. Liu, "Black start capability assessment in power system restoration," *IEEE Power and Energy Society General Meeting*, pp. 1–7, 2011.

[148] M. A. Perez, S. Ceballos, G. Konstantinou, J. Pou, and R. P. Aguilera, "Modular multilevel converters: Recent achievements and challenges," *IEEE Open Journal of the Industrial Electronics Society*, vol. 2, pp. 224–239, 2021.

[149] F. Muhammad and H. Rasheed, "Power loss distribution and characterization of modular multilevel converter for smart grid applications," *International Journal of Renewable Energy Research (IJRER)*, vol. 12, no. 3, pp. 1540–1551, 2022.

[150] R. H. Chandio, F. A. Chachar, J. B. Soomro, J. A. Ansari, H. M. Munir, H. M. Zawbaa, and S. Kamel, "Control and protection of mmc-based hvdc systems: A review," *Energy Reports*, vol. 9, pp. 1571–1588, 2023.

[151] L. Xu, L. Yao, and C. Sasse, "Power electronics options for large wind farm integration: VSC-based HVDC transmission," *2006 IEEE PES Power Systems Conference and Exposition, PSCE 2006 - Proceedings*, pp. 760–767, 2006.

[152] A. Alvarez-Bustos, B. Kazemtabrizi, M. Shahbazi, and E. Acha-Daza, "Universal branch model for the solution of optimal power flows in hybrid AC/DC grids," *International Journal of Electrical Power and Energy Systems*, vol. 126, no. PA, p. 106543, 2021. [Online]. Available: https://doi.org/10.1016/j.ijepes.2020.106543

[153] Y. Zhou, L. Zhao, W. J. Lee, Z. Zhang, and P. Wang, "Optimal Power Flow in Hybrid AC and Multi-terminal HVDC Networks with Offshore Wind Farm Integration Based on Semidefinite Programming," *2019 IEEE PES Innovative Smart Grid Technologies Asia, ISGT 2019*, pp. 207–212, 2019.

[154] C. Dierckxsens, K. Srivastava, M. Reza, S. Cole, J. Beerten, and R. Belmans, "A distributed DC voltage control method for VSC MTDC systems," *Electric Power Systems Research*, vol. 82, no. 1, pp. 54–58, 2012. [Online]. Available: http://dx.doi.org/10.1016/j.epsr.2011.08.006

[155] F. Gonzalez-Longatt, "Optimal power flow in MTDC systems based on a DC-independent system operator objective," *2015 IEEE Eindhoven PowerTech, PowerTech 2015*, 2015.

[156] H. Saadat *et al.*, *Power system analysis*. McGraw-hill, 1999, vol. 2.

[157] A. S. Abdel-Khalik, A. M. Massoud, A. A. Elserougi, and S. Ahmed, "Optimum power transmission-based droop control design for multi-terminal HVDC of offshore wind farms," *IEEE Transactions on Power Systems*, vol. 28, no. 3, pp. 3401–3409, 2013.

[158] N. Lianhui, X. Chunxiao, B. Huiyuan, and W. Di, "The amelioration of control strategy of VSC-MTDC based on voltage droop control," *2017 2nd International Conference on Power and Renewable Energy, ICPRE 2017*, pp. 157–161, 2018.

[159] W. Wang and M. Barnes, "Power flow algorithms for multi-terminal VSC-HVDC with droop control," *IEEE Transactions on Power Systems*, vol. 29, no. 4, pp. 1721–1730, 2014.

[160] L. Dewangan and H. J. Bahirat, "Comparison of HVDC grid control strategies," *Asia-Pacific Power and Energy Engineering Conference, APPEEC*, vol. 2017-Novem, pp. 1–6, 2018.

[161] L. F. Grisales-Noreña, J. C. Morales-Duran, S. Velez-Garcia, O. D. Montoya, and W. Gil-González, "Power flow methods used in AC distribution networks: An analysis of convergence and processing times in radial and meshed grid configurations," *Results in Engineering*, vol. 17, no. November 2022, p. 100915, 2023. [Online]. Available: https://doi.org/10.1016/j.rineng.2023.100915

[162] B. Stott and O. Alsaç, "Optimal power flow: Basic requirements for real-life problems and their solutions," in *SEPOPE XII Symposium, Rio de Janeiro, Brazil*, vol. 11, 2012, pp. 1–10.

[163] J. Zhu, *Optimization of power system operation*. John Wiley & Sons, 2015.

[164] T. K. Vrana, J. Beerten, R. Belmans, and O. B. Fosso, "A classification of dc node voltage control methods for hvdc grids," *Electric power systems research*, vol. 103, pp. 137–144, 2013.

[165] N. Hatziargyriou, J. Milanovic, C. Rahmann, V. Ajjarapu, C. Canizares, I. Erlich, D. Hill, I. Hiskens, I. Kamwa, B. Pal *et al.*, "Definition and classification of power system stability–revisited & extended," *IEEE Transactions on Power Systems*, vol. 36, no. 4, pp. 3271–3281, 2020.

[166] T. Van Cutsem and C. Vournas, *Voltage stability of electric power systems*. Springer Science & Business Media, 2007.

[167] M. Shahidehpour, F. Tinney, and Y. Fu, "Impact of security on power systems operation," *Proceedings of the IEEE*, vol. 93, no. 11, pp. 2013–2025, 2005.

[168] T. Werner and J. Verstege, "An evolution strategy for short-term operation planning of hydrothermal power systems," *IEEE Transactions on power systems*, vol. 14, no. 4, pp. 1362–1368, 1999.

[169] A. Poulin, M. Dostie, M. Fournier, and S. Sansregret, "Load duration curve: A tool for technico-economic analysis of energy solutions," *Energy and buildings*, vol. 40, no. 1, pp. 29–35, 2008.

[170] A. Mansoori, A. S. Fini, and M. P. Moghaddam, "Power system robust day-ahead scheduling with the presence of fast-response resources both on generation and demand sides under high penetration of wind generation units," *International Journal of Electrical Power & Energy Systems*, vol. 131, p. 107149, 2021.

[171] J. Deane, G. Drayton, and B. Ó. Gallachóir, "The impact of sub-hourly modelling in power systems with significant levels of renewable generation," *Applied Energy*, vol. 113, pp. 152–158, 2014.

[172] X. Zhu and M. G. Genton, "Short-term wind speed forecasting for power system operations," *International Statistical Review*, vol. 80, no. 1, pp. 2–23, 2012.

[173] A. J. Lamadrid, D. Munoz-Alvarez, C. E. Murillo-Sánchez, R. D. Zimmerman, H. Shin, and R. J. Thomas, "Using the m atpower optimal scheduling tool to test power system operation methodologies under uncertainty," *IEEE Transactions on Sustainable Energy*, vol. 10, no. 3, pp. 1280–1289, 2018.

[174] J. Zhao, T. Zheng, and E. Litvinov, "A unified framework for defining and measuring flexibility in power system," *IEEE Transactions on power systems*, vol. 31, no. 1, pp. 339–347, 2015.

[175] H. Nosair and F. Bouffard, "Flexibility envelopes for power system operational planning," *IEEE Transactions on Sustainable Energy*, vol. 6, no. 3, pp. 800–809, 2015.

[176] R. D. Zimmerman and C. E. Murillo-Sánchez, "Matpower optimal scheduling tool most 1.0 user's manual," *Power Systems Engineering Research Center (PSerc)*, 2016.

[177] M. Haugen, H. Farahmand, S. Jaehnert, and S.-E. Fleten, "Representation of uncertainty in market models for operational planning and forecasting in renewable power systems: a review," *Energy Systems*, pp. 1–36, 2023.

[178] A. Maheshwari and Y. R. Sood, "Solution approach for optimal power flow considering wind turbine and environmental emissions," *Wind Engineering*, vol. 46, no. 2, pp. 480–502, 2022.

[179] P. O. Dorile, D. R. Jagessar, and R. A. McCann, "Security of a power system under high penetration of wind energy considering contingencies and stability margins," in *2021 IEEE 19th Student Conference on Research and Development (SCOReD)*. IEEE, 2021, pp. 450–455.

[180] A. Devis, N. P. Van Lipzig, and M. Demuzere, "Should future wind speed changes be taken into account in wind farm development?" *Environmental Research Letters*, vol. 13, no. 6, p. 064012, 2018.

[181] Y. Zhang, A. Chowdhury, and D. Koval, "Probabilistic wind energy modeling in electric generation system reliability assessment," *IEEE Transactions on Industry Applications*, vol. 47, no. 3, pp. 1507–1514, 2011.

[182] M. U. Fahad and N. Arbab, "Factor affecting short term load forecasting," *Journal of Clean Energy Technologies*, vol. 2, no. 4, pp. 305–309, 2014.

[183] R. Ma, F. Jiang, J. Song, H. Chen, and H. Dong, "The short-term load forecasting based on the rate of load fluctuation," in *2011 Fourth International Conference on Intelligent Computation Technology and Automation*, vol. 1. IEEE, 2011, pp. 983–986.

[184] E. Ela and M. O'Malley, "Studying the variability and uncertainty impacts of variable generation at multiple timescales," *IEEE Transactions on Power Systems*, vol. 27, no. 3, pp. 1324–1333, 2012.

[185] J. Ma, V. Silva, R. Belhomme, D. S. Kirschen, and L. F. Ochoa, "Evaluating and planning flexibility in sustainable power systems," in *2013 IEEE power & energy society general meeting*. IEEE, 2013, pp. 1–11.

[186] B. Hu, Y. Gong, and C. Chung, "Flexible robust unit commitment considering sub-hourly wind power ramp behaviors," in *2019 IEEE Canadian Conference of Electrical and Computer Engineering (CCECE)*. IEEE, 2019, pp. 1–4.

[187] A. Lorca and X. A. Sun, "The adaptive robust multi-period alternating current optimal power flow problem," *IEEE Transactions on Power Systems*, vol. 33, no. 2, pp. 1993–2003, 2017.

[188] A. E. Feijoo and J. Cidras, "Modeling of wind farms in the load flow analysis," *IEEE transactions on power systems*, vol. 15, no. 1, pp. 110–115, 2000.

[189] A. E. Feijoo, J. Cidras, and J. G. Dornelas, "Wind speed simulation in wind farms for steady-state security assessment of electrical power systems," *IEEE transactions on Energy Conversion*, vol. 14, no. 4, pp. 1582–1588, 1999.

[190] P. Zhang, J. Marti, and H. Dommel, "Network partitioning for real-time power system simulation," in *Proc. 2005 International Conference on Power System Transients*, 2005, pp. 1–6.

[191] J. Arifin, T. A. Z. Siregar *et al.*, "Improving transmission reliability and reducing cost of supply in bangka island through sumatra-bangka interconnection: A contingency analysis approach," in *2023 4th International Conference on High Voltage Engineering and Power Systems (ICHVEPS)*. IEEE, 2023, pp. 766–770.

[192] S. E. G. Mohamed, A. Y. Mohamed, and Y. H. Abdelrahim, "Power system contingency analysis to detect network weaknesses," in *Zaytoonah University International Engineering Conference on Design and Innovation in Infrastructure, Amman, Jordan, pp. I3-4 Jun*, 2012.

[193] S. Meliopoulos, D. Taylor, C. Singh, F. Yang, S. W. Kang, and G. Stefopoulos, "Comprehensive power system reliability assessment," *PSERC Publication*, vol. 4, pp. 05–13, 2005.

[194] H. Huang, M. Kazerooni, S. Hossain-McKenzie, S. Etigowni, S. Zonouz, and K. Davis, "Fast generation redispatch techniques for automated remedial action schemes," in *2019 20th International Conference on Intelligent System Application to Power Systems (ISAP)*. IEEE, 2019, pp. 1–8.

[195] K. N. Patulak and H. S. Dini, "Contingency analysis of batam transmission system network post additional pv system in 2025 using performance index," in *2022 International Conference on Technology and Policy in Energy and Electric Power (ICT-PEP)*. IEEE, 2022, pp. 283–288.

[196] B. O. Adewolu and A. K. Saha, "Evaluation of performance index methodology for power network contingency ranking," in *2020 International SAUPEC/RobMech/PRASA Conference*. IEEE, 2020, pp. 1–6.

[197] G. Bhakta and A. B. Birchfield, "Applying remedial action schemes using sensitivity analysis for undergraduate research," in *2021 North American Power Symposium (NAPS)*. IEEE, 2021, pp. 1–6.

[198] U. NERC, "Glossary of terms used in nerc reliability standards," 2012.

[199] F. Sass, T. Sennewald, and D. Westermann, "Automated corrective actions by vsc-hvdc-systems: A novel remedial action scheme," *IEEE Transactions on Power Systems*, vol. 35, no. 1, pp. 385–394, 2019.

[200] Y. Zhu, N. Bacalao, and S. Conn, "Develop remedial action scheme to ensure system reliability with retirement of traditional baseload generators," in *2019 IEEE Power & Energy Society General Meeting (PESGM)*. IEEE, 2019, pp. 1–5.

[201] N. G. ESO, "Ncer: System defence plan: Issue 1," https://www.nationalgrideso.com/document/135226, December 2018.

[202] K. Meng, W. Zhang, J. Qiu, Y. Zheng, and Z. Y. Dong, "Offshore transmission network planning for wind integration considering ac and dc transmission options," *IEEE Transactions on Power Systems*, vol. 34, no. 6, pp. 4258–4268, 2019.

[203] Y. Zhang, M. E. Raoufat, and K. Tomsovic, "Remedial action schemes and defense systems," *Smart Grid Handbook, 3 Volume Set*, vol. 3, p. 235, 2016.

[204] H. Khoshkhoo, S. Yari, A. Pouryekta, V. K. Ramachandaramurthy, and J. M. Guerrero, "A remedial action scheme to prevent mid/long-term voltage instabilities," *IEEE Systems Journal*, vol. 15, no. 1, pp. 923–934, 2020.

[205] A. A. Bustos and B. Kazemtabrizi, "Flexible general branch model unified power flow algorithm for future flexible ac/dc networks," in *2018 IEEE International Conference on Environment and Electrical Engineering and 2018 IEEE Industrial and Commercial Power Systems Europe (EEEIC/I&CPS Europe)*. IEEE, 2018, pp. 1–6.

[206] M. I. Alizadeh, M. Usman, and F. Capitanescu, "Toward stochastic multi-period ac security constrained optimal power flow to procure flexibility for managing congestion and voltages," in *2021 International Conference on Smart Energy Systems and Technologies (SEST)*. IEEE, 2021, pp. 1–6.

[207] C. J. F. Cervantes, B. Kazemtabrizi, and M. C. Troffaes, "Contingency ranking in power systems via reliability rates," in *2018 IEEE International Conference on Environment and Electrical Engineering and 2018 IEEE Industrial and Commercial Power Systems Europe (EEEIC/I&CPS Europe)*. IEEE, 2018, pp. 1–6.

[208] S. Chatzivasileiadis, T. Krause, and G. Andersson, "Hvdc line placement for maximizing social welfare—an analytical approach," in *2013 IEEE Grenoble Conference*. IEEE, 2013, pp. 1–6.

[209] R. Kannan, "The development and application of a temporal markal energy system model using flexible time slicing," *Applied Energy*, vol. 88, no. 6, pp. 2261–2272, 2011.

[210] K. Neuhoff, A. Ehrenmann, L. Butler, J. Cust, H. Hoexter, K. Keats, A. Kreczko, and G. Sinden, "Space and time: Wind in an investment planning model," *Energy Economics*, vol. 30, no. 4, pp. 1990–2008, 2008.

[211] S. Impram, S. V. Nese, and B. Oral, "Challenges of renewable energy penetration on power system flexibility: A survey," *Energy Strategy Reviews*, vol. 31, p. 100539, 2020.

[212] B. Tarroja, F. Mueller, J. D. Eichman, and S. Samuelsen, "Metrics for evaluating the impacts of intermittent renewable generation on utility load-balancing," *Energy*, vol. 42, no. 1, pp. 546–562, 2012.

[213] M. A. Ortega-Vazquez and D. S. Kirschen, "Assessing the impact of wind power generation on operating costs," *IEEE Transactions on Smart Grid*, vol. 1, no. 3, pp. 295–301, 2010.

[214] T. Ackermann, N. B. Negra, J. Todorovic, and L. Lazaridis, "Evaluation of electrical transmission concepts for large offshore wind farms," in *Copenhagen Offshore Wind Conference and Exhibition*. Citeseer, 2005, pp. 26–28.

[215] D. Van Hertem and M. Ghandhari, "Multi-terminal vsc hvdc for the european supergrid: Obstacles," *Renewable and sustainable energy reviews*, vol. 14, no. 9, pp. 3156–3163, 2010.

[216] S. Cole, K. Karoui, T. K. Vrana, O. B. Fosso, J. Curis, A. M. Denis, and C. C. Liu, "A european supergrid: present state and future challenges," in *Proc. 17th Power Systems Computation Conference*, 2011.

[217] G. Arcia-Garibaldi, P. Cruz-Romero, and A. Gómez-Expósito, "Future power transmission: Visions, technologies and challenges," *Renewable and Sustainable Energy Reviews*, vol. 94, pp. 285–301, 2018.

[218] A. Raza, A. Shakeel, A. Altalbe, M. O. Alassafi, and A. R. Yasin, "Impacts of mt-hvdc systems on enhancing the power transmission capability," *Applied Sciences*, vol. 10, no. 1, p. 242, 2019.

[219] Z. Li, R. Zhan, Y. Li, Y. He, J. Hou, X. Zhao, and X.-P. Zhang, "Recent developments in hvdc transmission systems to support renewable energy integration," *Global Energy Interconnection*, vol. 1, no. 5, pp. 595–607, 2018.

[220] R. Irnawan, F. F. da Silva, C. L. Bak, and T. C. Bregnhøj, "An initial topology of multi-terminal hvdc transmission system in europe: A case study of the north-sea region," in *2016 IEEE International Energy Conference (ENERGYCON)*. IEEE, 2016, pp. 1–6.

[221] M. ENTSO-E, "Completing the map—power system needs in 2030 and 2040," *ENTSO-E*, 2020.

[222] C. Li, L. Xiao, Y. Cao, Q. Zhu, B. Fang, Y. Tan, and L. Zeng, "Optimal allocation of multi-type facts devices in power systems based on power flow entropy," *Journal of Modern Power Systems and Clean Energy*, vol. 2, no. 2, pp. 173–180, 2014.

[223] A. A. Bhandakkar and L. Mathew, "Optimal placement of unified power flow controller and hybrid power flow controller using optimization technique," in *2018 IEEE/IAS 54th Industrial and Commercial Power Systems Technical Conference (I&CPS)*. IEEE, 2018, pp. 1–7.

[224] S. Gerbex, R. Cherkaoui, and A. J. Germond, "Optimal location of multi-type facts devices in a power system by means of genetic algorithms," *IEEE transactions on power systems*, vol. 16, no. 3, pp. 537–544, 2001.

[225] S. Singh and A. David, "Placement of facts devices in open power market," in *2000 International Conference on Advances in Power System Control, Operation and Management, APSCOM-00*, vol. 1, 2000, pp. 173–177 vol.1.

[226] A. Fuchs and M. Morari, "Placement of hvdc links for power grid stabilization during transients," in *2013 IEEE Grenoble Conference*. IEEE, 2013, pp. 1–6.

[227] Y. Yang, Q. Gong, C. Lv, S. Guo, H. Li, and W. Cai, "Evaluation index and method of equipment utilization rate in distribution network with the integration of pv," in *2019 IEEE International Conference on Mechatronics and Automation (ICMA)*. IEEE, 2019, pp. 125–129.

[228] M. E. El-Hawary and G. S. Christensen, "Optimal economic operation of electric power systems," *(No Title)*, 1979.

[229] N. I. Yusoff, A. A. M. Zin, and A. B. Khairuddin, "Congestion management in power system: A review," in *2017 3rd international conference on power generation systems and renewable energy technologies (PGSRET)*. IEEE, 2017, pp. 22–27.

[230] A. Narain, S. Srivastava, and S. Singh, "Congestion management approaches in restructured power system: Key issues and challenges," *The Electricity Journal*, vol. 33, no. 3, p. 106715, 2020.

[231] E. Acha, C. R. Fuerte-Esquivel, H. Ambriz-Perez, and C. Angeles-Camacho, *FACTS: modelling and simulation in power networks*. John Wiley & Sons, 2004.

[232] N. Acharya and N. Mithulananthan, "Locating series facts devices for congestion management in deregulated electricity markets," *Electric power systems research*, vol. 77, no. 3-4, pp. 352–360, 2007.

[233] C. Dierckxsens, K. Srivastava, M. Reza, S. Cole, J. Beerten, and R. Belmans, "A distributed dc voltage control method for vsc mtdc systems," *Electric Power Systems Research*, vol. 82, no. 1, pp. 54–58, 2012.

[234] Y. Huang, X. Yuan, J. Hu, and P. Zhou, "Modeling of vsc connected to weak grid for stability analysis of dc-link voltage control," *IEEE Journal of emerging and selected topics in power electronics*, vol. 3, no. 4, pp. 1193–1204, 2015.

[235] Y. Wang, F. Qiu, G. Liu, M. Lei, C. Yang, and C. Wang, "Adaptive reference power based voltage droop control for vsc-mtdc systems," *Journal of Modern Power Systems and Clean Energy*, vol. 11, no. 1, pp. 381–388, 2021.

[236] F. Thams, J. A. Suul, S. D'Arco, M. Molinas, and F. W. Fuchs, "Stability of dc voltage droop controllers in vsc hvdc systems," in *2015 IEEE Eindhoven PowerTech*. IEEE, 2015, pp. 1–7.

[237] J. Beerten, S. Cole, and R. Belmans, "Modeling of multi-terminal vsc hvdc systems with distributed dc voltage control," *IEEE Transactions on Power Systems*, vol. 29, no. 1, pp. 34–42, 2013.

[238] N. M. Kangwa, C. Venugopal, and I. E. Davidson, "A review of the performance of vsc-hvdc and mtdc systems," *2017 IEEE PES PowerAfrica*, pp. 267–273, 2017.

[239] Y. Zhang, W. Qian, J. Shao, F. Zhang, L. Wang, Q. Hu, and W. Li, "Adaptive voltage reference based controls of converter power sharing and pilot voltage in hvdc system for large-scale offshore wind," *IEEE Open Access Journal of Power and Energy*, 2024.

[240] A. G. Abo-Khalil, "Impacts of wind farms on power system stability," *Intecopen," In Muyeen, SM, Al-Durra, A., Hasanien, HM (eds.): Wind Farmâ€™(InTechOpen, UK, 2013), ISBN 980â€“953â€“307â€“562â*, vol. 9, p. 133â, 2013.

[241] D. Westermann, D. Van Hertem, G. Real, T. Rauhala, M. Meisingset, M. Kurrat, B. Deppe, R. Atmuri, A. Küster, D. Soerangr *et al.*, "Voltage source converter (vsc) hvdc for power transmission–economic aspects and comparison with other ac and dc technologies," *Nil*, 2012.

[242] I. Okakwula, A. S. Alayande, and P. E. Orukpe, "Accurate probability distribution model determination and forecasting of peak load demand in nigeria," *Jordan J. Electr. Eng*, vol. 4, no. 4, pp. 186–194, 2018.

[243] T. B. Ouarda, C. Charron, J.-Y. Shin, P. R. Marpu, A. H. Al-Mandoos, M. H. Al-Tamimi, H. Ghedira, and T. Al Hosary, "Probability distributions of wind speed in the uae," *Energy conversion and management*, vol. 93, pp. 414–434, 2015.

[244] T. R. Ayodele *et al.*, "Determination of probability distribution function for modelling global solar radiation: case study of ibadan, nigeria," *International Journal of Applied Science and Engineering*, vol. 13, no. 3, pp. 233–245, 2015.

[245] O. Dzobo, C. Gaunt, and R. Herman, "Investigating the use of probability distribution functions in reliability-worth analysis of electric power systems," *International Journal of Electrical Power & Energy Systems*, vol. 37, no. 1, pp. 110–116, 2012.

[246] Y. Yang and F. Guo, "Reliability analysis of aero-equipment components life based on normal distribution model," in *2018 IEEE 4th Information Technology and Mechatronics Engineering Conference (ITOEC)*. IEEE, 2018, pp. 1070–1074.

[247] T. Zhang, W. Sheng, X. Song, X. Meng, and C. Shi, "Probabilistic modelling and simulation of stochastic load for power system studies," in *2013 UKSim 15th International Conference on Computer Modelling and Simulation*. IEEE, 2013, pp. 519–524.

[248] K. Yuan, K. Zhang, Y. Zheng, D. Li, Y. Wang, and Z. Yang, "Irregular distribution of wind power prediction," *Journal of Modern Power Systems and Clean Energy*, vol. 6, no. 6, pp. 1172–1180, 2018.

[249] T.-L. Zang, Y. Wang, and Z.-Y. Ma, "A detection method for abnormal harmonic current monitoring data using three-parameter weibull distribution," in *2016 IEEE 11th Conference on Industrial Electronics and Applications (ICIEA)*. IEEE, 2016, pp. 2366–2371.

[250] S. Burada, D. Joshi, and K. D. Mistry, "Contingency analysis of power system by using voltage and active power performance index," in *2016 IEEE 1st International Conference on Power Electronics, Intelligent Control and Energy Systems (ICPEICES)*. IEEE, 2016, pp. 1–5.

[251] S. Limanto, F. D. Kartikasari, and M. Oeitheurisa, "Improved learning outcomes of descriptive statistics through the test room and data processing features in the mobile learning model," in *2020 2nd International Conference on Industrial Electrical and Electronics (ICIEE)*. IEEE, 2020, pp. 139–142.

[252] R. A. Donnelly, *The complete idiot's guide to statistics, 2nd Edition*. Penguin, 2007.

[253] T. Halswanter, *An Introduction to Statistics with Python: With Applications in the Life Sciences*. Springer, 2016.

[254] Q. Zhao, J. García-González, O. Gomis-Bellmunt, E. Prieto-Araujo, and F. Echavarren, "Impact of converter losses on the optimal power flow solution of hybrid networks based on vsc-mtdc," *Electric Power Systems Research*, vol. 151, pp. 395–403, 2017.

[255] K. Vivek, "Design and analysis of voltage droop control technique for dc microgrids," in *2019 3rd International conference on Electronics, Communication and Aerospace Technology (ICECA)*. IEEE, 2019, pp. 795–799.

Appendix

Appendix A

A.1 Power system: Fundamental Concepts

A.1.1 Complex Power

The complex power can be express as:

$$S = P + jQ = VI^* \tag{A.1}$$

The current between buses i and j can be calculated as:

$$I_{ij} = Y_{ij}V_j \tag{A.2}$$

Substitute (A.2) into the (A.1), the revised formulation becomes:

$$S = P + jQ = V_S \sum_{i=1}^{n} (Y_{ij}V_j)^* \tag{A.3}$$

A.1.2 Complex Power across Transmission Line

The power transfer across the transmission line can be calculated using the formula provided below. To simplify the formulation, the line resistance and capacitance are neglected and only the purely inductive is considered for the complex impedance. Therefore, the impedance formula become:

$$\begin{aligned} Z &= j\omega L = jX \\ S &= V_r I^* = V_r \left[\frac{V_s - V_r}{jX}\right]^* \\ S &= \frac{V_r e^{-j\emptyset_2}\left(V_s e^{-j\emptyset_s} - V_r e^{-j\emptyset_2}\right)}{-jX} \\ S &= j\frac{V_s V_r}{X} e^{-j(\emptyset_r - \emptyset_s)} - j\frac{V_r^2}{X} \end{aligned} \tag{A.4}$$

Replace δ into the $\emptyset_r$-$\emptyset_s$, then the modified formula become:

$$\begin{aligned} S &= j\frac{V_s V_r}{X}e^{-j\delta} - j\frac{V_r^2}{X} \\ S &= j\frac{V_s V_r}{X}(\cos\delta - j\sin\delta) - j\frac{V_r^2}{X} \\ S &= \frac{V_s V_r}{X}\sin\delta + j\frac{V_s V_r}{X}\cos\delta - j\frac{V_r^2}{X} \\ S &= \frac{V_s V_r}{X}\sin\delta + j\frac{V_r}{X}\left(\frac{V_s V_r}{X}\cos\delta - V_r\right) \end{aligned} \tag{A.5}$$

A.1.3 State Variables in Traditional OPF

In the standard OPF equality constraint, the following state variables are present:

$$g(x) = \begin{bmatrix} g^i_{P_b}(x) = 0 \\ g^i_{Q_b}(x) = 0 \end{bmatrix} \quad \forall i \in \mathcal{I}_{bus} \tag{A.6}$$

A.2 FUBM Formulation

A.2.1 State Variables in the FUBM

The following are the additional state variables in the FUBM related to the equality constraint.

$$g(x) = \begin{Bmatrix} g^i_{P_b}(x) = 0 \\ g^i_{Q_b}(x) = 0 \\ g^i_{P_f}(x) = 0 \\ g^i_{Q_z}(x) = 0 \\ g^i_{V_f}(x) = 0 \\ g^i_{Q_t}(x) = 0 \\ g^i_{V_t}(x) = 0 \\ g^i_{P_{dp}}(x) = 0 \end{Bmatrix}, \quad x = \begin{Bmatrix} V^i_a & \forall i \in I_{pv} \cup I_{pq} \\ V^i_m & \forall i \in I_{pq} \\ \theta^i_{sh} & \forall i \in I_{sh} \\ B^i_{eq} & \forall i \in I_{Q_z} \\ B^i_{eq} & \forall i \in I_{vscII} \\ m^i_a & \forall i \in I_{v_t} \\ m^i_a & \forall i \in I_{Q_t} \\ \theta^i_{sh} & \forall i \in I_{vscII} \end{Bmatrix} \tag{A.7}$$

where $g(x)$ refers to the equality constraint and x is the state variables. i is the number of buses and I_{pv}, I_{pq} denote the PV and PQ buses, respectively. The sets of element indices I_{sh}, I_{Qz}, $I_{vsc_{II}}$, $I_{vsc_{III}}$, I_{Vt} , I_Qt , indicate the FubM elements for shift angle control, zero constraint control, VSC-FUBMs type II, VSC-FubMs type III, elements of V_t nodal control and elements for Q_t power control. The following is a list of state variables:

$$x = \begin{bmatrix} V_a & V_m & P_g & Q_g & B_{eq} & \theta_{sh} & m_a & G_{sw} \end{bmatrix}^\top$$

A.2.2 Comprehensive Admittance in the FUBM

$$\begin{bmatrix} i_f \\ i_t \end{bmatrix} = \begin{bmatrix} Y_{ff} & Y_{ft} \\ Y_{tf} & Y_{tt} \end{bmatrix} \begin{bmatrix} v_f \\ v_t \end{bmatrix} = \begin{bmatrix} Y_{br} \end{bmatrix} \begin{bmatrix} v_f \\ v_t \end{bmatrix} \tag{A.8}$$

$$Y_{fubm} = \begin{bmatrix} G_{sw} + \left(y_s + j\frac{b_c}{2} + jB_{eq} \right) & \frac{-y_s}{m'_a e^{-j\theta_{sh}}} \\ \frac{-y_s}{m'_a e^{j\theta_{sh}}} & y_s + j\frac{b_c}{2} \end{bmatrix} \tag{A.9}$$

$$Y_f = \begin{bmatrix} Y_{ff} \end{bmatrix} C_f + \begin{bmatrix} Y_{ft} \end{bmatrix} C_t \tag{A.10}$$

$$Y_t = \begin{bmatrix} Y_{tf} \end{bmatrix} C_f + \begin{bmatrix} Y_{tt} \end{bmatrix} C_t \tag{A.11}$$

$$Y_{bus} = C_f^\top Y_f + C_t^\top Y_t + \begin{bmatrix} Y_{sh} \end{bmatrix} \tag{A.12}$$

A.2.3 Power Injection the FUBM

1. Nodal complex power injections

$$[S_{br}] = [V_{br}] \times [I_{br}^*] \tag{A.13}$$

$$S_f = [v_f][i_f^*] = [v_f] \left[Y_{ff} v_f + Y_{ft} v_t \right]^* \tag{A.14}$$

$$S_t = [v_t][i_t^*] = [v_t] \left[Y_{ft} v_f + Y_{tt} v_t \right]^* \tag{A.15}$$

2. Nodal active power injections

$$P_f = \text{Real}(S_f) = \text{Real}\left([v_f][Y_{ff} v_f + Y_{ft} v_t]^* \right) \tag{A.16}$$

$$P_t = \text{Real}(S_t) = \text{Real}\left([v_t][Y_{ft} v_f + Y_{tt} v_t]^* \right) \tag{A.17}$$

3. Nodal reactive power injections

$$Q_f = \text{Imag}(S_f) = \text{Imag}\left([v_f][Y_{ff} v_f + Y_{ft} v_t]^* \right) \tag{A.18}$$

$$Q_t = \text{Imag}(S_t) = \text{Imag}\left([v_t][Y_{ft} v_f + Y_{tt} v_t]^* \right) \tag{A.19}$$

Appendix B

B.1 IEEE30 bus system

Table B.1: Bus Data

Bus	Demand P (MW)	Demand Q (MVAR)	Voltage Magnitude (p.u)	Voltage Angle (Degree)	baseKV	Vmax (p.u)	Vmin (p.u)
1	0	0	1	0	135	1.05	0.95
2	21.7	12.7	1	0	135	1.1	0.95
3	2.4	1.2	1	0	135	1.05	0.95
4	7.6	1.6	1	0	135	1.05	0.95
5	0	0	1	0	135	1.05	0.95
6	0	0	1	0	135	1.05	0.95
7	22.8	10.9	1	0	135	1.05	0.95
8	30	30	1	0	135	1.05	0.95
9	0	0	1	0	135	1.05	0.95
10	5.8	2	1	0	135	1.05	0.95
11	0	0	1	0	135	1.05	0.95
12	11.2	7.5	1	0	135	1.05	0.95
13	0	0	1	0	135	1.1	0.95
14	6.2	1.6	1	0	135	1.05	0.95
15	8.2	2.5	1	0	135	1.05	0.95
16	3.5	1.8	1	0	135	1.05	0.95
17	9	5.8	1	0	135	1.05	0.95
18	3.2	0.9	1	0	135	1.05	0.95
19	9.5	3.4	1	0	135	1.05	0.95
20	2.2	0.7	1	0	135	1.05	0.95
21	17.5	11.2	1	0	135	1.05	0.95
22	0	0	1	0	135	1.1	0.95
23	3.2	1.6	1	0	135	1.1	0.95
24	8.7	6.7	1	0	135	1.05	0.95
25	0	0	1	0	135	1.05	0.95
26	3.5	2.3	1	0	135	1.05	0.95
27	0	0	1	0	135	1.1	0.95
28	0	0	1	0	135	1.05	0.95
29	2.4	0.9	1	0	135	1.05	0.95
30	10.6	1.9	1	0	135	1.05	0.95

Table B.2: Branch Data

Branch	from_bus	to_bus	R (p.u)	X (p.u)	Half line charging (p.u)	Line limit (MVA)
1	1	2	0.02	0.06	0.03	130
2	1	3	0.05	0.19	0.02	130
3	2	4	0.06	0.17	0.02	65
4	3	4	0.01	0.04	0	130
5	2	5	0.05	0.2	0.02	130
6	2	6	0.06	0.18	0.02	65
7	4	6	0.01	0.04	0	90
8	5	7	0.05	0.12	0.01	70
9	6	7	0.03	0.08	0.01	130
10	6	8	0.01	0.04	0	32
11	6	9	0	0.21	0	65
12	6	10	0	0.56	0	32
13	9	11	0	0.21	0	65
14	9	10	0	0.11	0	65
15	4	12	0	0.26	0	65
16	12	13	0	0.14	0	65
17	12	14	0.12	0.26	0	32
18	12	15	0.07	0.13	0	32
19	12	16	0.09	0.2	0	32
20	14	15	0.22	0.2	0	16
21	16	17	0.08	0.19	0	16
22	15	18	0.11	0.22	0	16
23	18	19	0.06	0.13	0	16
24	19	20	0.03	0.07	0	32
25	10	20	0.09	0.21	0	32
26	10	17	0.03	0.08	0	32
27	10	21	0.03	0.07	0	32
28	10	22	0.07	0.15	0	32
29	21	22	0.01	0.02	0	32
30	15	23	0.1	0.2	0	16
31	22	24	0.12	0.18	0	16
32	23	24	0.13	0.27	0	16
33	24	25	0.19	0.33	0	16
34	25	26	0.25	0.38	0	16
35	25	27	0.11	0.21	0	16
36	28	27	0	0.4	0	65
37	27	29	0.22	0.42	0	16
38	27	30	0.32	0.6	0	16
39	29	30	0.24	0.45	0	16
40	8	28	0.06	0.2	0.02	32
41	6	28	0.02	0.06	0.01	32

Table B.3: Generator Data

Generator	**Pg**	**Qg**	**Qmax**	**Qmin**	**Vg**	**Pmax**
1	23.54	0	150	-20	1	80
2	60.97	0	60	-20	1	80
3	21.59	0	62.5	-15	1	50
4	26.91	0	48.7	-15	1	55
5	19.2	0	40	-10	1	30
6	37	0	44.7	-15	1	40